UNIVERSITY OF SOUTHAMPTON

Numerical Failure Modeling of Composite Structures

by

Gouri S Padhi

A Thesis submitted for the Degree of
Doctor of Philosophy

Computational Engineering and Design Center

School of Engineering Sciences

March 2000

UNIVERSITY OF SOUTHAMPTON

ABSTRACT

SCHOOL OF ENGINEERING SCIENCES
COMPUTATIONAL ENGINEERING AND DESIGN CENTER

Doctor of Philosophy

NUMERICAL FAILURE MODELING OF COMPOSITE STRUCTURES

by Gouri S Padhi

This thesis is concerned with the damage assessment of composite structures under static loading case with geometric non-linearity. Both the finite element method and the boundary element method are studied for this purpose. A finite element based computational damage model is developed for predicting the nonlinear response, first-ply failure and ultimate collapse strength of uni-directional laminated composite plates. The damage model is implemened into the finite element program ABAQUS. It contains theory of large deformation and large strain. The model is then extended to laminated composite structures with woven fabric plies. A simplified model is developed for prediction of stiffness properties of woven fabric composite plates. In both the cases numerical results are compared against test values. It is demonstrated that excellent correlation with experimental results can be achieved. In the context of the boundary element method (BEM) the present research focuses on stress analysis of 2-D orthotropic structures. A novel technique is proposed for accurately computing the singular integrals in the 2-D boundary element method.

Acknowledgments

First and foremost, I would like to thank my supervisor, Prof. Ajit Shenoi, for providing constant encouragement and support throughout this research. Sincere thanks are due to Dr. S S J Moy for his guidance throughout the course of this research. The author is deeply indebted to both Prof. Shenoi and Dr. Moy for providing the experimental results, which were crucial for this research.

I would like to thank Dr. Guy Hawkins, who had been cheerful and supportive throughout. He had been particularly helpful during the initial stage of this research.

My sincere gratitude to Prof. A J Keane, Director, Computational Engineering and Design Center (CEDC), for his valuable advice on computational aspects of this research.

I would like to thank Prof. W G Price, Head, Department of Ship Science, for making the departmental facilities (computational and experimental) available to me. Thanks to Mr. P A Wilson, for giving continuous support regarding the computer problems.

I would like to thank Dr. Z N Feng, for his consistent support, in my understanding and exploration of the experimental data.

Thanks to Dr. N W Bressloff (CEDC) for his consistent support towards computer related problems.

I would like to thank Dr. P B Nair (CEDC) for his constructive suggestions on preparing the thesis.

Thanks are also due to my colleagues in the CEDC, Dr. Yuvi Kahana, Dr. David Antony, Dr. Bahri Uzunoglu, and Dr. H K Jeong (Ship Science) for their stimulating supports and suggestions towards my research.

Finally, the financial assistance from the Faculty of Engineering and Applied Science, in the form of a studentship is deeply acknowledged.

Contents

List of Figures

List of Tables

Chapter 1

Introduction

1.1 Motivation

Composite materials are increasingly used in the construction of mechanical, aerospace, marine and automotive structures, because of their outstanding strength, stiffness and light-weight properties. Another advantage of composites is that stiffness and strength can be tailored to specific design loads. In the last few years there has been a dramatic increase in the usage of composite materials in non-aerospace products. Another class of innovative composite materials are advanced textile composites (3-D woven, braided, knitted, stitched) having complex reinforcement geometries. Textile Composites are extensively used for structural applications in aircraft construction[1,2] because of their ease of handling, low fabrication costs and high impact resistance. Reference[2] reviews the current research works on woven fabric composites at NASA as part of the Advanced Composites Technology(ACT) program. A principal opportunity to implement the out-of-plane reinforcements with these composite materials provides a huge variety of possible spatial orientations of substantially curved yarns. This can be realized in the current manufacturing using modern textile machinery. Textile reinforced composites have been considered promising materials for structural applications since the 1960s. The initial drive in the 1960s and 70s was for the perceived improvement in damage tolerance compared to laminated composites. The fact that a three dimensionally woven or braided reinforcement has no layers implies that delamination is not a failure mode for these materials, whereas delamination is a critical design criteria for

laminated composites.

Under service conditions, composite structures develop matrix cracks, fiber-matrix debonds, fiber fractures, and delaminations. These effects, which cause permanent loss of integrity within the structure, are termed damage, and they result in the loss of stiffness and strength of the material. Thus the load carrying capacity and the service life of the structure is reduced. These local damage events which are typically constrained from forming a major damage and are therefore nucleated under increasing load at many sites distributed through the volume of the composite material. For example the micro cracks observed within a structure constitute damage. As these micro cracks grow in size and number, they coalesce and develop into debonds, resulting in a reduction of the load-carrying capacity of the structure. In order to arrive at a reliable load-deformation response of the structure, it's load carrying capacity and service life, it is necessary to include the damage parameters and their subsequent effects in the numerical model.

1.2 Background

Damage assessment of composite structures is an aspect of design where there are few design synthesis techniques available and one that is relevant to almost all engineering composite structures. This is an area where many traditional techniques have been tried with relatively little success. Traditionally, in the analysis of laminated composite structures, the uni-directionally reinforced lamina is considered the fundamental material block. Hence both the tension and compression test methods for them have been standardized by ASTM. The other experimental methods for composite materials are : biaxial testing, short beam bending, rail shear test, off-axis tension test, Iosipescu test etc.. However experimental methods for composite materials are not so reliable as are for isotropic materials. For example phenomenon such as premature failure initiated by local fibre-matrix debonding and fibre buckling, is typical for compressive loading, though, is not observed in the case of tensile tests.

The other numerical methods for solving continuum mechanics problems are : the finite difference (FD), the finite element (FE) and the boundary element (BE) ap-

proaches. The finite difference approach is the simplest of the three approaches and is relatively easy to program. However, it's main drawback in practical engineering problems is that it is not suitable for problems with awkward irregular geometries. Nowadays, finite difference methods are popular for heat transfer and fluid flow problems, rather than stress analysis problems.

The finite element method grew out of the need to solve accurately structural analysis problems in the aerospace industry during the late 1950's. Although the mathematical ideas had been outlined in the appendix of a paper by Courant[3], it was not until advanced electronic computers were widely available that the method could be effectively applied for engineering computations. Since this period, finite element techniques have evolved rapidly and are now established as a basic method for solving boundary and evolution problems in science and engineering. Applications of finite element method for composite material analysis is quite large and the literatures concerning them can be found in the subsequent review chapters.

One of the first finite-element-based failure analysis was performed by Lee[4]. Lee performed a three-dimensional finite element analysis and used his own direct-mode determining failure criterion to predict the failures. He determined the stresses at the center of each element and the stresses at the center of the interface of each element to identify failure. According to the modes of failure, the stiffness matrix of the element with failures was modified. Equilibrium was then re-established to give a new stress distribution and subsequent failure zones. The process was repeated until the ultimate strength of the laminate was obtained. The literature concerning further applications of the finite element analysis for failure prediction of composite plates can be found in chapter 2. Recently Coats[5,6] developed a nonlinear progressive failure analysis for laminated composites that used a constitutive model in which damage accumulation was predicted by damage evolution laws. The methodology was used to predict the initiation and growth of matrix cracks and fiber fracture.

Boundary element method constitutes a recent development in computational mechanics for the solution of boundary value problems in engineering. Unlike the 'domain

type' methods, e.g., the finite difference or the finite element methods, the order of dimensionality of the problem reduces by unity in boundary element formulation, thus simplifying the analysis and the computer code to a large extend by solving a small system of equations.

One more important reason for choosing the finite element and the boundary element methods in the composite failure analysis is their ability to solve computationally intensive problems. With these two methods, most of the scientific and engineering problems invariably reduce to solving systems of simultaneous equations. Currently, the solution of linear systems of equations on advanced parallel-vector computers is a key area of research with applications in many disciplines[7-8].

1.3 Objectives and Scope

The overall objective of this research is to develop computational models for failure analysis of composite structures. The composites of primary interest are those best suited to applications in aircraft structures. A progressive failure methodology is developed using the finite element program ABAQUS. Two important class of structures are consider for application purposes. They are (i)uni-directional composite structures, and (ii) woven-fabric composite structures. The methodology is then validated by comparing numerical predictions using nonlinear progressive failure analyzes with experimental data.

Next the boundary element method is applied stress analysis of 2-D orthotropic structures. Efficient computational procedures are developed for computation of the singular integrals in the boundary element method. Numerical results are compared against analytical results.

Specific goals of this research include:

1. Establish state-of-the-art perspective on computational models for failure analysis of composite structures.

2. Develop and implement a finite element based failure analysis methodology which accommodates various formulations for detecting failure and degrading material properties.

3. Development of computational strategies for accurate stress analysis of 2-D orthotropic structures using the boundary element method.

4. Validation of the computational models against test data or analytical solutions.

1.4 Layout of the Thesis

This thesis consists of eight chapters addressing the numerical modeling of composite structures. Each chapter starts with an extended introduction where the motivations and objectives are formulated. The ultimate objective of the thesis is to present computational models which provide an accurate correlation with experimental/exact results available in literatures.

After this introductory chapter, in chapter 2, an extensive review is made of the damage modeling issues for uni-directional laminated composite structures. A review is made of the past literatures on laminated plate theories. Summaries of some most relevant literatures are elaborately outlined. Chapter 3 reviews the literatures concerning the modeling issues for woven fabric composites.

The next two chapters are aimed at failure modeling of various composite structures. A comprehensive failure modeling of uni-directional composite structures is presented in chapter 4. An attempt has been made to systematically include all major composite failure criteria, to discuss their assumptions and procedures, present final equations and provide their mutual comparisons in the context of the damage prediction capability for the composite structures. This allowed to distinguish the best (most accurate and applicable) failure criteria which are recommended for practical applications.

Chapter 5 describes the failure analysis of woven fabric composite plates. This field of research is in it's infancy, as can be seen from the review of the existing publications. Hence a simplified model is developed to be suitable for analysis of the type of weave architecture, for which experimental results are available. Failure analysis is carried

out next. Numerical results are compared against experimental values.

Applications of the boundary element method for stress analysis of 2-D orthotropic structures is addressed in chapter 6. First, a detailed discussion and literature review on the fundamentals of the boundary element method and the associated singular integrals, in the context of 2-D orthotropic elasticity is presented. The approach is demonstrated on a number of specific plane stress, plane strain, cylindrical bending problems, and shows a unique accuracy in comparison to the benchmark solutions. The material of this chapter is supplemented by a short appendix on computation of singular integrals. Finally discussions and future research are presented in chapter 7 and conclusions are presented in the last chapter.

1.5 References

1. Poe, C.C., Dexter, H.B. and Raju, I.S., A Review of the NASA Textile Composites Research, AIAA Paper No. 97-1321, AIAA (1997)

2. Harris, C.E. and Poe, C.C., Role of Mechanics of Textile Perform Composites in the NASA Advanced Composites Technology Program, NASA CP-3311, pp. 1-5 (1994)

3. Courant, R., Variational Methods for the Solution of Problems of Equilibrium and Vibrations, *Bulletin of American Mathematical Society*, Vol. 43, pp. 1-23(1943).

4. Lee, J.D., Three Dimensional Finite Element Analysis of Damage Accumulation in Composite Laminate, Computers and Structures, Vol. 15, pp. 335-350(1982).

5. Lo, D.C., Coats, T.W., Harris, C.E. and Allen, D.H., Progressive Damage Analysis of Laminated Composite (PDLAC) (A Computational Model Implemented in the NASA COMET Finite Element Code, NASA TM 4724 (1996).

6. Coats, T.W. and Harris, C.E., A Progressive Damage Methodology for Residual Strength Predictions of Notched Composite Panels, NASA TM-1998-207646 (1998).

7. Utku, S., Salama, M. and Melosh, R., Concurrent Factorization of Positive Definite Banded Hermitian Matrices, *International Journal for Numerical Methods in Engineering* , Vol. 23, pp. 2137-2152 (1986).

8. Dongarra, J.J., Gustafson, F.G. and Karp, A., Implementing Linear Algebra Algorithms for Dense Matrices on a Vector Pipeline Machine, *SIAM Review*, Vol. 26, No. 1 (1984).

Chapter 2

Literature Review on Progressive Failure Analysis of Composite Structures

2.1 Background

Damage in composite materials has been and continues to be the subject of numerous investigations. One important observation regarding the damage propagation in composites is that the growth of an individual damage pattern such as a crack does not, by itself, cause conditions of criticality, but the total effect of cracks in a representative volume, brought about by their individual growth and mutual interaction, lead to degradation of the average properties, which eventually causes loss of integrity and failure of the composite.

A variety of computational techniques have been developed and applied to study the initiation and evolution of the damage mechanisms in these materials. The objective of this chapter is to review these models in the context of damage evolution laws, failure mechanisms and material property degradation schemes. However, one more important factor in the computational modeling of composite structures is the shear deformation theory used in the composite failure analysis. It has long been recognized that the classical two-dimensional laminated plate theory, based on the Kirchhoff hypotheses of straight in-extensional normals for the entire plate package yields sufficiently accurate

results only for thin composite plates.

This chapter is organized as follows. Next section reviews the various approaches for developing two-dimensional shear deformation theories and makes an assessment of the accuracy of the response predictions of these theories. Section 3 reviews the computational damage models for laminated composite structures. Each review discusses the type of analysis (linear or nonlinear) used in performing the progressive failure analyzes, failure criterion chosen, and prediction of progressive failure analyzes compared to experimental results. Based on these reviews, conclusions are drawn in the last section are drawn in the last section.

2.2 Assessment of Shear Deformation Theories for Laminated composite Plates

Plate and shell structures made of laminated composite materials are often modeled as an equivalent single-layer using classical laminate theory, in which the thickness stress components are ignored. The classical laminate theory is a direct extension of classical plate theory based on the kirchoff hypothesis for homogeneous plates. This theory is adequate when the thickness (to side or radius ratio) is small. However, laminated plates and shells made of such advanced filamentary composite materials as graphite-epoxy are susceptible to thickness effects because their effective transverse moduli are significantly smaller than the effective elastic modulus along the fiber direction. Refined theories provide improved global response estimates for deflections, vibration frequencies, and buckling loads of moderately thick composites when compared to the classical laminate theory.

The Classical laminated plate theory is based on Kirchoff's hypothesis and, in general, provides good estimates of gross behavior of the laminate. In addition, it is well known that the effect of transverse and normal strains is not negligible, as in the classical plate theory. Shear deformation theories aim at incorporating these effects. Reissener[1] and Mindlin[2] laid the foundations for such developments. In Reissener's approach assumptions are introduced concerning the variation of stresses, whereas in Mindlin's approach displacements are chosen in an appropriate form. Basically both

the approaches offer the possibility of further refinement by considering a more general form of the field variables.

The first theory for laminated anisotropic plates is that of Yang, Norris, and Stavsky[3]. Their work called the Yang-Norris-Stavsky (YNS) theory represents a generalization of Reissner-Mindlin plate theory for homogeneous isotropic plates to arbitrarily laminated anisotropic plates and includes shear deformation and rotary inertia effects.

Lo *et al.*[4], utilized a straight forward power series expansion of the displacement to improve the laminate characteristics. Although the theory gives a much better approximation to the behaviour of laminated plates as compared to that of CLPT, it suffers from the same drawbacks as that of FSDT, namely: (i)it does not satisfy the conditions of zero transverse shear stresses on the top and bottom surfaces of the plate, (ii)it requires a shear correction factor to the transverse shear stiffnesses. Moreover it contains more dependent unknowns as compared to other improved shear deformation theories with equal accuracy.

Reddy[5], used expressions for in-plane displacements satisfying the free-surface zero shear conditions. The theory accounts not only for transverse strains, but also for a parabolic variation of the transverse shear strains through the thickness, and consequently there is no need to use shear correction coefficients in computing the shear stresses. Moreover the theory contains the same number of dependent variables as in first order shear deformation theory, but results in more more accurate prediction of deflections and stresses. However this theory does not satisfy the continuity condition of the transverse shear stresses at the interfaces.

Toledano and Murakami[6] used Legendre polynomials for the approximation of in plane displacement distribution across the plate thickness. The theory gave accurate results for in plane responses.

Levinson[7] and Murthy[8] presented third order theories that assume transverse inextensibility. However both authors used the equilibrium equations of the first order theory in their analysis. In other words, the higher order terms of the displacement are accounted for in the calculation of the strains but not in the governing differential equations or in the boundary conditions.

A recently proposed theory by Knight and Qi[9] assumes physically that only in some average sense does a straight line originally normal to the mid plane remain straight and rotate relative to the normal of the mid-plane after deformation. Hence the in-plane displacement is still approximated, in an average sense, as linear and the transverse deflection as constant through the plate thickness. The associated nominal-uniform transverse shear strain directly derived from these displacement field assumptions is identified as the weighted average transverse shear strain through the plate thickness with the corresponding transverse shear stress as the weighting function, while the actual transverse shear strain is permitted to vary through the thickness and satisfies the constitutive law with it's stress counter part. Likewise, the average rotation of the line is identified as it's weighted-average value, instead of the one evaluated from a linear regression of the in-plane displacement with the least-square method. This restated FSDT possesses the advantages of both equivalent single-layer theories and layer-wise theories. It accounts for a variable distribution of transverse shear strain to which higher-order theories are developed. It satisfies proper continuity requirement of transverse shear stress at layer interfaces, which layer-wise theories are proposed to achieve. The constitutive law and traction boundary conditions are automatically satisfied.

The theory proposed by Whitney and Pagano[10] is an extension of the theory proposed by Yang and Norris[3] to laminated composite plates. The displacement assumption is similar to that of first order shear deformation theory. However the stresses calculated were identical to that of the CLPT, although the prime purpose of the investigation was to predict gross laminate response characteristics.

Pagano[11] has very successfully adopted Reissner's approach for estimating interlaminar stresses by restating the variational principle to laminated body, composed of several layers. In this theory both stresses and displacements are subject to variation. Therefore (i)traction and displacement continuity conditions at interfaces between adjacent layers are satisfied, (ii)it considers a region within the laminate that is arbitrarily located except that it is bounded by any two of the parallel interfaces. Numerical results show that for laminates with free edge class of boundary value problems, in which very steep stress gradient occurs, this theory gives more accurate results. However the theory results in a mathematical model consisting of 23N partial differential equations

in the mid-plane coordinates of the laminate and 7N edge boundary conditions; N is the number of layers in the laminate. The storage and computational costs, especially for geometrically nonlinear problems or transient analysis using the finite element analysis precludes the use of such a theory. Because it gives as accurate a global response as the three-dimensional theory, it is considered efficient for problems not involving regions of acute discontinuities.

Three dimensional elasticity models have been applied to the stress, free vibrations, and buckling problems of laminated orthotropic rectangular plates. Both the cylindrical bending case and the simply-supported boundary conditions have been considered[12,13]. In quasi-three dimensional models, simplifying assumptions are made regarding the stress or strain state in the laminate, but no *a priori* assumptions are made about the distribution of the different response quantities in the thickness direction.. However the use of three- dimensional and quasi three-dimensional models for predicting the response characteristics of laminated anisotropic plates with complicated geometry is computationally expensive and, therefore, is not feasible for practical plates. On the other hand two-dimensional models are adequate for predicting the gross response characterics of medium-thick laminated plates, but they are not adequate for the accurate prediction of the transverse stresses and deformations.

The conventional variational formulation of the classical lamination theory as well as the third-order theory[5] involves higher order (i.e. second-order) derivatives of the transverse displacement. Therefore, in the finite-element modeling of such theories the continuity of not only the transverse displacement should be imposed but also it's derivatives along the element boundary. In other words, a conforming plate bending element based on a displacement formulation of these theories requires the continuity of transverse displacements and their derivatives across the inter-element boundaries. The construction of such an element is algebraically complicated, requiring for example, a quintic polynomial with 21 degrees of freedom for a six-node triangular element.

To overcome the stringent continuity requirements of the conventional variational formulation, several alternative formulations and associated elements have been developed. These include hybrid finite elements, mixed finite elements, and shear flexible elements based on the FSDT. Hybrid elements are based on variational statements

that use independent variation of displacements inside the domain

Much of the research in the analysis of composite plates is limited to linear problems. This is perhaps due to the complexity of the nonlinear partial differential equation associated with the large-deflection theory of composite plates. Approximate solutions to the large-deflection theory (in the Von Karman sense) of laminated composite plates have been attempted. Chandra[14] and Chia[15] employed the Galerkin method to reduce the governing nonlinear partial differential equations to an ordinary differential equation in time for the mode shape; the perturbation technique was used to solve the resulting equation. Zaghloul and Kennedy[16] used a finite-difference successive iteration technique in their analysis. In all of these studies the transverse shear effects were neglected.

Many of the cited theories can be considered as special cases of a general theory based on the following through-the thickness displacement assumptions[17]:

$$u_\alpha(x_\beta, x_3) = u_\alpha^0(x_\beta) + U_\alpha(x_\beta, x_3), \tag{2.1}$$

$$w(x_\beta, x_3) = w^0(x_\beta) + W(x_\beta, x_3), \tag{2.2}$$

Where u_α^0 and w^0 are the displacement components of the reference plane of the plate ($x_3 = 0$), U_α and W are the functions of x_3 which vanish at $x_3 = 0$, $\alpha, \beta = 1, 2$. The different theories can be identified by the assumed functional dependence of U_α and W on x_3 (table 5.1). Also various models that are usually considered for numerical analysis are presented in table 5.2.

2.3 Review of Progressive Failure Analysis of Composite Structures

Reddy and Pandey[18] developed a finite element procedure based on first-order, shear-deformation theory for first-ply analysis of laminated composite plates subjected to

Table 2.1: Displacement assumptions in different laminated plate theory

Theory	Type	U_α	W	Comments
Classical theory		$-x_3\partial_\alpha w^0$	0	C^1 Continuity for w
First-order shear deformation theory	5 Parameters Pagano[10]	$x_3\phi_\alpha^0$	0	C^0 Formulation
Higher-order theory	11-Parameters Lo[4]	$x_3\phi_\alpha^0 + (x_3)^2\psi_\alpha^0 + (x_3)^3\zeta_\alpha^0$	$x_3\epsilon_3^0 + (x_3)^2\psi_3^0$	Transverse stresses do not satisfy continuity at layer interfaces
Higher order theory	5-Parameters Reddy[5]	$-x_3\partial_\alpha w^0 + \left[1 - \frac{4}{3}\left(\frac{x_3}{h}\right)^2\right]\phi_\alpha^0$	0	
Discrete layer theory	transverse strain included	$\sum_{i=1}^{k} U_{alpha}^{(k)}\phi(k,i)$	$\sum_{i=1}^{k} W^{(k)}\phi(k,i)$	$\phi(k,i) = 1 for k \neq i$ $= \frac{x-3-h_{k-1}}{h_k - h_{k-1}} for k = i$
Discrete layer theory	transverse strain neglected	$\sum_{i=1}^{k} U_{alpha}^{(k)}\phi(k,i)$	0	For convenience, the bottom surface selected to be the reference surface (only in the discrete layer theories)

Table 2.2: Modeling Approaches

Model number	Type	Through the thickness displacement assumptions	Constraint conditions on stress	Total number of generalized displacement parameters
1	First-order shear deformation theory	Linear u_α Constant w	$\sigma_{33} = 0$	5
2	Higher-order shear deformation theory	Cubic u_α quadratic w Lo[4]	None	11
3	Simplified Higher-order theoory	Cubic u_α constant w Reddy[5]	σ_{33}=0 through and $\sigma_{3\alpha}$=0 at top and bottom surfaces	5
4	Discrete layer theory	Piecewise linear u_α, constant w through out thickness	σ_{33}=0	2*NL+3
5	Simplified discrete layer theory	Piecewise linear u_α, constant w through out thickness	σ_{33}=0 continuity of $\sigma_{3\alpha}$ at layer interfaces	5
6	Predictor Corrector approach	Predictor Phase: Linear u_α Constant w Corrector Phase: Matching displacements	Predictor Phase $\sigma_{33} = 0$	5

in-plane and/or transverse loads. The well established failure criteria including the maximum stress, maximum strain, Hill's, Tsai-Wu and Hoffmann's are reviewed in the context of first-ply failure.

Rosen[19] presented a theoretical and experimental study of the failure of a composite, consisting of a matrix stiffened by uni-axially oriented fibers, when subjected to a uni-axial tensile load parallel to the fiber direction. The fibers were treated as having a statistical distribution of flaws or imperfections that result in fiber failure under applied stress. It was demonstrated that the statistical accumulation of the flaws or imperfections within the composite was the cause of composite failure.

Reddy and Reddy[20] developed a three-dimensional (3-D) progressive failure algorithm for composite laminates under axial tension. The finite element analysis used Reddy's layerwise laminated plate theory (LWLT) and predicted both in-plane and interlaminar stresses at the reduced integration Gauss points. A parametric study was performed to investigate the out-of-plane material properties, 3-D stiffness reduction methods, and boundary conditions on the failure loads and strains of a composite laminate under axial tension.

Singh *et al.*[21] carried out a progressive failure analysis of symmetric thin square laminates under in-plane shear. The finite element method along with first order shear deformation theory was used for this purpose. Geometric non-linearity was included in the analysis in the Von Karman sense. The paper discusses failure loads, associated maximum transverse displacements and locations and modes of failure associated with the laminates.

Chang and Chang[22] developed a progressive failure model for laminated composites containing stress concentrations. A non-linear finite element method was used for this purpose. For fiber failure, both the transverse modulus E_{22} and and Poisson's ratio ν_{12} were set to zero, and the longitudinal modulus, E_{11} and shear modulus, G_{12} were reduced according to the exponential Weibull distribution. For matrix cracking in a lamina, the transverse modulus and the Poisson's ratio were reduced to zero, whereas the longitudinal and shear moduli remained unchanged.

Chang and Lessard[23] conducted an analytical investigation to study the progressive damage in laminated composites containing an open hole and subjected to compressive

loading. A finite element analysis based on finite deformation theory, and with material and geometric non-linearities was used for this purpose. Non-linear shear stress-strain behavior was included in the analysis. The effect of the lay-up sequence and loading direction on the strength of the laminate was studied.

Sleight[24] developed a progressive failure model for predicting failure of laminated composite structures under geometrically non-linear deformations. The progressive failure analysis used C^1 shell elements based on classical lamination theory for calculating the in-plane stresses. Stiffness reductions were carried out at the ply level. Numerical results were presented for in-plane loading conditions. These results were then compared against experimental values.

Sahid and Chang[25] developed a progressive failure model for predicting the accumulated damage and the effect of such damage on the in-plane response of laminated composites subjected to tensile and shear loads. The main focus of the paper was on internal damage in composites induced by matrix cracking under in-plane tensile and shear loads. The finite element method was used for this purpose. Predictions from the analysis were compared against experimental results.

The failure analysis of composite laminates subjected to out-of-plane load causing bending has not received as much as attention as in plane loading. It is complicated due to both material and geometric non-linearities that come into play when the loads are increased beyond the first ply failure. Material non-linearity results from the damage mentioned earlier, and the geometric non-linearity is due to the large displacements experienced by the structure during loading.

Reddy and Reddy[26] used generalized layerwise plate theory and a progressive failure model to determine first ply and ultimate failure loads of a three-point bend specimen. Stiffness reduction was carried out at the reduced integration Gauss points of the finite element mesh depending on the mode of failure. Geometric non-linearity was taken into account in the Von Karman sense.

Kam and Sher[27] studied progressive failure of centrally loaded laminated composite plates. The Ritz method, with geometric non-linearity, in the Von Karman sense, was used to construct the load displacement behavior. Echaabi and others[28] presented a theoretical and experimental study of damage progression and failure modes of com-

posite laminates under three point bending. Linear CLPT was used for the stress analysis.

Kim *et al.*[29] carried out a progressive failure analysis for laminated composite beams using a beam finite element. Maximum stress and Tsai-Wu failure criteria are used to assess failure at the Gauss points. Stiffness reduction was carried out with material property degradation factors. Distinct degradation factors were used for fiber failure and matrix failure. Convergence of the finite element mesh and the load increment size on the failure load was studied. The predictions correlated well with the experimental data.

Tolson and Zabaras[30] studied the first and last ply failure loads of a laminated composite plate subjected to both in-plane and sinusoidal transverse loads. A higher-order shear deformation theory was used for this purpose. Stiffness reductions were carried out at the Gauss integration points. However no comparison was made to test results for the transverse load case.

Gummadi and Palazotto[31] used a geometrically non-linear finite-element formulation based on the total Lagrangian approach, for predicting the onset of various failure modes in laminated composite beams and arches. Failure modes such as matrix cracking, fiber breakage, and delamination were included in the analysis. Large strain effects on load displacement characteristics were studied. Load-carrying capabilities of the composite beam and arch structures, were discussed.

2.4 Conclusion

On the basis of the above reviews, the following conclusions seem to be justified.

- The classical laminated plate theory yields sufficiently accurate results only for thin composite plates. The first order shear deformation theory is more accurate than the classical laminated plate theory. Higher order theories give still more accurate results, with however, an increase in the computational cost. For the present study, the composite plates considered were very thin, with aspect ratios of order of more than 200. Therefore the first order theory was considered to be the most suitable shear deformation theory to use in the composite analysis

procedure.

- Most of the computational damage models have been developed for in-plane and simple bending conditions. In the latter case, the state of stress was not strongly bi-axial in nature. In these cases the numerical implementation becomes simpler. However, it does not take into account the effect of the interaction between the multi-axial stresses in a composite layer.

- In some literatures comparison with experimental results has not been reported. For practical applications of a computational model, it is essential that it is validated against standard test results. Correlation of numerical results(such as deformations, strains and damage patterns) with the experimental values gives an added robustness to the numerical model.

- In most of the literatures geometric non-linearity and large deformation effects have been ignored. Inclusion of these effects significantly complicates the implementation aspects. However, as can be seen later in this thesis the first-ply failure load and the ultimate collapse loads of composite plates are found to be strongly sensitive to the effect of geometric non-linearity.

The overall objective of the current research is to develop progressive failure analysis methodology for laminated composite structures under bending loading conditions. The model contains large deformation and large strain theories. Geometric non-linearity is included to simulate the experimental behavior. Most of the well established failure criteria are included in the damage model. A simple post-failure material property degradation scheme is proposed for carrying out the progressive failure analysis. The numerical results are compared against test results. Numerical damage predictions are compared and assessed against experimental observations. All the failure criteria are assessed with respect to their prediction capability for damage initiation and failure.

2.5 References

1. Reissner, E., The Effect of Transverse Shear Deformation on The Bending of Elatsic Plates *J. of Appl. Mech.* pp. A69-A77(1945)

2. Mindlin, R.D., Influence of Rotary Inertia and Shear on Flexural Motions of Isotropic, Elastic Plates *App. Mech Divn., Proceedings of the ASME*, pp. 31-38(1950)

3. Yang, P.C. and Norris, C.H., Elastic Wave Propagation in Heterogeneous Plates, *Int. J. of Solids and Struc.*, Vol. 2 pp. 665-684(1966)

4. Lo, K.H. and Christensen, R.M., A Higher-Order Theory of Plate Deformation: Part-2 Laminated Plates, *J. of Appl. Mech.* pp. 669-676, Dec. 1977

5. Reddy, J.N., A Simple Higher Order Theory for Laminated Composite Plates, *J. of Appl. Mech*, Vol. 51, pp. 745-752 Dec.(1984)

6. Toledano, A., A High-Order Laminated Plate Theory With Improved In-Plane Responses *Int. J. Of Solids and Structures*, vol. 23, pp.111-131(1987)

7. Levinson, M., An Accurate Simple Theory of Statics and Dynamics of Elastic plates, *Mechanics Research Communications*, Vol. 7, pp. 343-350(1980).

8. Murthy, M.V.V., An Improved Transverse Shear Deformation Theory for Laminated Anisotropic Plates, *NASA Technical Paper 1903*, Nov. 1981.

9. Knight, N.F. Jr and Qi, Yunqian, Restatement of First-Order Shear Deformation Theory For Laminated Plates, *Int. J. Of Solids and Structures*, vol. 34, pp. 481-492(1997)

10. Pagano, N.J. and Whitney, J.M. Shear Deformation in Heterogeneous Anisotropic Plates, *J. of Appl. Mech*, pp. 1031-1036, Dec.(1970)

11. Pagano, N.J., Exact Solutions for Composite Laminates in Cylindrical Bending, *J. of Comp. Mat.* 3, 398-411(1969).

12. Pagano, N.J., Exact Solutions for Composite Laminates in Cylindrical Bending, *J. of Comp. Mat.*, Vol. 3, pp. 398-411(1969)

13. Pagano, N.J., Exact Solutions for Rectangular Bidirectional Composites and Sandwich Plates, *J. of Comp. Mat.*, Vol. 4, pp. 20-34(1970)

14. Chandra, R., Large deflection Vibration of Cross-Ply Laminated Plates with Certain Edge Conditions, *J. of Sound Vib.* Vol. 47(4), pp.509-514(1976)

15. Chia, C.Y. and Prabhakar, M.K., A General Mode Approach to Nonlinear Flexural Vibrations of Laminated Rectangular Plates, *ASME J. of Appl. Mech.*, Vol. 45 pp. 623-628(1978)

16. Zaghloul, S.A. and Kennedy, J.B., Nonlinear Analysis of Unsymmetrically Laminated Plates, *ASME J. of Engg. Mech Div.*, 101(EM3), pp.169-185(1975)

17. Reddy, J.N., Finite-Element Modeling of Layered, Anisotropic Composite Plates and Shells: A Review of Recent Research, *Shock and Vibn. Digest*, Vol. 13, No. 12, pp.3-12(1981)

18. Reddy, J.N. and Pandey, A.K., A First-Ply Failure Analysis of Composite Laminates, Comput. and Struct., Vol. 25, pp. 371-393(1987).

19. Rosen, B.W., Tensile Failure of Fibrous Composites, AIAA Journal, Vol. 2, pp. 1985-1991(1964).

20. Reddy, Y.S. and Reddy, J.N., Three-Dimensional Finite Element Progressive Failure Analysis of Composite Laminates Under Axial Extension, J. of Comp. Tech. and Res., Vol. 15, pp. 73-87(1993).

21. Singh, S.B., Kumar, A. and Iyengar, N.G.R., Progressive Failure of Symmetric LAminates Under In-plane Shear:II-Negative Shear, Structural Engineering and Mechanics, Vol. 6, pp. 757-772(1998).

22. Chang, F.K. and Chang, K.Y., A Progressive Damage Model for Laminated Composites containing Stress Concentrations, J. of Comp. Mat., Vol. 21, 1987 pp.834-855

23. Chang, F.K. and Lessard, L.B., Damage Tolerance of Limanted Composites Containing an Open Hole and Subjected to Compressive Loadings: Part I-Analysis, Journal of Composite Materials, Vol. 25, pp. 2-43(1991).

24. Sleight, D.W., Progressive Failure Analysis Methodology for Laminated Composite Structures, NASA TP-1999-209107 (1999).

25. Shahid, I. and Chang, F.K., An Accumulative Damage Model for Tensile and Shear Failures of Laminated Composite Plates, J. of Comp. Mat., Vol. 29, 1995, pp. 926-981

26. Reddy, Y.S.N. and Reddy, J.N., An Accurate Prediction of Failures in Composite Laminates Using a Layerwise Model, Proc. of Int. Conf. on Comp. Mat. ICCM-9 Madrid, Vol. 3,1993, pp 15-22

27. Kam, T.Y. and Sher, H.F., Non-linear and First Ply Failure Analyses of Laminated Composite Cross Ply Plates, J. of Comp. Mat., Vol. 29, 1995, pp.-463-482

28. Echaabi, J., Trochu, F., Pham, X.T. and Ouellet, M., Theoritical and Experimental Investigation of Failure and Damage Progression of Graphite-Epoxy Composites in Flexural Bending Test, J. of Reinf. Plast. and Comp., Vol. 15, 1996, pp. 740-755

29. Kim, Y., Davalos, J.F. and Barbero, E.J., Progressive Failure Analysis of Laminated Composite Beams, Journal of Composite Materials, Vol. 30, pp. 536-559(1996).

30. Tolson, S. and Zabaras, N., Finite Element Analysis of Progressive Failure in Laminated Composite Plates, Comput. and Struct., Vol.38 1991, pp. 361-376

31. Gummadi, L.N.B. and Palazotto, A.N., Progressive Failure Analysis of Laminated Beams and Arches Undergoing Large Rotations, Mechanics of Composite Materials and Structures, Vol. 6, pp. 69-93(1999).

Chapter 3

Review of Modeling Issues for Woven Fabric Composite Structures

3.1 Background

Textile reinforced composites are fiber reinforced composites whose unit structures are characterized by more than one fiber orientation. Figure 3.1 shows a schematic illustration of the hierarchical nature of textile materials. As illustrated, the fiber is the basic unit from which textile materials are formed. Fibers can be converted into laminated tapes, yarns, or direct formed fabrics. Laminated tapes can also be cut into thin strips called slit tape and used as a type of yarn. Yarns can then be converted into a variety of fabric structures. These fabrics can be classified according to the processes used in creating them. Some relevant ones are given below.

3.1.1 Woven Fabrics

A woven structure is characterized by the orthogonal interlacing of two sets of yarns, called warp and weft warns. The warp yarns are aligned with the direction of the fabric leaving the loom, which is also called the warp direction. The weft yarns run perpendicular to the warp direction, and are sometimes called fill yarns. Weaves may be classified by the pattern of interlacing. The simplest pattern is the plain weave shown in figure 3.2. Another class of woven fabrics are the satin weaves and are shown

in figure 3.3. The satin weave pattern is defined by the number of yarn widths between exchanges. For example, the five harness satin weave shown in figure 3.3 has a 4-over, 1-under pattern. In addition, the exchanges are arranged so as not to connect continuous diagonals.

3.1.2 Braided Fabrics

Braided fabrics are formed by the mutual intertwining, or twisting of yarns about each other. Figure 3.4 shows the interlacing patterns for braided fabrics. In a 2D braid, the designation "$n \times n$" refers to the number of bias yarns between crossover points. Longitudinal or axial yarns can be introduced into the braiding process to create a triaxial braid. The axial yarns are trapped within the crossovers of the bias yarns. Figures 3.4(b), (c), and (d) show three possible patterns for triaxial braids. These figures show the braid patterns with gaps between the yarns for clarity; the actual braid would normally have complete coverage.

3.1.3 Orthogonal Non-woven Composites

Orthogonal 3D materials are fabricated by fixing a series of yarns in one direction, and then inserting planar yarns in the two orthogonal directions around the fixed yarns. Figure 3.5 shows a typical arrangement of fiber bundles that might be obtained in this process.

Among the above mentioned fabric structures, woven fabrics are by far the most used textile system for composite applications. Woven composites provide an excellent opportunity to radically improve the rather poor impact resistance and damage tolerance of traditional laminates. They are able to survive a greater number of matrix and debonding cracks without ultimate failure. Due to random crack orientation, there are no obvious weak directions which would allow extensive crack propagation and result ultimately in failure of the structural part. Also, the local breakage planes of curved yarns, which are perpendicular to the corresponding local longitudinal yarn axes, appear to be spatially dis-oriented. All of this leads to highly dispersed fracture phenomenon in woven composites and, accordingly, allows one to increase tremendously

both impact energy absorption and damage tolerance.

However, formulating a proper mathematical model for mechanical characterization of these materials is a complex task. The intricate geometry of the weave combined with geometrical and material irregularities poses a formidable problem in the modeling and analysis of such composites. The existence of the matrix pockets adds to the complexity of the geometry. In the past, various approaches have been proposed in literatures for developing homogenized (simplified) models and computing the equivalent homogenized material properties for textile composites. This chapter reviews the prominent ones which are relevant to this thesis. The next section explains the concept of a unit cell (or RVE) in the context of woven fabric composite, which is extensively used in the subsequent review sections.

3.2 Unit Cells (or RVEs)

Woven composite is a heterogeneous material. However, very often structural analysis on woven and other textile composite materials is being carried out treating it as a homogeneous material. In this case it is necessary to determine some set of elastic properties which characterize the homogeneous material, mechanically equivalent to the actual material. If there is a representative volume element (RVE) whose mechanical response represents the response of the structural component, it will be sufficient to concentrate on the mechanical characterization of such RVEs. RVE is also synonymously used as unit cell in textile nomenclature. The unit cell (or the RVE) is defined by the requirement that the entire textile can be constructed from spatially translated copies of it, without the use of rotations or reflections. Typical unit cells for a plain weave and satin weave composites are shown in figures 3.2 and 3.3 respectively. Even though, the weave pattern in figure 3.2 looks two dimensional, geometrically they are three dimensional in nature. Figure 3.6 illustrates the actual 3-D geometry of a unit cell. This is the actual shape of the unit cell marked as a dotted block in figure 3.2. The geometry of a woven fabric composite plate can be obtained by simply translating this unit cell in orthogonal directions. Figure 3.7 shows the schematics of an RVE with the matrix pockets removed. This is necessary when one would attempt to analyze the RVE with the finite element method, in which case, both the yarn system and the

resin are modeled separately.

3.3 The Finite Element Approach

Woo and Whicomb[1] used a global/local finite element approach for analysis of textile composite structures. At the global level, an initial global solution was obtained using a coarse global mesh. At the local level, a small portion of the textile composite was modeled with a refined local mesh.

Tan *et al.*[2] presented a unit cell model and a laminate model for predicting engineering elastic constants of 3D orthogonal woven composites. The effect of the geometrical parameters on the elastic constants was studied. The results were compared against experimental values.

Kollegal and Sridharan[3] analyzed the compressive behavior of a unit cell of a plain weave fabric using three-dimensional finite elements. A detailed examination of the internal stresses and strains was carried out. Geometric nonlinearity effects, arising due to the the undulation of the yarns, and the material nonlinearity of the resin were included in the analysis.

Marrey and Sankar[4] developed a finite element based micro-mechanical method for computing the plate stiffness coefficients of a textile composite modeled as a homogeneous plate. The unit cell was modeled using eight-node brick elements. The effect of inhomogeneity within a finite element was accounted by considering appropriate elastic constants in the Gauss integration of the stiffness matrix. Numerical studies were conducted on both plain weave and satin weave composites. Numerical results, such as the plate stiffness coefficients are compared with those derived from the homogenized elastic constants in conjunction with the classical plate theory.

Whicomb and Srirengan[5] conducted a three-dimensional finite element analysis to study the effect of quadrature order, mesh refinement on the failure of plain weave composites. The loading consisted of a nominal uniaxial stress along one of the fiber tow directions. Sensitivity of the predictions to the tow waviness was also studied. Other contributions on three-dimensional finite element models of textile composites can be found in references[6–15].

3.4 Simplified Models for Structural Analysis of Textile Composites

3.4.1 Bridging Model

The bridging model of Ishikawa and Chou[16] specifically focuses on satin woven composites. The RVE of the composite is presented in five 'bricks', as shown in figure 3.8. Brick III represents an interlacing in the structure, while bricks I, II, IV are considered equivalent to [0/90] laminates. The mechanical properties of brick III are calculated using an analogy to the 'curved fibers model', and the properties of the other bricks through a reduced stiffness averaging approach, following the tradition of laminated plate theory. This model has been extended to consider hybrid materials[17] by introducing additional bricks in the RVE which belong to one or the other reinforcement system.

3.4.2 Mosaic Model

Ishikawa and Chou[18] developed the mosaic model (figure 3.9) in which the continuity of fibers in the yarn direction is neglected and the woven lamina is idealized as two layers with discontinuous fibers in orthogonal directions to form a mosaic pattern. In this way the undulation of the fibers is also neglected. Thus the woven lamina is regarded as an assemblage of pieces of asymmetric cross-ply ([0/90]) laminates.

3.4.3 Modified Matrix Method

The modified matrix method by Tarnopolskii *et al*[19] was developed to predict the elastic response of orthogonally cross-lapped XYZ type composites. The concept behind this method is to reduce the complexity of the problem by solving each system of reinforcement, x, y, and z separately. For example, the yarns in the z direction may be combined with the matrix material to create an effective medium in the sense of unidirectional micro-mechanics. The structure is now considered to be composed of x and y oriented fibers embedded in this modified matrix. This process may be repeated

to eliminate an additional system of fibers.

3.4.4 Stiffness Averaging Approach

The stiffness averaging method for textile reinforced composites was initially presented by Kregers and Melbardis[20]. In this method, as a first step, the elastic properties for a unidirectional rod, presenting a yarn and an equal volume fraction of matrix around it, are calculated using any acceptable micro-mechanics approach. From this the local unidirectional compliance matrix is constructed. This compliance matrix is now inverted to get the local stiffness matrix. The stiffness matrix is then transformed to account for the individual yarn orientation. And lastly, the stiffness matrix of all unidirectional elements are volumetrically averaged to obtain the total stiffness matrix for the textile composite. Related information on this approach can be found in references[21,22,23].

3.5 Conclusion

From the above review, the following conclusions seem to be justified.

- The simplified models are based on averaging material properties rather than treating matrix and fiber as discrete components as is done in the finite element method. However, these methods are easy to code and apply to simple textile composite structures. Moreover, depending on the type of reinforcement and the textile composite structure considered, they give very good precision at a reasonably low computational cost.

- The finite element approaches consider detailed geometric descriptions of the reinforcing system for prediction of material properties. Hence, they give detailed information on the stress and strain fields throughout the representative volume element (RVE). However, this involves defining the reinforcement geometry at each point inside the composite, which is a complex task. Moreover, a realistic textile structure might consist of a large number of (the order of hundred) unit cells.

In this case, the finite element analysis may not be possible with conventional computing power due to huge requirements in CPU time and memory.

- For a yarn system with high curvature, in which case quantification of the reinforcement may not be well estimated by the simplified models, the finite element method might be useful. However, from the scanning electron microscope (SEM) results for the woven fabric plates, for which results are reported in this thesis, it appears that the yarn reinforcement was nearly flat.

3.6 References

1. Woo, K. and Whitcomb, J.D., Three-Dimensional Failure Analysis of Plain Weave Composites Using a Global/Local Finite Element Method, *Journal of Composite Materials*, Vol. 30, pp. 984-1003(1996).

2. Tan, P., Tong, L. and Steven, G.P., Modeling Approaches for 3D Orthogonal Woven Composites, *Journal of Reinforced Plastics and Composites*, Vol. 17, pp. 545-577(1998).

3. Kollegal, M.G. and Sridharan, S., Compressive Behavior of Plain Weave Lamina, *Journal of Composite Materials*, Vol. 32, pp. 1334-1355(1998).

4. Marrey, R.V. and Sankar, B.V., A Micro-mechanical Model for Textile Composite Plates, *Journal of Composite Materials*, Vol. 31, pp. 1187-1213 (1997).

5. Whitcomb, J. and Srirengan, K., Effect of Various Approximations on Predicted Progressive Failure in Plain Weave Composites, Composite Structures, Vol. 34, pp. 13-20 (1996)

6. Yoshino, T. and Ohtsuka, T., Inner Stress Analysis of Plain Woven Fiber Reinforced Plastic Laminates, Bulletin of the JASME, Vol. 25, pp. 485-492((1982).

7. Naik, N.K. and Ganesh, V.K., Prediction of on-axes Elastic Properties of Plain Weave Fabric Composites, Composites Science and Technology, Vol. 45, pp. 135-152(1992).

8. Lene, F. and Paumelle, P., Micro-mechanics of Damage in Woven Fabric Composites, Composite Material Technology PD-vol. 45, pp. 97-105(1992).

9. Lei, C. and Ko, F.K., Finite Element Analysis of 3-D Braided Composites, Proceedings of the ASME Winter Annual Meeting, ASME(1988).

10. Lei, C., Wang, A.S. and Ko, F.K., A Finite Cell Model for 3-D Cell Model, Proceedings of the ASME Winter Annual Meeting, ASME(1988).

11. Carter, W.C., Cox, B.N., Dadkhah, M.S. and Morris, W.L., An Engineering Model of Composites Based on Micro-Mechanics, Acta Metallurgica (1995).

12. Whitcomb, J.D., Three Dimensional Stress Analysis of Plain Weave Composites, 3rd Symposium on Composite Materials: Fatigue and Fracture, Philadelphia, PA., American Society of Testing Materials(1989).

13. Dasgupta, A., Bhandarkar, S., Pecht, M. and Barker,D., Thermo-elastic properties of woven fabric composites using Homogenization Techniques, Journal of Composites Technology and Research, Vol. 6, pp. 593-602(1992).

14. Blackketter, D.M., Walrath, D.E. and Hansen, A.C., Modeling Damage in a Plain Weave Fabric-Reinforced Composite Material, J. of Composite Technology and Research, Vol. 15, pp.136-142 (1993).

15. Glaesgen, E.H., pastore, C.M., Griffin, O.H. and Birger, A.B., Geometrical and Finite Element Modeling of Textile Composites, Composites Part B, Vol. 27B, pp. 43-50(1996).

16. Ishikawa, T. and Chou T.W., Stiffness and Strength Behavior of Woven Fabric Composites, J. of Materials Science, Vol. 17, pp. 3211-32220 (1982)

17. Ishikawa, T. and Chou T.W., Elastic Behavior of Woven Hybrid Composites, J. of Comp. Mat., Vol. 16, pp. 2-19 (1982)

18. Ishikawa, T. and Chou T.W., One-Dimensional Micro-mechanical Analysis of Woven Fabric Composites, AIAA Journal, Vol. 21, pp. 1714-1721 (1983)

19. Tarnopol'skii, Y.M., Pplyakov, V.A. and Zhigun, I.G., Composite Materials Reinforced with a System of Three Straight, Mutually Orthogonal Fibers, 1: Calculation of Elastic Characteristics, Polymer Mechanics, Vol. 5, pp. 853-860(1973).

20. Kregers, A.F. and Melbardis, Y.G., Determination of the Deformability of Three-Dimensionally Reinforced Composites by the Stiffness Averaging Method, Polymer Mechanics, Vol. 14, pp. 3-8(1979).

21. Kregers, A.F. and Teters, G.A., Use of Averaging Methods to Determine the Viscoelastic Properties of Spatially Reinforced Composites, Polymer Mechanics, Vol. 15, 617-624(1979).

22. Kregers, A.F. and Teters, G.A., Determination of the Elastoplastic Properties of Spatially Reinforced Composites by the Stiffness Averaging Method, Polymer Mechanics, Vol. 16, pp. 30-36(1981).

23. Roze, A.V. and Zhigun, I.G., Three-Dimensionally Reinforced Fabric Materials 1: Calculation Model, Polymer Mechanics, Vol. 6, pp. 311-318(1970).

24. Bogdanovich, A.E. and Pastore, C.M., Mechanics of Textile and Laminated Composites, Chapman and Hall, London(1996).

25. Cox, B.N. and Flanagan, G., Handbook of Analytical Methods for Textile Composites, NASA CR 4750, 1997.

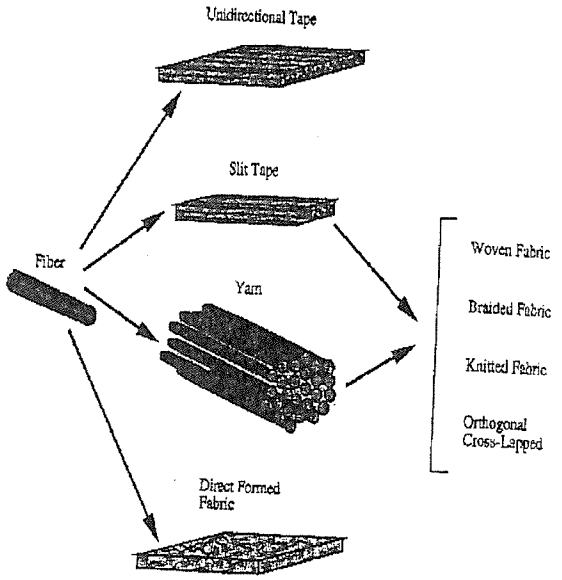

Figure 3.1: Schematic Illustration of the Hierarchy of Fibers, Yarns, and Fabrics in Textile Processes (after Bogdanovich[24])

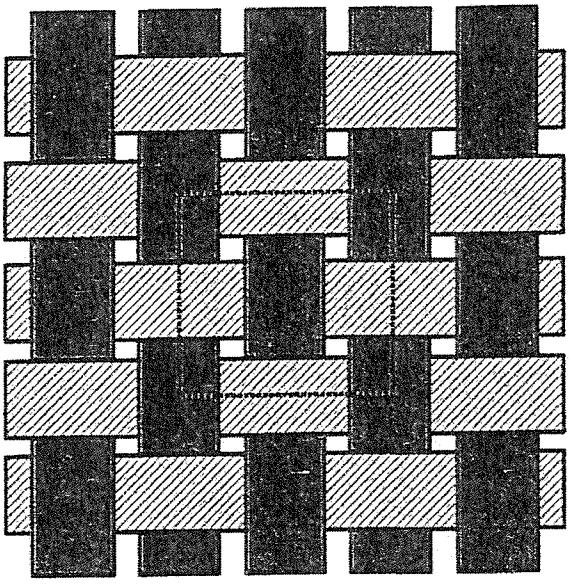

Figure 3.2: Yarn Pattern in a Plain Weave Perform (Unit-Cell Boundary in Dotted Lines) (after reference[25])

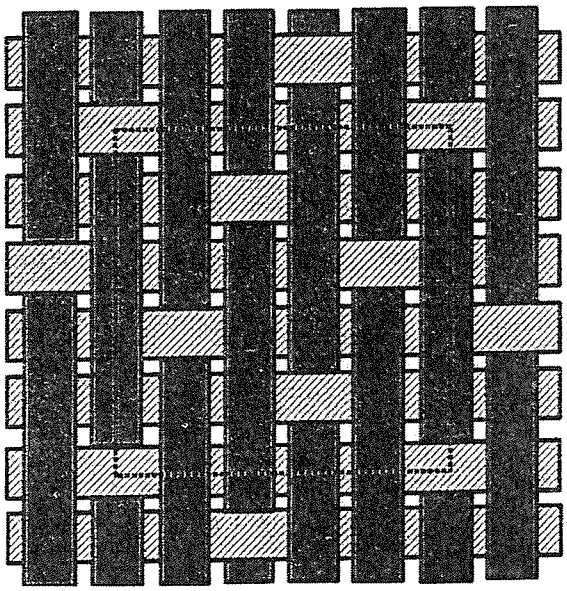

Figure 3.3: Yarn Pattern in a 5-Harness Satin Weave Perform (Unit-Cell Boundary in Dotted Lines) (after reference[25])

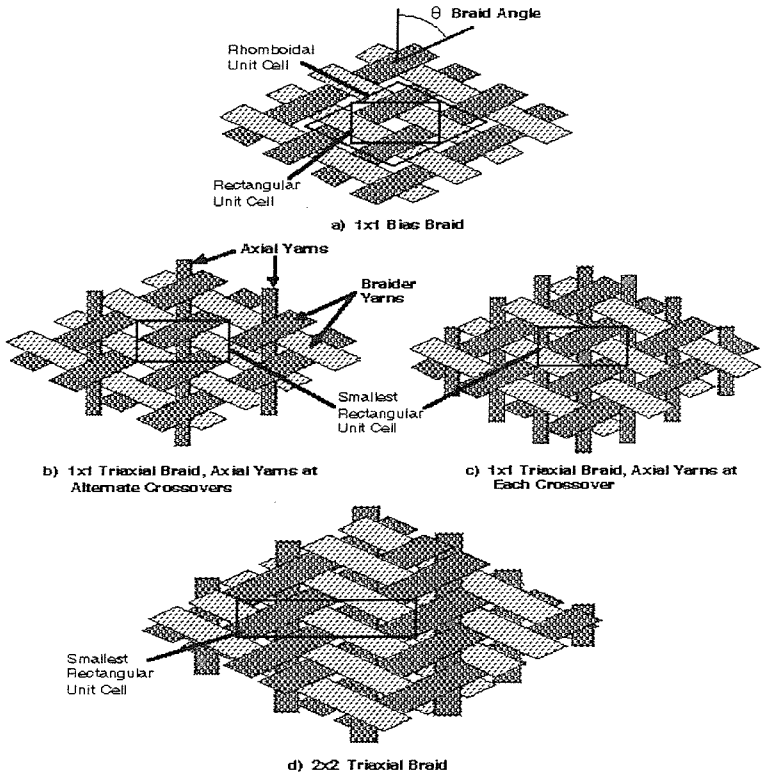

Figure 3.4: Some Common 2D Braid Patterns (after reference[25])

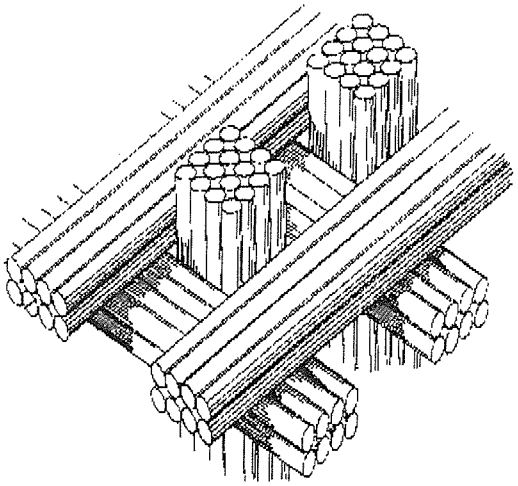

Figure 3.5: 3D Orthogonal Composite (after reference[25])

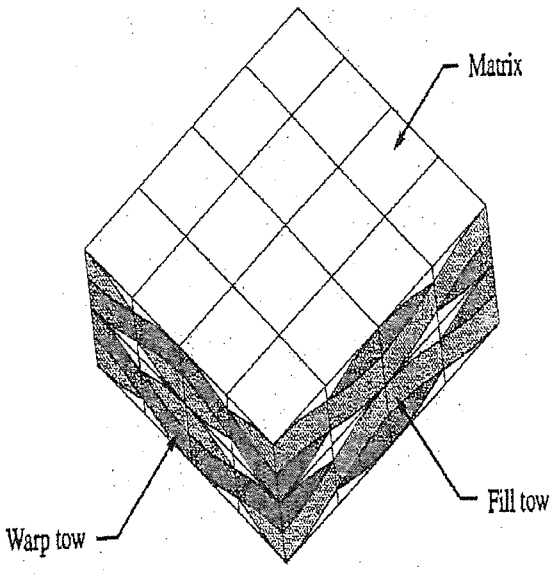

Figure 3.6: Schematics of Plain Weave Composite-Full RVE (Unit Cell)

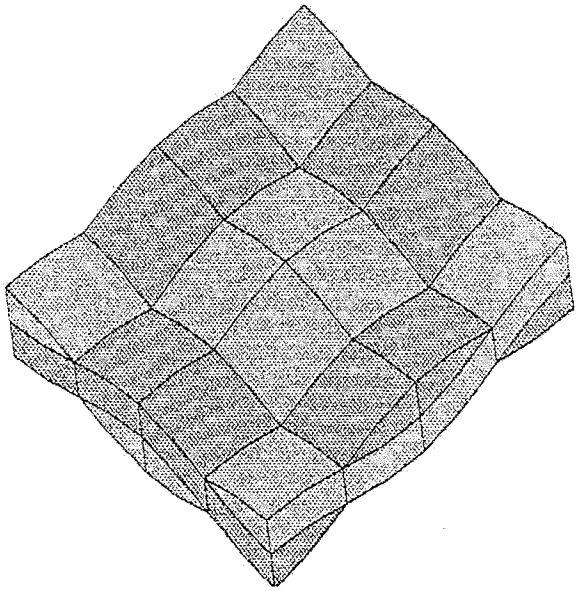

Figure 3.7: Schematics of Plain Weave Composite-Full RVE (Unit Cell) with Matrix Pockets Removed

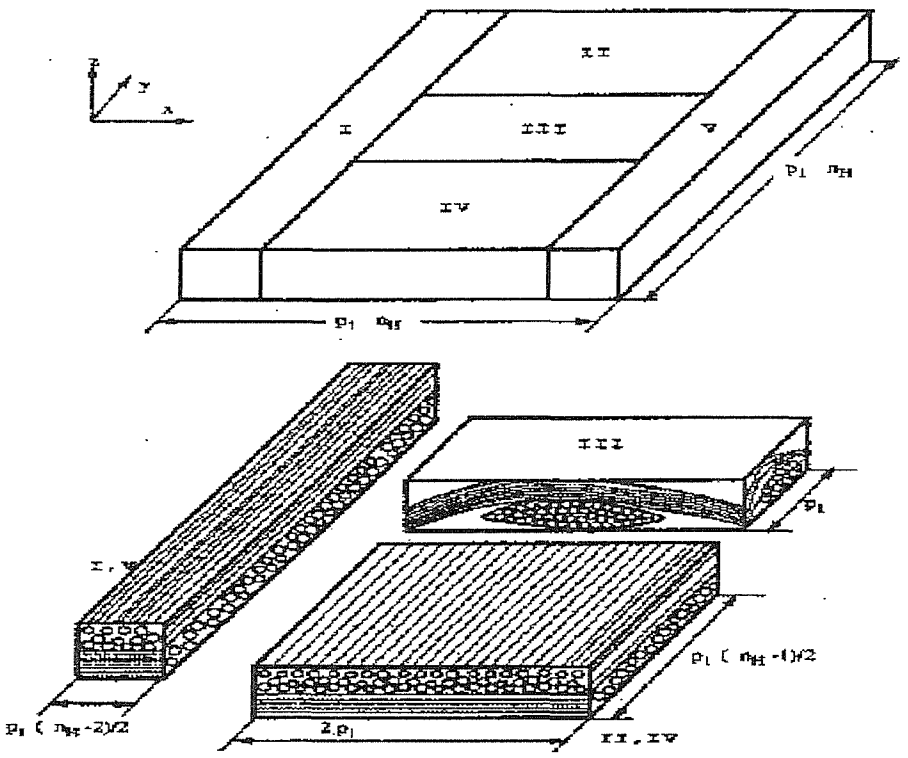

Figure 3.8: Schematic Illustration of RVE Representation of a Satin Weave for the Bridging Model of Ishikawa and Chou[16] (after Bogdanovich[24])

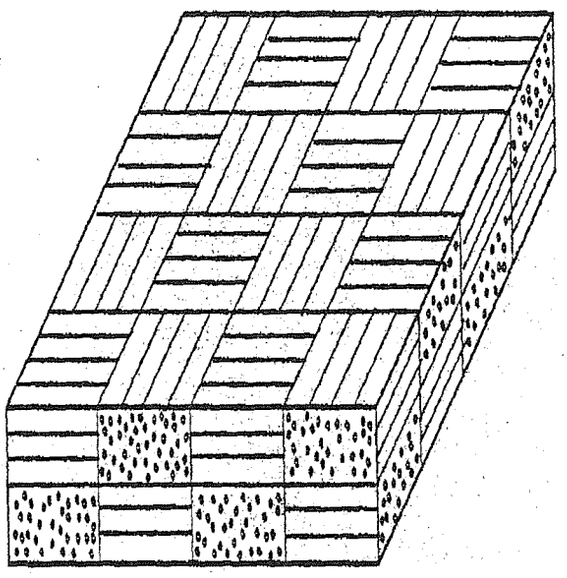

Figure 3.9: Ishikawa's Mosaic Model

Chapter 4

Progressive Failure Analysis of Uni-Directional Composite Structures

From the review made in chapter 2, it was clear that damage modeling of composite structures, with (1) geometric nonlinearity, (2) material nonlinearity because of local damage, and (3) presence of bi-axial stresses, has not been investigated. The objective of this chapter is to develop a progressive failure analysis methodology for predicting the failure of uni-directional laminated composite structures under geometrically nonlinear deformations. The method is used to study the non-linear behavior, first ply failure and ultimate collapse of laminated composite plates with clamped edges, subjected to transverse pressure. The chapter is organized as follows. In the next section, major steps for conducting a progressive failure analysis using the finite element method, are discussed. Section 2 outlines the nonlinear analysis procedure that has been adopted in this research. In section 3, the various failure criteria to be used in the progressive failure analysis are presented. Section 4 reviews some of the existing material property degradation models and suggests a suitable one for use in the progressive failure analysis. In section 5, the equilibrium aspects of the nonlinear solution procedure are discussed. Section 6 discusses the numerical modeling aspects of progressive failure analysis using the finite element program ABAQUS. In section 7, the experimental procedure which had been conducted on the composite plates, is briefly

described. In section 8 numerical results are presented. Discussions are presented in section 9 and conclusions are given in section 10.

4.1 Overview of Progressive Failure

A typical methodology for a progressive failure analysis is illustrated in figure 4.1. At each load step, a geometrically non-linear analysis is carried out until a converged solution is obtained. From this solution, stresses and strains at the Gauss integration points are calculated. If failure is detected in an element, as indicated by a failure criterion, the element properties are changed according to a particular degradation model. Since in this process the material properties for some or all elements might have changed, the displacement field corresponding to this load step does not correspond to an equilibrium state. Therefore, equilibrium of the structure is re-established using the modified material properties for the failed elements. Then the next load step is applied on the structure and the above process is repeated. Progressive failure analysis is continued until the structure fails.

Therefore, typical progressive failure analysis methods involve four key features. First, a nonlinear analysis capability is used to establish equilibrium. Second, an accurate stress recovery procedure is needed in order to establish the local element stress state. Third, material degradation or damage models are needed in order to propagate the failure and establish new estimates for the local material properties. Finally, a procedure to re-establish equilibrium after modifying local element properties is needed.

4.2 Nonlinear Analysis

After local failures at an element integration point, the element stiffness, and the element's contribution to the global stiffness changes. Therefore the tangent stiffness matrix $[K_T]$ is a function of the material properties and the unknown displacement D. In this progressive failure analysis, a nonlinear analysis is performed until a converged

solution is obtained for a constant set of material properties. The nonlinear analysis involves solving the linearized finite element equations for the k^{th} iteration

$$\begin{aligned} [K_T]^{(k)}\,\delta D &= R^{(k)} \\ D^{(k+1)} &= D^{(k)} + \delta D \end{aligned} \tag{4.1}$$

Where $R^{(k)}$ is the force residual for the iteration. Both $[K_T]^{(k)}$ and $R^{(k)}$ are functions of the displacements $D^{(k)}$. Solution of equation (4.1) involves an iteration process where the k^{th} step requires computing the displacement increment δD for the $k+1$ load step using the k^{th} tangent stiffness matrix. The displacement vector D in the k^{th} load step is then updated using δD. With this new displacement, both the force imbalance vector R and the tangent stiffness matrix $[K_T]$ are updated, and the process is continued for the next iteration. If R is zero, then the structure is in perfect equilibrium. In a non-linear problem, this is usually not the case. Hence R is compared against a tolerance value. If R is less than the current tolerance value, the structure is considered to be in equilibrium and D is a valid equilibrium configuration. Therefore the non-linear analysis continues until the tolerance criteria are satisfied.

In the progressive failure analysis, at a given load step, this non-linear solution method is used to calculate the element stresses. Failure criteria are then used to assess whether any failures have occurred during this load increment. If no failures are detected, then the applied load is increased, and the analysis continues. If failures are detected in an element, it's stiffness is reduced using the appropriate material property degradation models. These models are discussed in the subsequent sections of this chapter.

In the present progressive failure analysis methodology, this nonlinear analysis procedure is implemented using the finite element program ABAQUS. Appendix A outlines the advanced computational capabilities (including the nonlinear features) available in ABAQUS. In addition, the strain measure used here is the approximate Koiter-Sanders theory, which includes both large rotation and large strain. The mathematical expressions of this theory can be found in reference[1]. The Newton-Raphson method is used to solve the set of equations at any load step. To achieve a good convergence in the non-linear analysis a force and moment residual convergence of 0.5% and displacement

correction convergence of 1 % were used.

4.3 Failure Analysis

The ultimate failure in a composite structure occurs as a result of accumulation of local material failures. Initial failure in a composite material can be predicted by application of a failure criterion. Prediction of ultimate failure requires an understanding of failure modes and failure propagation.

Laminated composites may fail by fiber breakage, matrix cracking, fiber-matrix shear or by delamination of layers. The mode of failure depends upon the loading, stacking sequence, and specimen geometry. or curing or out-of-plane effects.

Failure criteria are needed to predict the macroscopic failures in a composite material. In a progressive failure analysis, if a failure criterion in an element is exceeded, the material properties corresponding to that particular mode of failure are reduced depending on the material degradation model.

Failure criteria for composite materials are often classified into two groups: namely, non-interactive failure criteria and interactive failure criteria.

4.3.1 Non-Interactive Failure Criteria

In a non-interactive failure criterion, there is no interaction between the stress or strain components. These failure criteria are simple to apply and tell the mode of failure. However, they neglect the interaction of stresses in the failure mechanism. The maximum stress and maximum strain criteria belong to this category. The failure surfaces for these criteria are rectangular in stress and strain space, respectively.

4.3.2 Interactive Failure Criteria

Interactive failure criteria include stress interactions in the failure mechanism, but they do not tell the mode of failure. The Tsai-Wu and Tsai-Hill failure criteria belong to this category. The failure surfaces in these cases may not be rectangle when plotted

in the stress or strain space. Implementation of these failure criteria can be found in references[2-5].

Most of the failure criteria for composite materials are unable to predict all the failure modes of a composite materials. Also, not all are computationally efficient for implementation into finite element programs. The following subsection discusses the failure criteria which have been used in the present progressive failure analysis procedure.

4.3.3 Mathematical Representation of Failure Criteria

Most failure criteria for composite materials can be expressed in terms of a single tensor polynomial failure criterion such as that proposed by Tsai. Failure is assumed to occur if the following condition is satisfied[6].

$$F_i\sigma_i + F_{ij}\sigma_i\sigma_j + F_{ijk}\sigma_i\sigma_j\sigma_k + ... \geq 1 \tag{4.2}$$

The two dimensional form of the above polynomial is expressed as:

$$F_1\sigma_1 + F_2\sigma_2 + 2F_{12}\sigma_1\sigma_2 + F_{11}\sigma_1^2 + F_{22}\sigma_2^2 + F_{66}\sigma_6^2 \geq 1 \tag{4.3}$$

Various forms of this general representation are given below. In the expressions, the notations σ_1, σ_2 and σ_6 ($\sigma_6 = \sigma_{12}$) are the in-plane stresses in the material coordinate directions, X_T, X_C, Y_T, Y_C and SC are the strength parameters as defined in table(4.1).

- Tsai-Wu Criterion:

The failure indices for the Tsai-Wu criterion are

$$\begin{gathered} F_1 = \frac{1}{X_T} - \frac{1}{X_C},\ F_2 = \frac{1}{Y_T} - \frac{1}{Y_C},\ F_{12} = -\frac{1}{2}\sqrt{F_{11}F_{22}}, \\ F_{11} = \frac{1}{X_T X_C},\ F_{22} = \frac{1}{Y_T Y_C},\ F_{66} = \frac{1}{SC^2} \end{gathered} \tag{4.4}$$

- Maximum Stress Criterion:

The failure indices for Maximum Stress criterion are

$$F_1 = \frac{1}{X_T} - \frac{1}{X_C},\ F_2 = \frac{1}{Y_T} - \frac{1}{Y_C},\ F_{12} = -\frac{F_1 F_2}{2},$$
$$F_{11} = \frac{1}{X_T X_C},\ F_{22} = \frac{1}{Y_T Y_C},\ F_{66} = \frac{1}{SC^2} \tag{4.5}$$

- Hoffmann Criterion:

The failure indices for Hofffmann criterion are

$$F_1 = \frac{1}{X_T} - \frac{1}{X_C},\ F_2 = \frac{1}{Y_T} - \frac{1}{Y_C},\ F_{12} = -\frac{1}{2X_T X_C},$$
$$F_{11} = \frac{1}{X_T X_C},\ F_{22} = \frac{1}{Y_T Y_C},\ F_{66} = \frac{1}{SC^2} \tag{4.6}$$

- Tsai-Hill Criterion:

The failure indices for Tsai-Hill criterion are

$$F_1 = 0,\ F_2 = 0,\ F_{12} = -\frac{1}{2X^2},\ F_{11} = \frac{1}{X^2} F_{22} = \frac{1}{Y^2} \tag{4.7}$$

where

If $\sigma_1 > 0,\ X = X_T$; otherwise, $X = X_C$. If $\sigma_2 > 0,\ Y = Y_T$; otherwise, $Y = Y_C$.

- Azzi-Tsai-Hill Criterion:

The Azzi-Tsai-Hill failure theory is the same as the Tsai-Hill theory, except that the absolute value of the cross product term is taken as

$$F_1\sigma_1 + F_2\sigma_2 + 2F_{12} \mid \sigma_1\sigma_2 \mid + F_{11}\sigma_1^2 + F_{22}\sigma_2^2 + F_{66}\sigma_6^2 \geq 1 \tag{4.8}$$

The F_i coefficients are the same as those of the Tsai-Hill criterion.

- Hashin's Criterion

The two dimensional Hashin's criterion[7] is expressed in a different form as follows:

Fiber failure

$$\left(\frac{\sigma_1}{X_T}\right)^2 + \frac{\sigma_{12}^2}{SC^2} = 1, \qquad \sigma_1 > 0 \tag{4.9}$$

$$\sigma_1 = -X_C, \qquad \sigma_1 < 0 \tag{4.10}$$

Matrix Failure

$$\left(\frac{\sigma_2}{Y_T}\right)^2 + \frac{\sigma_{12}^2}{SC^2} = 1, \qquad \sigma_1 > 0 \tag{4.11}$$

$$\frac{1}{Y_C}\left[\left(\frac{Y_C}{2\,SC}\right)^2 - 1\right]\sigma_2 + \frac{\sigma_2^2}{4\,SC^2} + \frac{\sigma_{12}^2}{SC^2} = 1, \qquad \sigma_1 < 0 \tag{4.12}$$

4.4 Material Property Degradation

If failure is detected in a particular element of the composite material, the properties of that element must be adjusted according to a material property degradation model. A survey of some post-failure theories for laminated composites is presented in reference[8]. Most of these material degradation models belong to one of the three general categories: instantaneous unloading, gradual unloading, or constant stress at ply failure. Figure 4.2 illustrates these three categories.

For the instantaneous unloading case, the stiffness and strength of a failed ply are reduced to zero, although the ply is physically present. This approach may lead to an underestimation of the laminate strength, because it does not recognize that ply-failure is localized, and that the remaining stiffness of a failed ply is not necessarily zero. This approach therefore has limited applicability.

In the constant stress category, it is assumed that the failed layer can carry no further load in the failed direction. For example, if a lamina fails in the resin cracking mode, the value of the Young's modulus in the direction perpendicular to the fiber direction, becomes zero. Implementation of this property degradation model can be found in reference[9].

In the gradual unloading model, it is assumed that after failure in a lamina, the material elastic properties are gradually reduced depending upon the extent of damage within the lamina. Implementation of this property degradation model can be found in references[10–12].

Chang and Chang[11] used a stiffness reduction model in which after matrix failure(due to either tension or compression), the ply in the damaged region was assumed to lose all its transverse strength. For fiber failure, stiffness of the failed layer was assumed to depend upon the extend of the damage, which was determined using a micro-mechanics approach. Chang and Lessard[13] used a similar approach, but fiber breakage was not included in the degradation model. Sahid and Chang[14] used the crack density as a parameter to characterize the ply stiffness, which is complicated for macro-numerical modeling.

In addition to the above methods of material property degradation, another method is the residual property method, in which continuum damage models are used to predict progressive damage and the stiffness drop in the laminate[15]. Damage accumulation during loading is predicted by damage evolution laws, which are too complicated and therefore will not be discussed here.

This brief review indicates that some methods, such as the ply-discount method, underestimate the laminate strength, while others are too complicated to implement, without any significant improvement in the prediction capability of the failed ply properties. In this research, a simple, yet effective, stiffness reduction model(similar to reference[11] and reference[16]) based on the experimental observations, is proposed.

For matrix cracking at a material integration point, the transverse modulus E_y, and Poisson's ratio ν_{yx} are reduced to zero. However the longitudinal modulus E_x and the shear modulus G_{xy} remain unchanged. When fiber-matrix shearing is predicted at a material point, the transverse modulus G_{xy} and the Poisson's ratio ν_{yx} are reduced to zero. However the longitudinal modulus E_x and the transverse modulus E_y remain unchanged. If fiber failure is detected, then the material is deemed to have lost its stiffness at the integration point.

Hashin's criterion as discussed in the previous section, directly gives the mode of failure. For the other interactive polynomial criteria, if failure occurs the following

expressions are used to determine the failure mode:

$$H_1 = F_1\sigma_1 + F_{11}\sigma_1^2$$

$$H_2 = F_2\sigma_2 + F_{22}\sigma_2^2$$

$$H_6 = F_{66}\sigma_6^2 \tag{4.13}$$

The largest H_i term is selected as the dominant failure mode and the corresponding modulus is reduced to zero. Thus H_1 corresponds to fiber failure, H_2 corresponds to matrix crack and H_6 corresponds to fiber matrix shearing failure.

The contribution of each stress component towards the failure index(H_i) is computed and the stress component which contributes the maximum is identified. Depending on the largest H_i term the failure mode is determined and the corresponding material properties are degraded as mentioned above.

4.5 Re-establishment of Equilibrium

In a progressive failure analysis, once failures are detected in a ply, the corresponding material properties are degraded. However, the structure may not be in equilibrium with these degraded material properties and the present deformation configuration. Therefore, it is necessary to carry out some more iterations to establish equilibrium. However, if the load steps chosen in the non-linear analysis are sufficiently small, such a procedure may not be needed.

In the present research, equilibrium is re-established in the non-linear analysis procedure, in the sense that the failure index is kept within a tolerance of 0.01. The first ply failure load reported here is the lowest pressure at which the failure index($F_i\sigma_i + F_{ij}\sigma_i\sigma_j$) first reached a value of unity at any material integration point. At some point in the analysis a dramatic change in slope of the load deflection graph indicates inability to support additional load. This location is identified as the failure load.

4.6 Numerical Modeling Using ABAQUS

The classical (e.g. Kirchoff-Love) shell theory is based on an assumption of infinite rigidity in the transverse direction (i.e. neglect of transverse strains), and hence is not used in the present analysis. The first order theory considering shear deformation, which is by far the most efficient theory(i.e., increased accuracy without an increase in computational effort) is used in this research. The finite element formulation aspects of a shell element are discussed extensively elsewhere[12,17,18,19], and therefore not covered here.

The progressive failure analysis methodology uses the C^0 four node shell element S4R of the ABAQUS element library based on first order shear deformation theory, due to its better performance in large deformation analysis. The element has six degrees of freedom(three displacement and three rotation components). To avoid shear locking[6] the element uses reduced (lower order) integration to form the element stiffness. The element has one in-plane integration point and three through-the-thickness integration points for each layer. Gauss quadrature is used to calculate the shell behavior.

Since the damage initiation was observed along all the edges of the specimen, a uniform mesh size of 20×20(400 elements) was used. A standard user subroutine USDFLD in ABAQUS was written, which allows the user to define material properties as functions of the field variables at a material point, which instead can be function of any of the available material point quantities. The material properties of the laminated plate were defined to be dependent upon three field variables. The first field variable was the contribution of σ_1 towards the failure index (H_1). The second and third field variables were the contributions of σ_2 and σ_{12} respectively (H_2, H_6) to the failure index.

The computing work was done on a single node of the IBM SP2 parallel computer running under the AIX 4.1.4 operating system. It has a 66Mhz Power2 processor, 256 Mbyte RAM and 32 Kb instruction cache. On average the CPU time taken for one complete analysis with one failure criterion was about 50 hours .

4.7 Experimental Background

The experiments for the composite plates had been conducted by Moy *et al.* (see reference[20]). Thirty four fiber reinforced composite plates were tested to failure to investigate the effects of material composition, method of manufacture and panel aspect ratio on strength and stiffness under transverse pressure loading. The panels relevant to this research were of an E-Glass/polyester type. The weight density of the reinforcement was 620 g/mm^2, the matrix was isophthalic polyester, Scott Bader Crystic-489. The panels were made up of five unidirectional plies, each with about 90% of the fibers concentrated in the fiber direction. The fiber weight fraction was 0.415. The material properties for this lay-up, taken from ref[21], are shown in table 4.1. The plate specifications are given in table 4.2. All the test specimens reported here were fabricated using the hand lay up method. In this the dry reinforcement was placed on a flat mould and the appropriate quantity of resin was applied. The wet composite was then rolled by hand to distribute the resin evenly. Another layer of reinforcement was then laid on the top and more catalyzed resin was poured and rolled over the reinforcement. This sequence was then continued until the desired thickness was reached. The layered structure was then left to harden and cure under normal laboratory conditions. The test rig (figure 4.3) consists of identical upper and lower steel frames. The specimen is sandwiched between the frames which are then bolted tightly together by two lines of bolts all round. The heavy steel frames give in-plane and rotational restraints to the edges of the panel to simulate fixed boundary conditions. Water pressure is provided through a synthetic bag placed between the specimen and the lower steel frame (figure 4.4). During a test the bag is filled with water from a rigid pressure vessel. Pressure is increased by introducing compressed air into the top of the pressure vessel and is controlled manually and measured by a pressure transducer and a mechanical pressure gauge. Strain gauges and displacement transducers were mounted on all of the panels. Some selected panels were heavily strain gauged. The test procedure was the same for all the panels. Initial readings were taken on all instruments and pressure was then increased in small increments. At each increment pressure and deformations were allowed to settle down before readings were taken. Pressure load was increased continuously up to failure.

The geometry and coordinate system used for the present analysis is shown in figure 4.5. All the plates considered here were clamped on all the edges, and were loaded by water pressure applied to the bottom surface. Each specimen was instrumented with displacement potentiometers placed at five locations on the surface. Although deformation data was available at more than one point, only the central deflection is compared with the analytical result.

The three panels considered here, referred to as A, B, and C, had aspect ratios of 1, 1.5 and 2 respectively. Typical load-deflection curves are given in figure 4.6. The progression of failure for the panels was observed visually. A typical sequence of damage progression is given below. Initial damage was due to resin cracking along the edges. This was characterized by noise emitted during loading. When cracking started the resin lost its sheen and appeared dull. These cracks started from the loaded face where the edge was in tension. Up to aspect ratio 1.5, there were cracks parallel to the edges and also at 45° to the edges. At aspect ratio 2 there were cracks only parallel to the long edges. At higher load there was visible damage with considerable resin cracking. Failure occurred at the edges of the panels and usually along a long side. There was little warning of failure in terms of rapid increases in deflection, but it was obvious when failure was imminent. At failure the break-up of fibers along edges was accompanied by very loud noises, different from the resin cracking noises. Figure 4.7 shows a typical failure pattern at final collapse for plate C of aspect ratio 2.

4.8 Numerical Results

Figure 4.8 shows the load-central deflection graph for plate A. As can be seen the progressive failure results (using Tsai-Wu) agree very well with the test results. The load-central deflection data using other failure criteria are also available. However they are almost identical to the Tsai-Wu curve and are not presented to maintain clarity.

Summaries of the first ply failure loads, dominant failure mode type and the failure location, using different failure criteria are presented in tables(4.3 to 4.5). Table 4.3 summarizes the first ply failure results for plate A, having aspect ratio 1. Pressure at which the failure index first reached one, according to different failure criteria, is

listed and compared with the test pressure at which first audible crack was heard. The numerical procedure could provide the exact location, where failure initiated, i.e. top, middle or bottom of a ply. Since bending dominated in the initial stage of loading, the stress state was high in the bottom of a ply, at which the ply failed first. Due to the low transverse lamina strength, first ply failure was invariably due to matrix crack. For increased aspect ratio ($\frac{a}{b}$ in figure 4.5), the bending stresses being higher along the long edges, the initial failure was even less for plates B and C, as can be seen in tables 4.4 and 4.5. However the central deflection at first ply pressure was higher as the aspect ratio increased.

Summaries of the ultimate failure loads, dominant failure mode type and the failure deflection, using different failure criteria are presented in tables(4.6 to 4.8). Table 4.6 summarizes the ultimate collapse load results for plate A. The failure load corresponds to the pressure at which there was rapid large increase in deflection with a small increase in pressure. The dominant failure mode presented in the table is that which was responsible for the collapse of the structure. For plate A failure was due to fiber-breakage, which indicates that the in-plane normal stress σ_1 was responsible. However for increased aspect ratios, as can be seen in tables 4.7 and 4.8, the dominant failure mode was fiber-matrix shear, which means the bond between the matrix and the fiber was lost. This indicates that at higher aspect ratios the in-plane shear stress caused the final collapse of the structure. Additional discussion on the first ply failure, ultimate failure and damage propagation is given in the next section.

Internal damage and failure modes predicted by the model for all the plates are presented graphically in figures 4.9 to 4.24. In these figures a solid sphere indicates a matrix crack at that location, a cube indicates fiber-matrix shear, and a triangular prism indicates fiber breakage.

- Plate A

The first ply failure was due to matrix cracking. Almost all the failure criteria predicted the same ply and same location for failure initiation.The predicted first ply failure pressure does not agree well with the test pressure at first audible crack. This may be due to the fact that the background noise in the test laboratory, made it difficult to identify when the crack started[20]. The first crack started almost at the middle of

the edge(Y=15). Immediately after, cracks also penetrated through the depth from the bottom surface. As shown in figures 4.9 to 4.14 at 0.1 MPa cracks started on top surface along the edge(y=45mm). With further increase in pressure cracks advanced towards the center. At 0.30 MPa about 67 percent of the material points failed by matrix cracking. Just before failure about 75 percent of the material points had failed by matrix cracking and about 8 percent of the material points had failed by fiber breakage. Fiber breakage first began at a pressure of 0.15 MPa in the second ply. With further increase in pressure it propagated to the fourth ply. Gradually it was advancing towards the center, although the damaged region due to fiber breakage was narrow(width of 90mm) and ran parallel to the x axis. In each ply the damage was symmetric. The damage in the bottom two plies was always more than that of the upper two plies. Tsai-Hill criterion predicts the failure pressure most accurately, with plate failure mainly due to fiber failure.

- Plate B

The first ply failure was again due to matrix cracking. Almost all the failure criteria predicted the same ply and same location for failure initiation.The inaccuracy in predicting first ply failure pressure may be attributed to the same reason as mentioned for plate A. After the first crack, cracks penetrated through the depth from the bottom surface. With further increase in pressure cracks advanced towards the center and towards the top surface. As shown in figures 4.15 to 4.19 at 0.30 MPa about 67 percent of the material points failed by matrix cracking. For plate B fiber Matrix shearing first began in the second ply at a pressure of about 0.10 MPa. With further increase in pressure it propagated to the fourth ply, although damage in the second ply was always higher. Gradually it advanced towards the center, at a rate greater than that of plate A. The damaged region due to fiber-matrix shear was also more than that of plate A. Just before failure more than 75 percent of the material points had failed by matrix cracking and about 15 percent of the material points had failed by fiber matrix shear. Tsai-Wu criterion predicts the failure pressure most accurately, although it over estimates the failure deflection. The plate failure was mainly due fiber matrix shear.

- Plate C

The first ply failure was invariably due to matrix crack. The propagation of damage for plate C was similar to that of plate B, with more damage occurring at an early stage. As shown in figures 4.20 to 4.24 the damage zone due to fiber-matrix shear was wider and more in the second and fourth plies than that of the other two plates. Almost all the failure criteria predicted the same ply and same location for failure initiation. Tsai-Hill criterion predicts the failure pressure most accurately. The plate failure was mainly due fiber matrix shear.

4.9 Discussion

- Choice of Failure Criterion

There was little difference in prediction of first ply failure load from all the failure criteria, which indicates that at ply level it is immaterial which failure criterion is used. This can be explained as follows.

Referring to eqs. 4.4 to 4.8 and table 4.1, it can be seen that the expression for the coefficient F_{22} is the same for most of the failure criteria and the expression for the coefficient F_2 is the same for Tsai-Wu's, maximum-stress and Hoffmann's criteria, which makes the contribution of σ_2 towards failure (H_2) almost equal by most of the failure criteria. This means that most of the failure criteria predict the same load for matrix failure. The coefficient F_2 is about 40 times larger than F_1 and F_{22} is about 80 times larger than F_{11}, although for Tsai-Hill criterion, F_1 and F_2 are zero. In the very initial stage of loading, the in-plane stresses in the first ply are of the same order of magnitude. Along the long edges, F_2 and F_{22} are much higher than the other coefficients. Consequently, the contribution of σ_2 ($H_2 = F_2\sigma_2 + F_{22}\sigma_2^2$) towards failure was much higher and the contribution of the other two in-plane stresses towards failure was negligible. This means that with the transverse lamina strength being much less than the corresponding longitudinal ones, and the transverse lamina stresses in the initial loading stage being of the same order of magnitude as the other in-plane stresses, it is the transverse stress σ_2(and hence H_2), which determines the onset of initial failure. H_2 is almost the same for most of the failure criteria. Hence they predicted nearly same first-ply pressure.

The load deflection curve due to all the failure criteria was almost the same for each of the panels. The ultimate load and ultimate deflection were better predicted by the Tsai-Hill criterion for all the panels in contrast to Tsai-Wu or the maximum stress criterion predicting better for beam bending cases as reported in ref[16,22]. The reason for this may be as follows. The maximum stress criterion does not take stress interaction into account(i.e. rectangle in two-dimensional stress space). Furthermore, in beam bending cases, the state of stress is not strongly bi-axial in nature, and therefore could predict failure load more accurately. Plates, however curve in two directions. Stresses along the two in-plane axes could both become significant. This implies that coupling or interaction effects would become significant. Although Tsai-Wu and Tsai-Hill include stress interaction(both are ellipses), Tsai-Wu is more close towards the maximum stress criterion. Therefore the failure pressure for the present plate bending case was better predicted by Tsai-Hill criterion.

- Load Increment

The progressive(ultimate) failure loads in the non-linear failure analysis were found to be sensitive to both load increment size and finite element mesh size. The first ply failure load and ultimate load were strongly dependent on the load increment size chosen. In a test the load and displacement increase continuously, but in a numerical simulation discrete load increments are used for failure prediction. A large load step will not represent damage progression well, and a very small load step will require significant computational effort. In the present analysis a load increment size of approximately 0.2 percent of the first ply failure load (or about thirty thousand load steps) and a mesh size of 20 by 20 (or 400 elements) was chosen, after conducting a convergence study for a fixed failure criterion.

- Damage in the Panels

The initial bending at the edges of the panels caused cracks in the resin, which ran along, particularly, the long edges of the loaded surface of the panel. Cracks propagated from bottom to top and advanced towards the center. Fiber failure in the form of fiber-matrix shear or fiber breakage started in the second and fourth plies, along the edges

and gradually propagated towards the center. The width of the damage zone due to fiber failure mode was larger for plates having larger aspect ratio. In each case the middle ply remained un-damaged up to a pressure of 0.10 MPa. In addition to matrix crack, the final dominant failure mode was either fiber-matrix shear or fiber breakage.

As shown in figure 4.9 in the initial stage, fiber content being more in the x-direction, ply 1 and ply 5 were stressed more than the others. Cracks formed in these plies when the transverse tensile or compressive strain reached its limit. However since the transverse compressive strength(Y_C) of the ply is significantly more than its transverse tensile strength, more cracks appeared in the first ply. The middle layer acted as a neutral layer and remained unstressed, up to 0.10 MPa. With further increase in load, there was redistribution of stresses in two ways as follows:

(a) The damaged materials lost some of their stiffness, and consequently their contribution to global stiffness decreased. The undamaged material points,being stiffer than the damaged ones, carried a larger portion of the additional load and therefore were stressed more. In this way stress transfer occurred both in-plane and through the thickness. Therefore as shown in figure 4.10, there was sudden transfer of stress to the middle layer, which eventually cracked at several material points. In the other layers more in-plane material points cracked as stresses were transferred between material points as damage occurred.

(b) The damaged material points could not carry any more load in the failed mode, but still might carry some load, if not completely failed. For example if a material point fails in matrix cracking mode it cannot take additional stresses in the transverse direction, but it can still carry some load due to its longitudinal stiffness which is not necessarily zero. This results in increase in stress level in the fiber direction. As shown in figure 4.10 some of the materials points, which had failed by matrix cracking, failed in fiber mode.

With further increase in load there was continuous stress transfer, due to which there was increase in the number of cracked material points and the number of material points with fiber failure, the former occurring more rapidly as shown in figure 4.11. When about three quarter of the material points had lost their transverse strength and

about 15% of the material points had lost their longitudinal strength, the structure behaved as if plastic hinges had formed along the long edges as shown in figures 4.14, 4.19 and 4.24. At this stage there was a rapid increase in deflection and the plate was assumed to fail.

- Basic Panel Behavior

The panels studied were very thin, with a short span to thickness of ratio of approximately 175. Tables(4.6,4.7,4.8) show that for the same material and same lamination sequence, the larger the aspect ratio, the larger the deflections and the lower the failure load. As would be expected, the plates behaved non-linearly under transverse pressure(figure 4.8). At very low pressures the panels were very flexible, and there was rapid increase in deflection(figure 4.8), which confirms the nonlinear load-deflection curves obtained in the tests, as shown in figure 4.6. As the aspect ratio increased, the contribution of shear stress towards failure was greater than that of the normal stresses, so that plates B and C finally failed in the fiber-matrix shear mode(tables 4.7 and 4.8) , while the failure in plate A was mainly due to breakage of the fibers(table 4.6).

Figure 4.24 shows the failure pattern of plate C just before failure and figure 4.7 is a photograph of plate A taken in the laboratory at final failure. The deep black damage lines running parallel to the long edges (figure 4.7) show where the fibers were broken. They are in agreement with the predictions of the numerical results as shown in figure 4.24, which indicates that fiber failure in the form of fiber-matrix shearing was dominant along the long edges, leading eventually to the final collapse of the plate.

4.10 Concluding Remarks

A progressive failure methodology for uni-directional composite plates has been developed and successfully implemented. It accommodates various formulations in predicting failure such as the maximum stress criterion, Tsai-Wu criterion and Hashin's criterion and others.These different formulations are compared and assessed by performing analyzes on laminated composite panels. The results show improvement in accuracy with the progressive degradation model. The contribution of transverse stresses

towards failure was found to be negligible and hence is not included in the failure criterion. The progression of damage is shown graphically for easy understanding. The model can provide the following information: the type and extent of damage at a given load, the residual stiffness and strength of the laminated composite plates, the first ply failure load, the final collapse load, and the complete response of the composite plates from initial loading to final failure. The progressive(ultimate) failure loads in the non-linear failure analysis were found to be sensitive to both load increment size and finite element mesh size. In a test the load and displacement increase continuously, but in a numerical simulation discrete load increments are used for failure prediction. A large load step will not represent damage progression well, and a very small load step will require significant computational effort. In the present analysis about thirty thousand load steps and a mesh size of 20 by 20 (or 400 elements) were chosen, after conducting a convergence study for a fixed failure criterion.

4.11 References

1. ABAQUS/Theory Manual, Version 5.6, Hibbit,Karlsson and Sorensen, Inc, 1996, RI, USA, Chapter 3

2. Lee, J.D., Three Dimensional Finite Element Analysis of Damage Accumulation in Composite Laminate, Computers and Structures, Vol. 15, pp. 335-350(1982).

3. Christensen, R.M., Tensor Transformations and Failure Criteria for the Analysis of Fiber Composite Material, Vol. 22, pp. 874-897(1988).

4. Sandhu, R.S., Nonlinear Behavior of Uni-Directional and Angle Ply Laminates, AIAA J. of Aircraft, Vol. 13, pp. 104-111(1974).

5. Abu-Farsakh, G.A. and Abdel-Jawad, Y.A., A New Failure Criterion for Nonlinear Composite Materials, J. of Comp. Tech. and Res., Vol. 16, pp. 138-145(1994)

6. Ochoa, O.O. and Reddy, J.N., *Finite Element Analysis of composite Laminates*, Kluwer Academic Press (1992).

7. Hashin, Z., Failure Criteria for Unidirectional Fiber Composites, ASME J. of Appl. Mech., vol.47, 1980, pp 329-334

8. Nahas, M.N., Survey of Failure and Post-Failure Theories of Laminated Fiber-Reinforced Composites, J. of Comp. Tech. and Res., Vol. 8, No. 4, pp. 138-153(1986)

9. Hahn, H.T. and Tsai, S.W., On the Behavior of Composite Laminates after Initial Failures, Astronautics and Aeronautics, Vol. 21, pp. 58-62 (1983).

10. Petit, P.H. and Waddoups, M.E., A Method of Predicting the Nonlinear Behavior of Laminated Composites, J. of Comp. Mat., Vo. 3, pp. 2-19(1969).

11. Chang, F.K. and Chang, K.Y., A Progressive Damage Model for Laminated Composites containing Stress Concentrations, J. of Comp. Mat., Vol. 21, 1987 pp.834-855

12. Schmidt, R. and Reddy, J.N., A Refined Small Strain and Moderate Rotation Theory of Elastic Anisotropic Shells, ASME J. of Appl. Mech., Vol. 55, 1988, pp.611-617

13. Chang, F.K. and Lessard, L.B., Damage Tolerance of Laminated Composites Containing an Open Hole and Subjected to Compressive Loadings: Part I-Analysis, J. of Comp. Mat., Vol. 25 1991, pp. 2-43

14. Shahid, I. and Chang, F.K., An Accumulative Damage Model for Tensile and Shear Failures of Laminated Composite Plates, J. of Comp. Mat., Vol. 29, 1995, pp. 926-981

15. Lo, D.C., Coats, T.W., Harris, C.E. and Allen, D.H., Progressive Damage Analysis of Laminated Composite(PDALC)-A Computational Model Implementated in the NASA COMET Finite Element Code, NASA Tech. Memo.-4724(1996)

16. Reddy, Y.S.N. and Reddy, J.N., An Accurate Prediction of Failures in Composite Laminates Using a Layer-wise Model, Proc. of Int. Conf. on Comp. Mat. ICCM-9 Madrid, Vol. 3,1993, pp 15-22

17. Reddy, J.N., A Small Strain and Moderate Rotation Theory of Elastic Anisotropic Plates, ASME J. of Appl. Mech., Vol. 55, 1988, pp.611-617

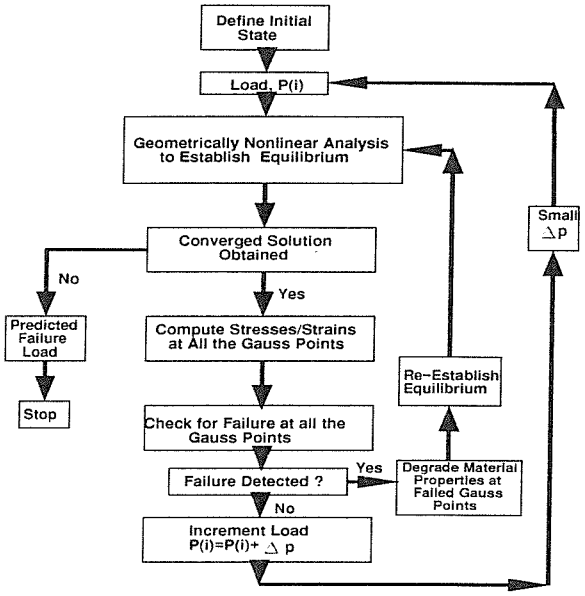

Figure 4.1: Progressive Failure Analysis

18. Palmerio, A.F., Reddy, J.N. and Schmidt, R., On a Moderate Rotation Theory of Laminated Anisotropic Shells, Part 1. Theory, Int. J. of Non Linear Mech., Vol. 25, 1990, pp.687-700

19. Pietraszkiewicz, W., Lagrangian Description of and Incremental Formulation in The Non-linear Theory of Thin Shells, Int. J. of Non-linear Mech., Vol. 19, 1983, pp. 115-140

20. Moy, S.S.J., Shenoi, R.A. and Allen, H.G., Strength and Stiffness of Fiber Reinforced Plastic Plates, Proceedings of the Institution of Civil Engineers, Vol. 116, No. 2 1996, pp. 204-220

21. Shenoi, R.A., Wellicome, J.F.(eds), Composite Materials in Maritime Structures, Vol. 1 and 2, Cambridge University Press(1993)

22. Echaabi, J., Trochu, F., Pham, X.T. and Ouellet, M., Theoretical and Experimental Investigation of Failure and Damage Progression of Graphite-Epoxy Composites in Flexural Bending Test, J. of Reinf. Plast. and Comp., Vol. 15, 1996, pp. 740-755

Table 4.1: Mechanical Properties of glass/polyester unidirectional Lamina.

Moduli Parameters	Symbol(units)	
Longitudinal modulus	E_x(GPa)	23.6
Transverse Modulus	E_y(GPa)	10.0
Shear Modulus	G_{xy}(GPa)	1.0
Poisson's ratio	ν_{xy}	0.23
Strength Parameters	**Symbol(units)**	
Longitudinal tension	X_T(MPa)	735
Longitudinal Compression	X_C(MPa)	600
Transverse tension	Y_T(MPa)	45
Transverse Compression	Y_C(MPa)	100
Inplane Shear	SC(MPa)	45

Table 4.2: Laminated Plate Specifications(refer to figure 4.5)

Plate	Lay-up	No. of Plies	Length(a) (mm)	Width(b) (mm)	Thickness (mm)
A	[0/45/90/-45/0]	5	600	600	3.43
B	[0/45/90/-45/0]	5	900	600	3.43
C	[0/45/90/-45/0]	5	1200	600	3.43

Table 4.3: First Ply Failure Analysis of Plate A

Failure Criterion	Failure Pressure	Central Deflection(mm)	Failed Ply	Failed Location (x,y-coordinates) (mm)	Dominant Failure Mode
Maximum Stress	0.0218	10.64	1 (bottom)	315, 15	Matrix Crack
Tsai-Hill	0.0218	10.64	1 (bottom)	315, 15	Matrix Crack
Tsai-Wu	0.0221	10.69	1 (bottom)	315, 15	Matrix Crack
Hoffmann	0.0219	10.65	1 (bottom)	315, 15	Matrix Crack
Hashin	0.0218	10.64	1 (bottom)	315, 15	Matrix Crack
Azzi-Tsai-Hill	0.0218	10.64	1 (bottom)	315, 15	Matrix Crack
Test result: Pressure at first audible Crack	0.035	-	-	-	-

Table 4.4: First Ply Failure Analysis of Plate B

Failure Criterion	Failure Pressure	Central Deflection(mm)	Failed Ply	Failed Location (x,y-coordinates) (mm)	Dominant Failure Mode
Maximum Stress	0.01615	11.67	1 (bottom)	465, 15	Matrix Crack
Tsai-Hill	0.01615	11.67	1 (bottom)	465, 15	Matrix Crack
Tsai-Wu	0.0164	11.74	1 (bottom)	465, 15	Matrix Crack
Hoffmann	0.0162	11.69	1 (bottom)	465, 15	Matrix Crack
Hashin	0.01615	11.67	1 (bottom)	465, 15	Matrix Crack
Azzi-Tsai-Hill	0.01615	11.67	1 (bottom)	465, 15	Matrix Crack
Test result: Pressure at first audible Crack	0.035	-	-	-	-

Table 4.5: First Ply Failure Analysis of Plate C

Failure Criterion	Failure Pressure	Central Deflection(mm)	Failed Ply	Failed Location (x,y-coordinates) (mm)	Dominant Failure Mode
Maximum Stress	0.01545	11.80	1 (bottom)	615, 15	Matrix Crack
Tsai-Hill	0.01545	11.80	1 (bottom)	615, 15	Matrix Crack
Tsai-Wu	0.015675	12.00	1 (bottom)	615, 15	Matrix Crack
Hoffmann	0.01550	11.90	1 (bottom)	615, 15	Matrix Crack
Hashin	0.015425	11.80	1 (bottom)	615, 15	Matrix Crack
Azzi-Tsai-Hill	0.01545	11.80	1 (bottom)	615, 15	Matrix Crack
Test result: Pressure at first audible Crack	0.040	-	-	-	-

Table 4.6: Ultimate Failure Load for Plate A

Failure Criterion	Failure Pressure (N/mm^2)	Central Deflection (mm)	Dominant Failure mode
Maximum Stress	0.612	41.0	Fiber-Failure
Tsai-Hill	0.608	40.90	Fiber Failure
Tsai-Wu	0.610	40.90	Fiber-Failure
Hoffmann	0.611	41.0	Fiber-Failure
Hashin	0.600	41.0	Fiber-Failure
Azzi-Tsai-Hill	0.608	40.90	Fiber-Failure
Test Results	0.605	41.70	Fiber-Failure

Table 4.7: Ultimate Failure Load for Plate B

Failure Criterion	Failure Pressure (N/mm^2)	Central Deflection (mm)	Dominant Failure mode
Maximum Stress	0.5450	54.40	Fiber-Matrix Shear
Tsai-Hill	0.5520	54.40	Fiber-Matrix Shear
Tsai-Wu	0.5530	55.20	Fiber-Matrix Shear
Hoffmann	0.5490	54.60	Fiber-Matrix Shear
Hashin	0.5450	56.20	Fiber-Matrix Shear
Azzi-Tsai-Hill	0.5520	54.40	Fiber-Matrix Shear
Test Results	0.550	53.30	

Table 4.8: Ultimate Failure Load for Plate C

Failure Criterion	Failure Pressure (N/mm^2)	Central Deflection (mm)	Dominant Failure mode
Maximum Stress	0.455	56.30	Fiber Matrix Shear
Tsai-Hill	0.462	56.50	Fiber Matrix Shear
Tsai-Wu	0.461	56.50	Fiber Matrix Shear
Hoffmann	0.441	55.70	Fiber Matrix Shear
Hashin	0.455	55.90	Fiber Failure
Azzi-Tsai-Hill	0.462	56.50	Fiber Matrix Shear
Test Results	0.480	51.0	

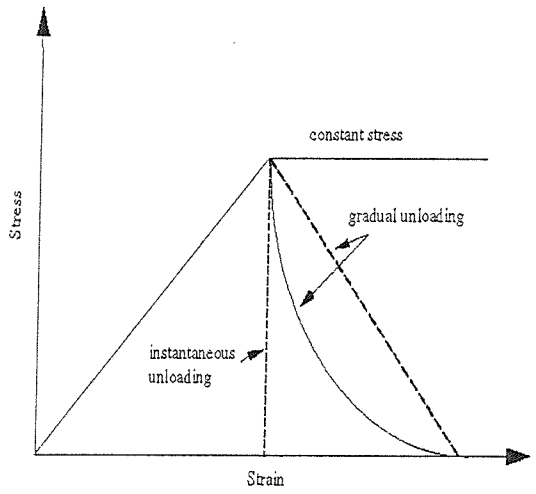

Figure 4.2: Post-Failure Degradation Behavior in Laminated Composite Plates

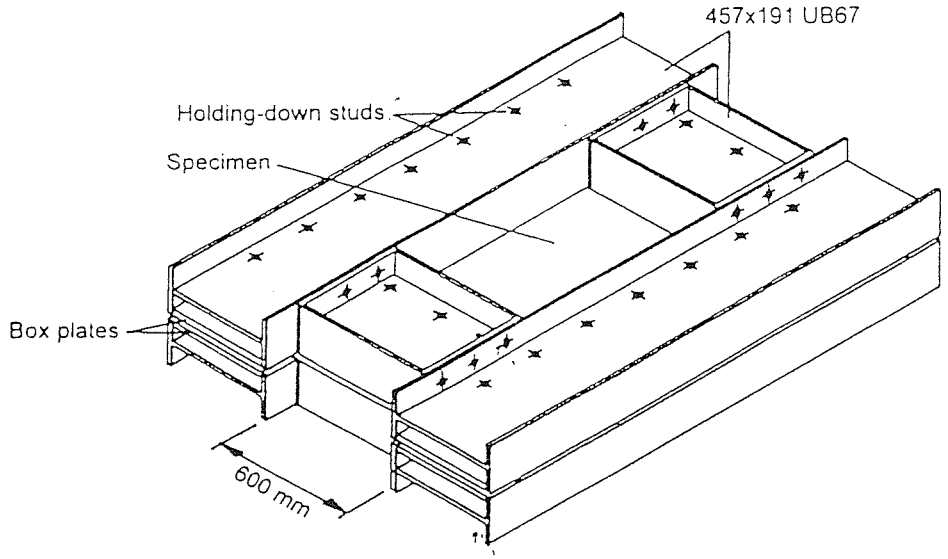

Figure 4.3: Isometric View of Test Rig

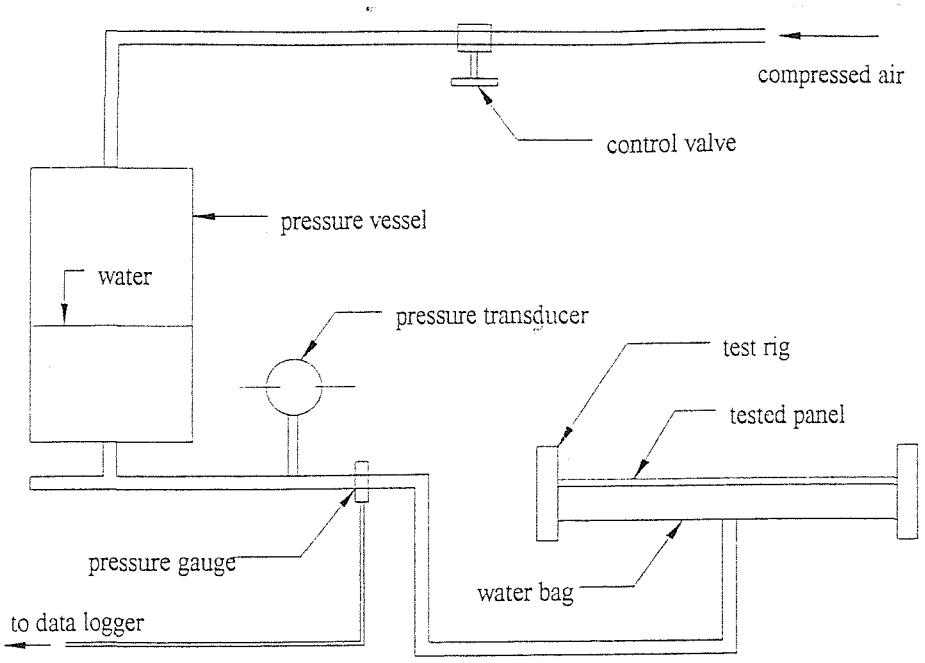

Figure 4.4: Demonstration of the Loading System

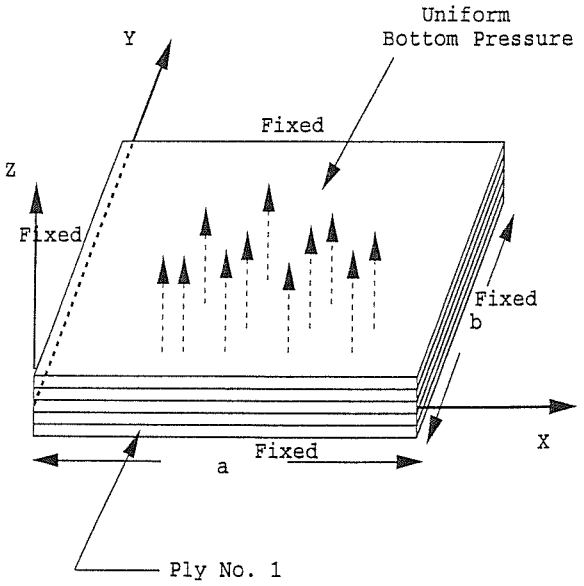

Figure 4.5: Geometry and Coordinate System Used

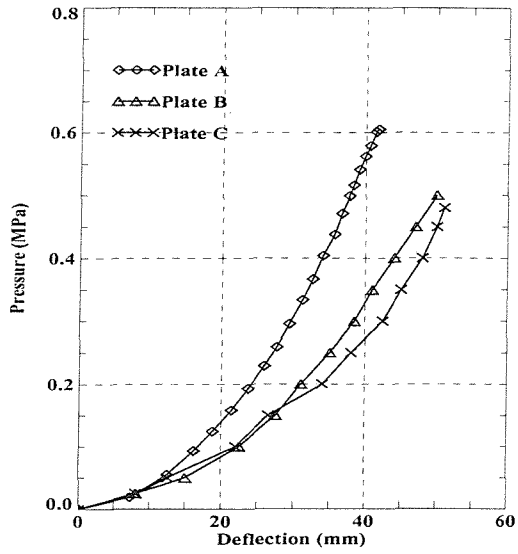

Figure 4.6: Load Central Deflection Graphs : Test Result

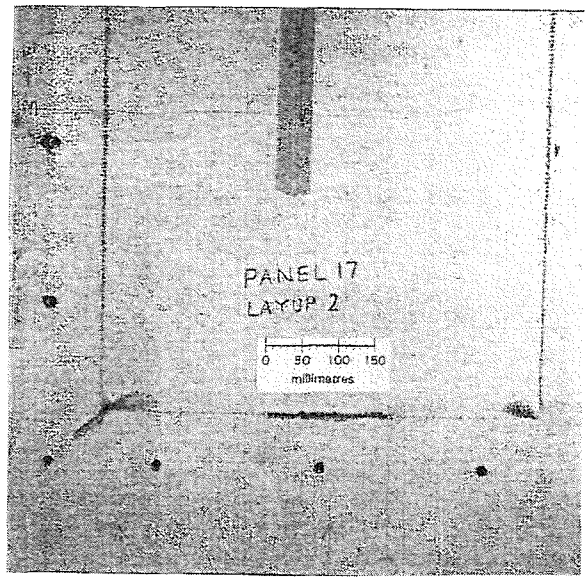

Figure 4.7: Test Failure Pattern for Plate C

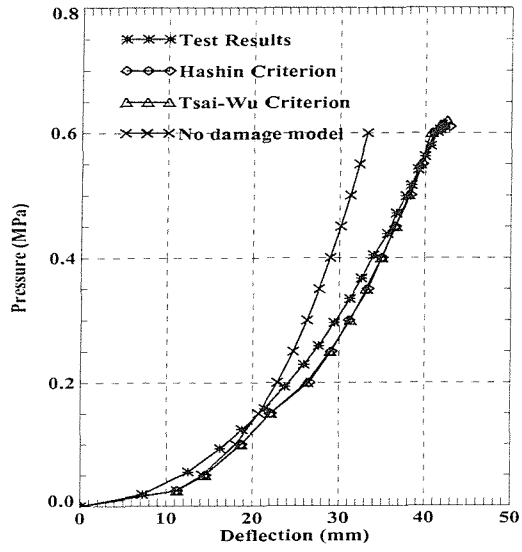

Figure 4.8: Central Deflection for Plate C

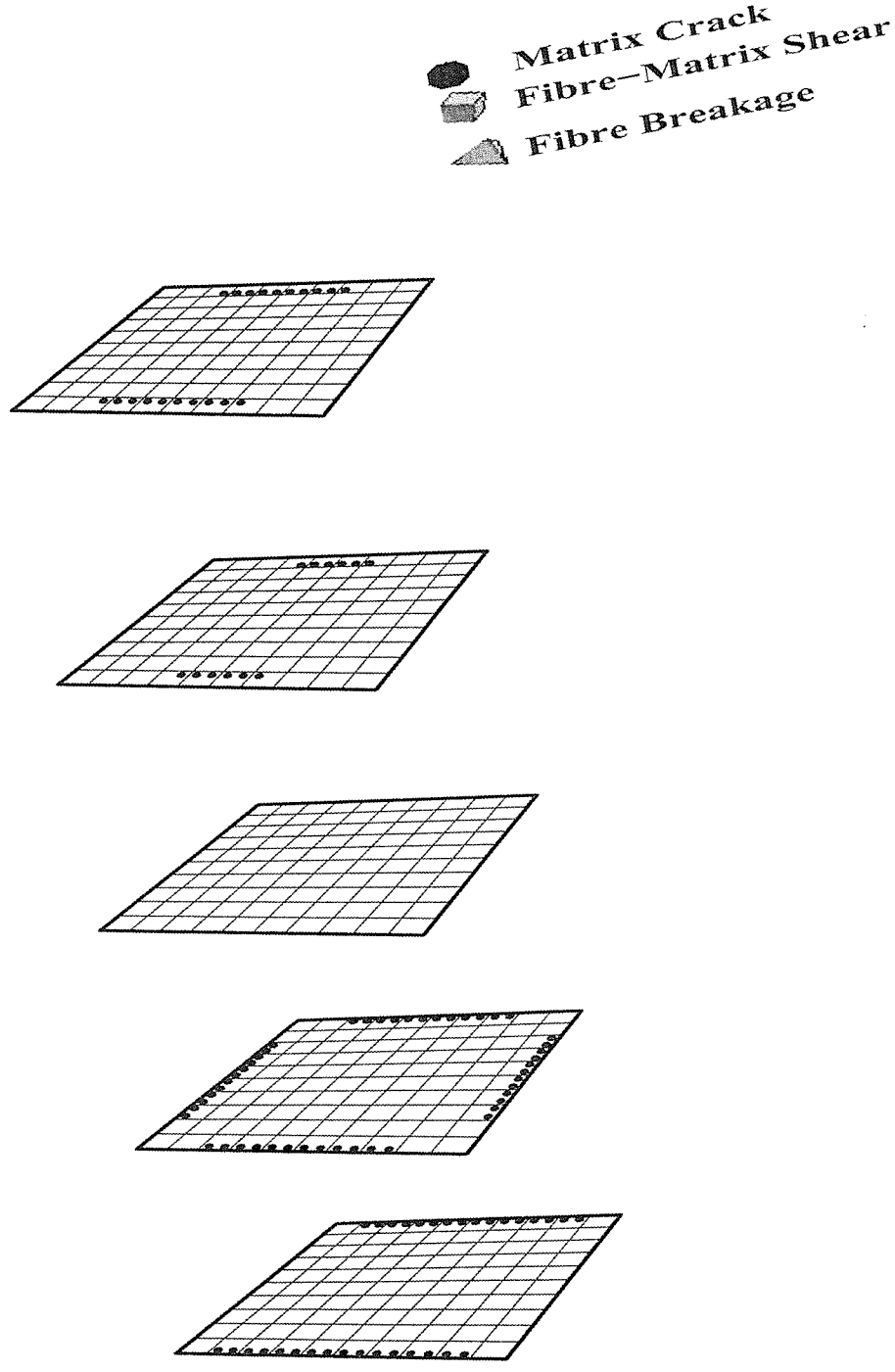

Figure 4.9: Damage Pattern for Plate A at 0.10 MPa

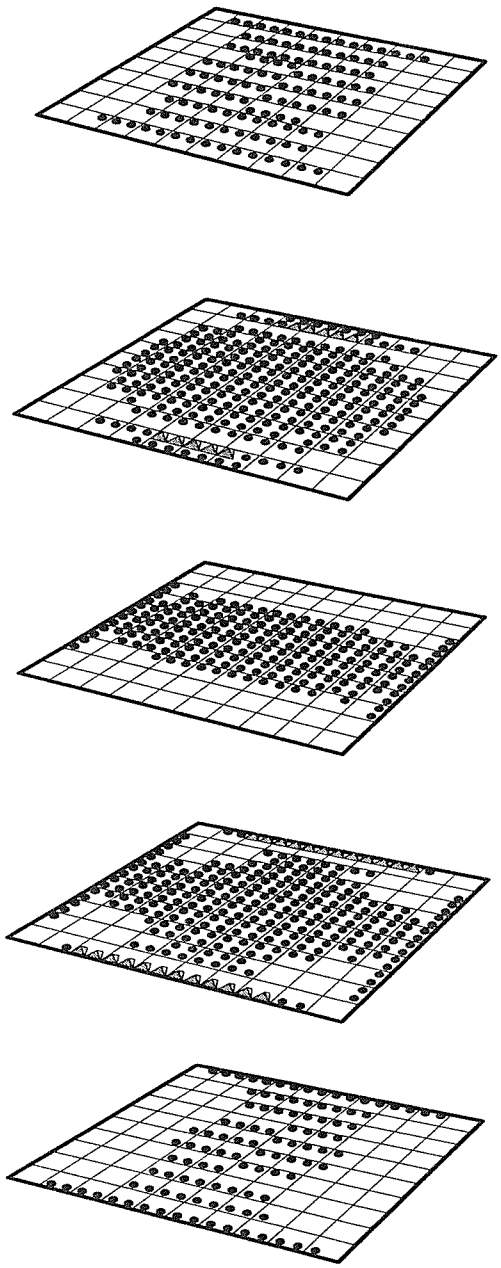

Figure 4.10: Damage Pattern for Plate A at 0.20 MPa

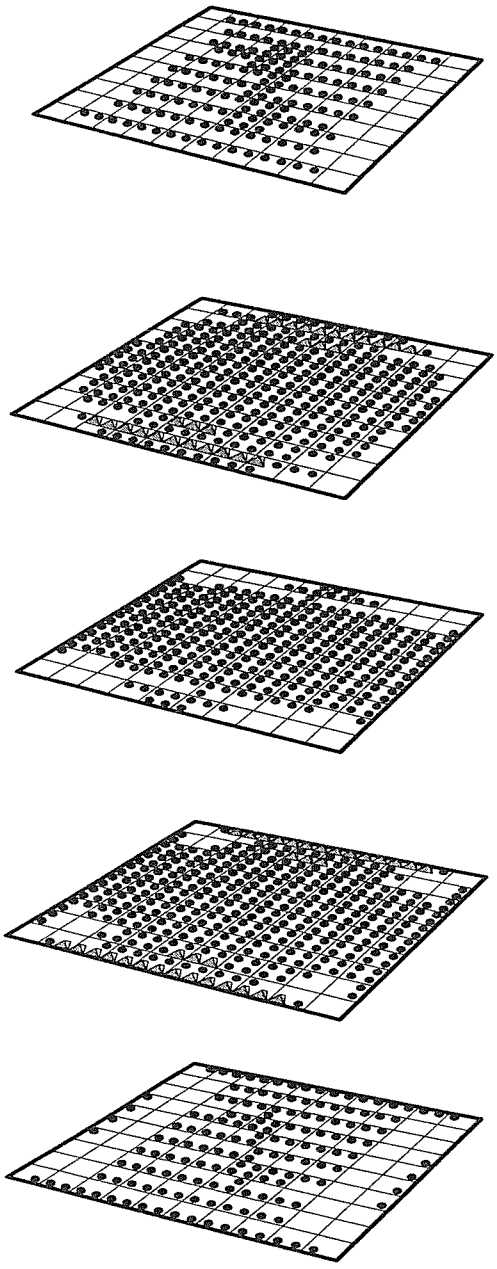

Figure 4.11: Damage Pattern for Plate A at 0.30 MPa

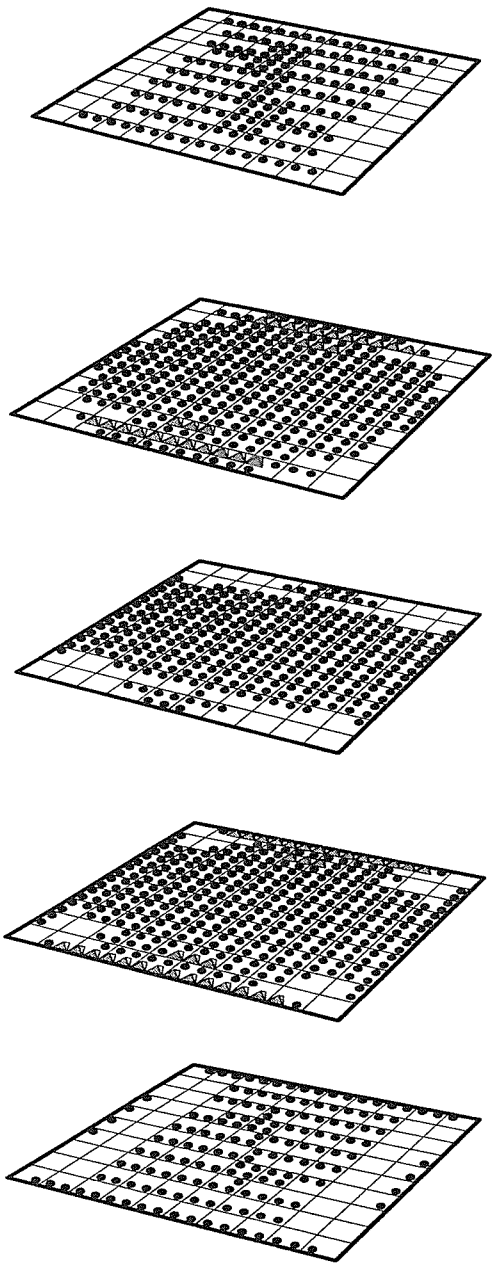

Figure 4.12: Damage Pattern for Plate A at 0.40 MPa

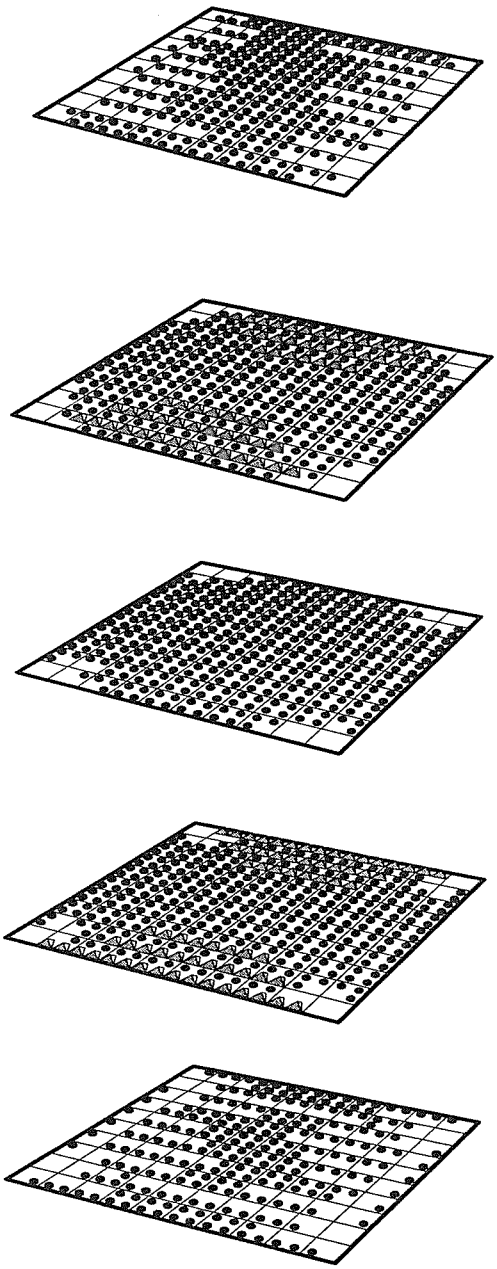

Figure 4.13: Damage Pattern for Plate A at 0.50 MPa

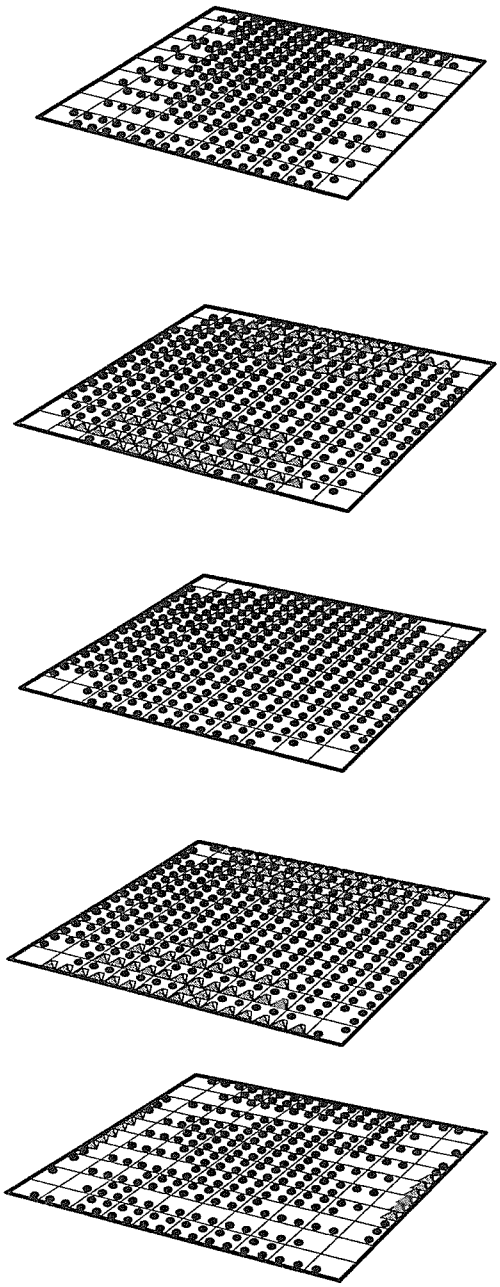

Figure 4.14: Damage Pattern for Plate A at 0.60 MPa (Just Before Failure)

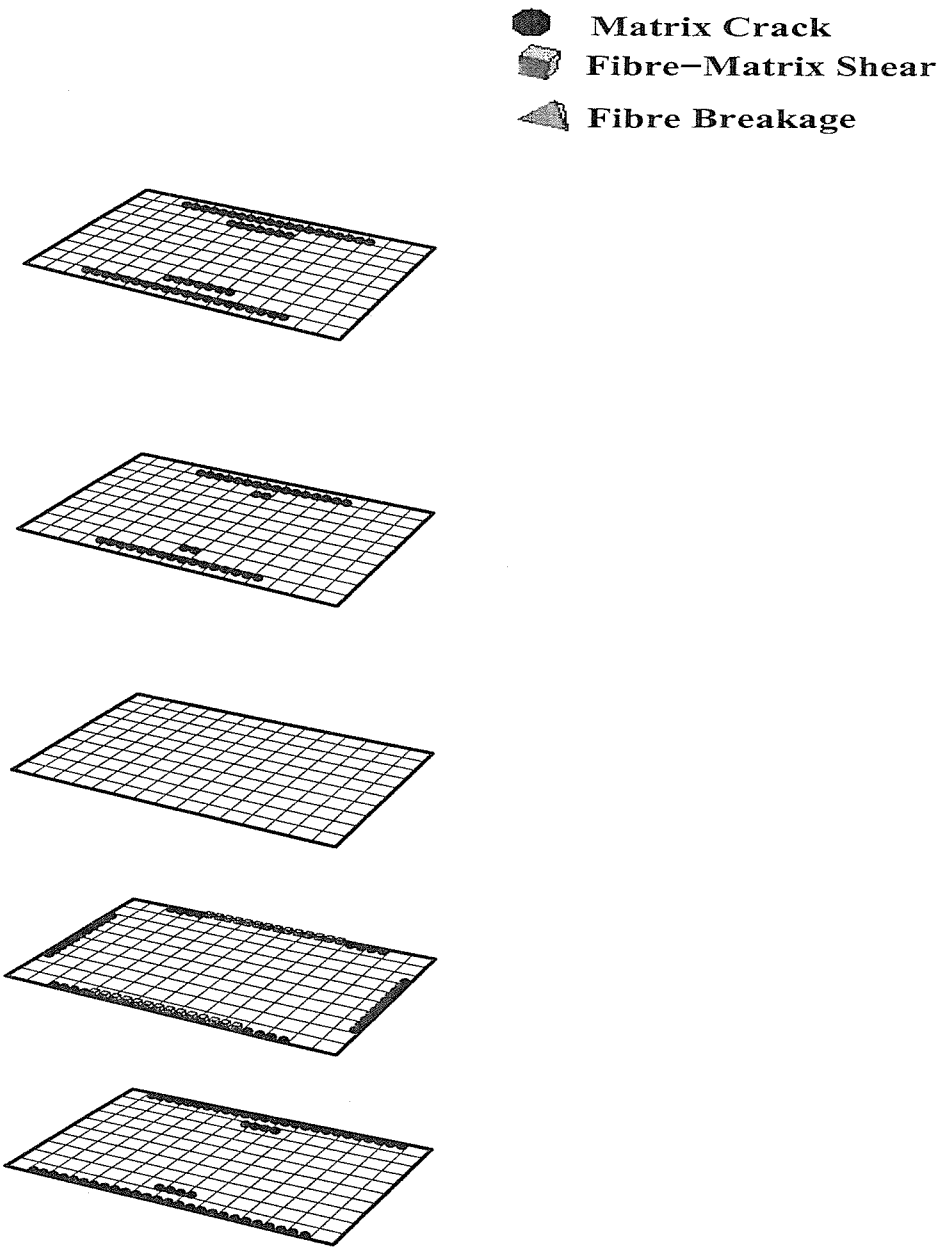

Figure 4.15: Damage Pattern for Plate B at 0.10 MPa

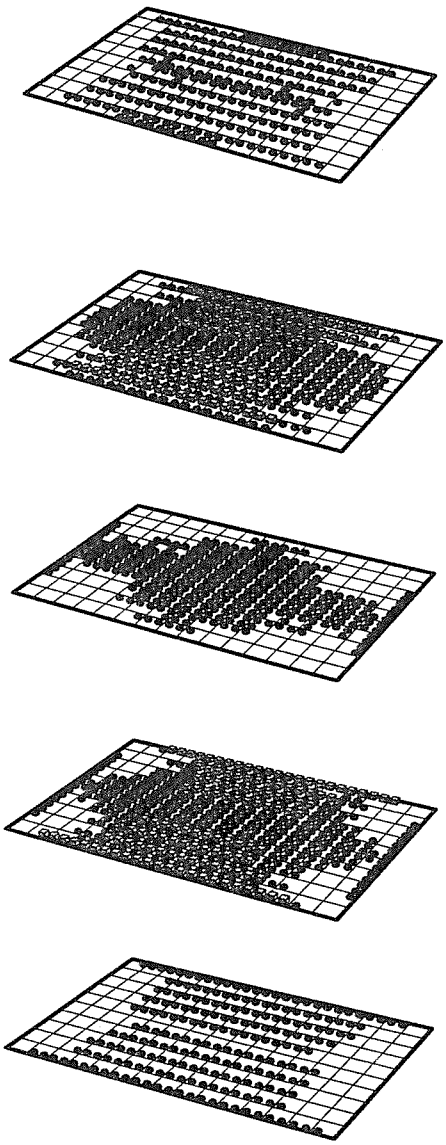

Figure 4.16: Damage Pattern for Plate B at 0.20 MPa

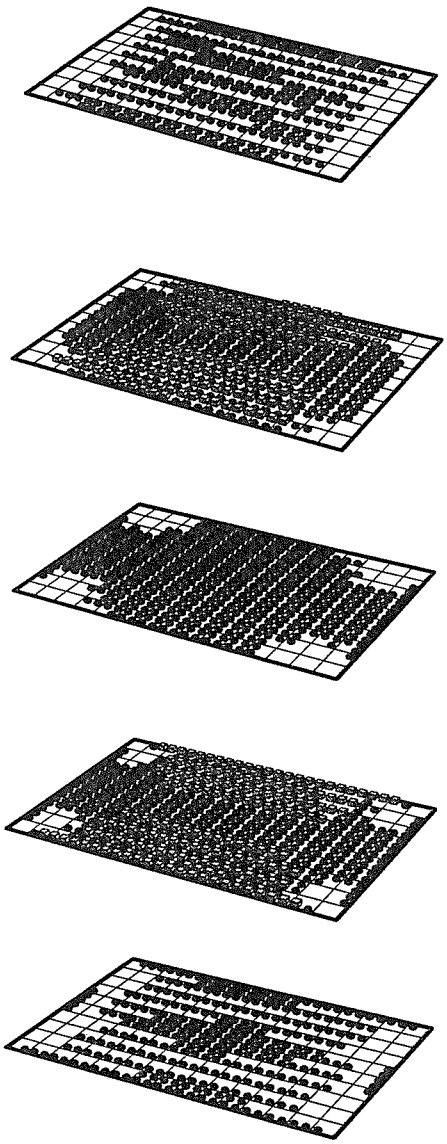

Figure 4.17: Damage Pattern for Plate B at 0.30 MPa

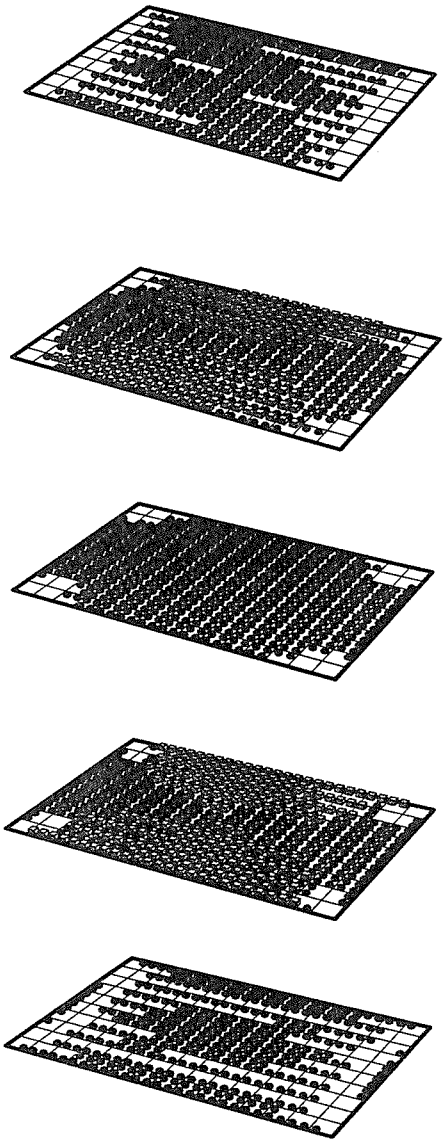

Figure 4.18: Damage Pattern for Plate B at 0.40 MPa

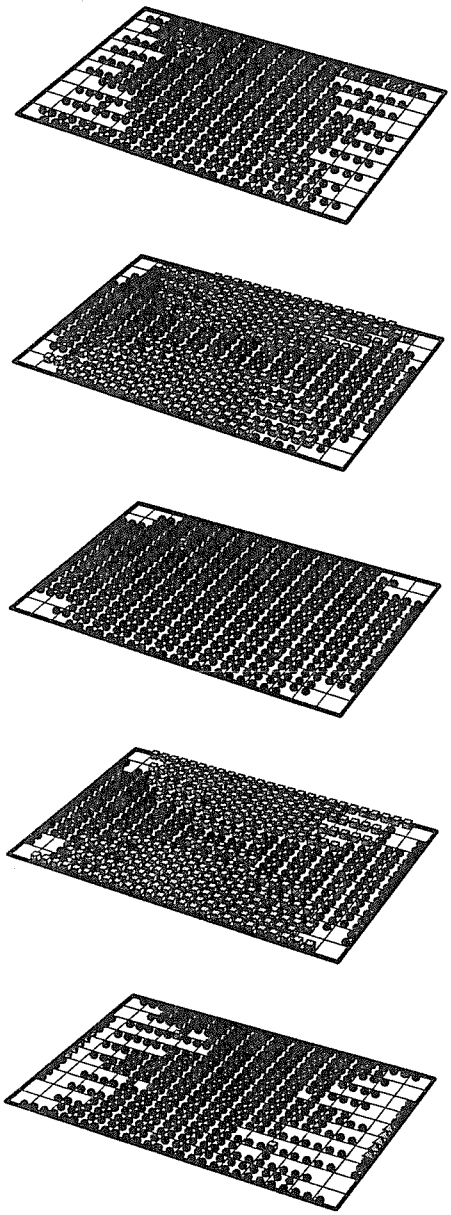

Figure 4.19: Damage Pattern for Plate B at 0.50 MPa (Just Before Failure)

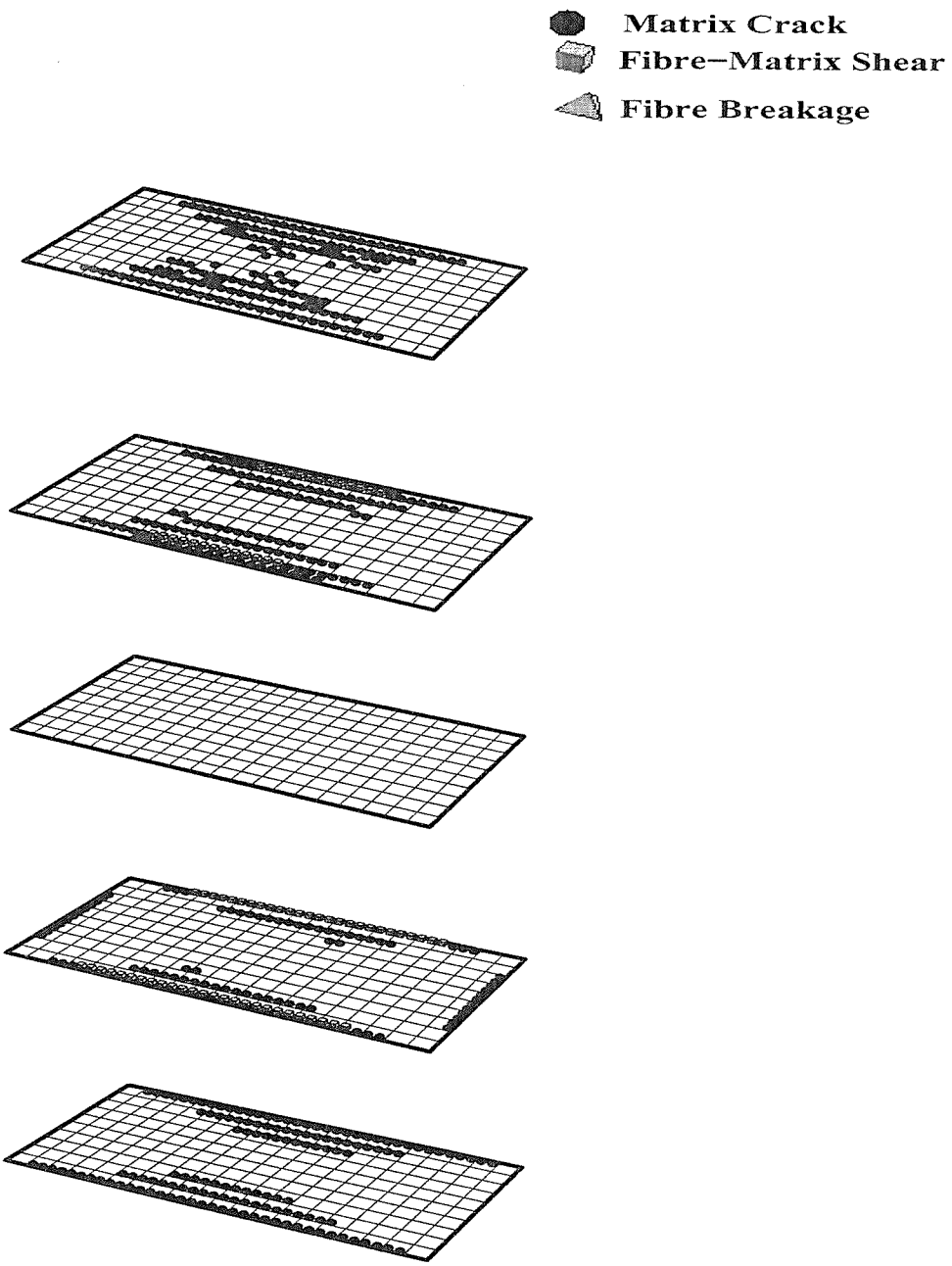

Figure 4.20: Damage Pattern for Plate C at 0.10 MPa

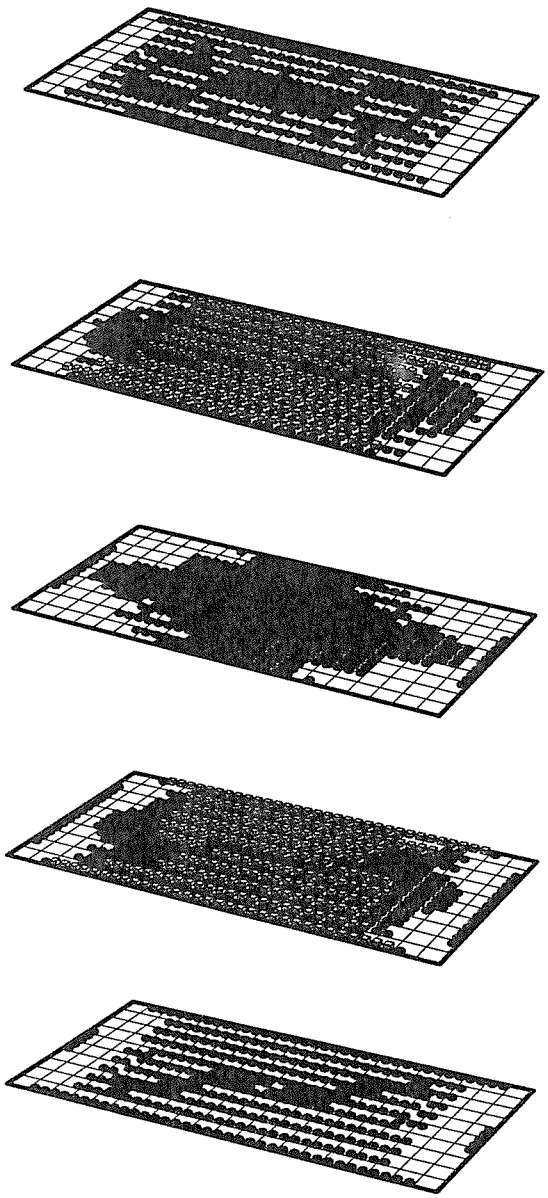

Figure 4.21: Damage Pattern for Plate C at 0.20 MPa

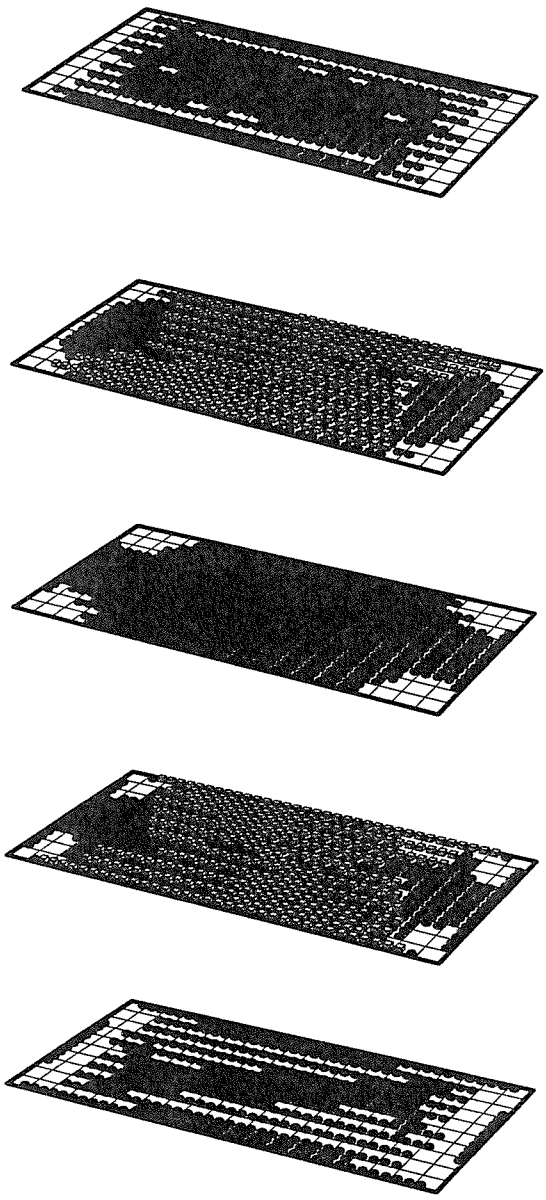

Figure 4.22: Damage Pattern for Plate C at 0.30 MPa

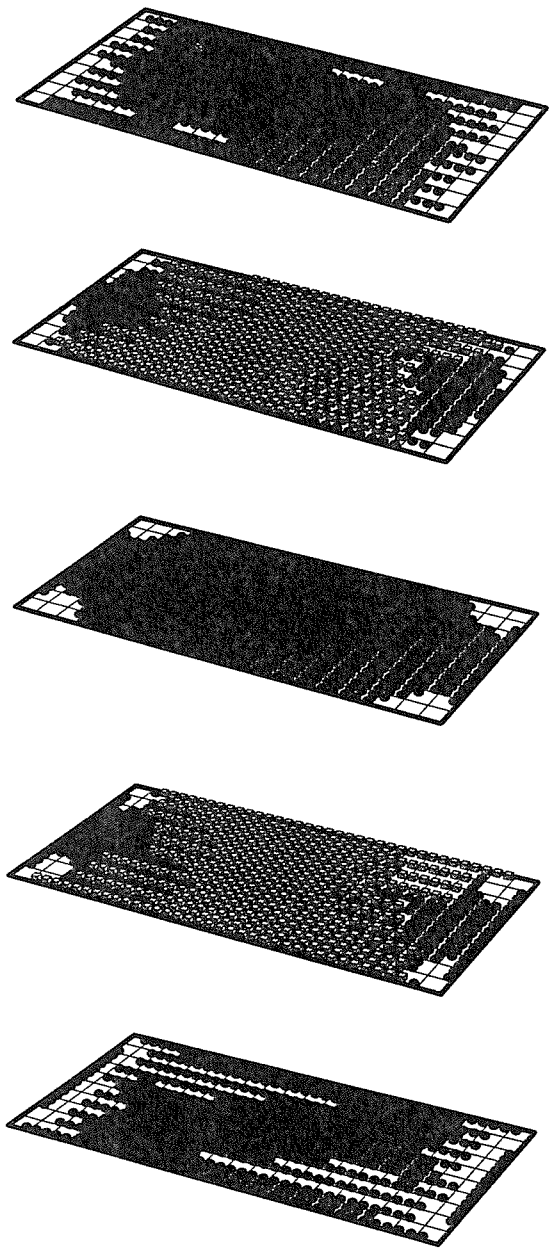

Figure 4.23: Damage Pattern for Plate C at 0.40 MPa

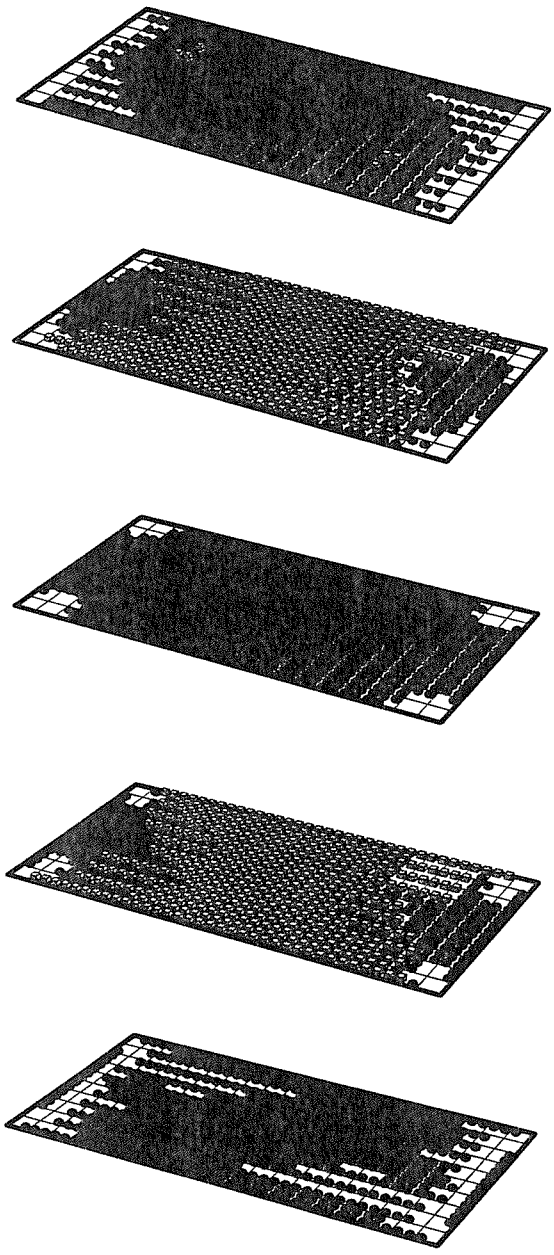

Figure 4.24: Damage Pattern for Plate C at 0.50 MPa (Just Before Failure)

Chapter 5

Failure Analysis of Woven Fabric Composite Structures

5.1 Introduction

In the previous chapter, a progressive failure methodology was developed and implemented into the general purpose finite element program ABAQUS. Damage propagation of three uni-directional composite plates was studied. Another class of composites which are extensively used in aerospace structures, is plain weave fabric composites. A thorough discussion of these composites and their numerical modelling aspects have been discussed in the third chapter. The objective of this chapter is to study the damage propagation and failure of laminated plates made of plain woven composite materials.

Few research projects have been done on damage modeling of woven fabric composite structures. Blackketter *et al*[1] studied the damage development in plain weave fabric reinforced composite laminates subjected to tension and shear loadings using 3-D finite element analysis. Whitcomb and Srirengan[2] studied the effects of quadrature order, mesh refinement and choice of material degradation model on the progressive failure of plain weave composites. Naik[3] in his work included non-linear shear response, yarn bending and straightening/wrinkling in woven materials. The stiffness reduction scheme used by Blackketter[1] was used in the analysis. Vandeurzen *et al*[4] studied the failure process in woven fabric composites in which the homogenization technique[5] was

used. The aim of this chapter is to study the failure behavior of woven fabric composite plates in bending, in contrast to the in-plane conditions considered in the literatures.

For studying the damage propagation of a woven fabric composite layer, detail finite element modeling of the reinforcement and the surrounding resin is often necessary. Analysis in this way is often called a micro-mechanics analysis. However, from the review made in chapter 3, it is clear that, if the woven fabric composite plate consists of large number of unit cells, the finite element method becomes computationally expensive. The woven fabric plate considered in this chapter consists of unit cells of order of thousands. Moreover, the progressive failure methodology developed in the previous chapter was developed for uni-directional composites. It cannot be directly applied to woven fabric composite structures.

In this chapter the progressive failure analysis of woven fabric composite plates are carried out as follows. A simplified model is developed in which a woven ply is simplified as a combination of two resin layers and two uni-directional composite layers. This is explained in the next section. Section 3 outlines the procedure for determining the mechanical properties of a composite plate with woven plies. Even though this section is not necessary for carrying out the progressive failure analysis, this is useful for validating the accuracy of the simplified model. Section 4 gives a brief description on the experiments on these plates. In section 5, the extension of the damage model developed in the previous chapter as applicable to the present simplified model is discussed. Numerical results are presented in section 6, and conclusions are drawn in the last section.

5.2 Simplified Model for a Woven Fabric Lamina

In the simplified model, a repeating unit element with width d in a single layer woven fabric composite (referred to as woven lamina) is simplified as a four-layer laminate which consists of upper and lower layers of pure resin and two orthogonal fiber/resin layers sandwiched between the two pure resin layers as shown in figure 5.1. The pure resin layers represent the coverings on the top and bottom of the rovings. The fiber/resin layers represent the warp roving and the weft roving, in which the fiber and the remainder

of the resin are mixed together.

The following notations are used.

- Notations for the composite plate as a whole:

  t = overall thickness

  V_f = Overall fiber content by volume

  E^f, E^m are Young's moduli of fiber and resin respectively

  ν^f, ν^m are Poisson's ratios of fiber and resin respectively

  G^f, G^m are Shear moduli of fiber and resin respectively

  $g_f = 1 - \nu^{f2}$ and $g_m = 1 - \nu^{m2}$

- Notations for the woven lamina:

  h = thickness of lamina

  h_{mi} = thickness of *top* or *bottom* pure resin layer

  t_i^1, t_i^2 are thickness of fiber/resin (*warp* and *weft*)

  S_{fi} = fiber content in fiber/resin (*warp* and *weft*)

  S_{mi} = resin content in fiber/resin (*warp* and *weft*)

  $S_{mi} = 1 - S_{fi}$

  μ = fraction of resin (by volume) in pure resin layer

  ξ_{1i} = lamina fiber fraction

  ξ_{2i} = warp fiber fraction

If μ is the proportion of the resin that lies in the uni-directional layers, which can be estimated from the scanning electron microscope(SEM) photograph of the composite plate, then the thicknesses of various layers in the simplified model can be calculated as follows. Total thickness of pure resin is $\mu(1 - V_f)t$. The amount allocated to each lamina is $\frac{\mu(1-V_f)t}{n}$. Hence the thickness of the top or bottom pure resin layer is $\frac{\mu(1-V_f)t}{2n}$. Here t is the total thickness of the composite plate and n is the number of woven fabric layers.

- Equivalent thickness of fiber in fiber/resin layer (warp or weft)

  Equivalent thickness of all fibers is $V_f t$.

  The amount allocated to each fiber/resin layer (warp or weft) is

  $\xi_{1i}\xi_{2i}V_f t$ for (warp fiber/resin layer)

  $\xi_{1i}(1-\xi_{2i})V_f t$ for (weft fiber/resin layer)

- Equivalent thickness of resin in fiber/resin layer (warp or weft)

  Equivalent thickness of resin in all the fiber/resin layers is $(1-\mu)(1-V_f)t$.

  The amount allocated to each fiber/resin layer (warp or weft) in lamina is

  $\xi_{1i}\xi_{2i}(1-\mu)(1-V_f)t$ for (warp fiber/resin layer)

  $\xi_{1i}(1-\xi_{2i})(1-\mu)(1-V_f)t$ for (weft fiber/resin layer)

- Equivalent thickness of fiber/resin layer (warp or weft)

  This can be obtained by adding the equivalent thicknesses of the fiber and the resin together.

  $t_i^1 = (1-\mu(1-V_f))\xi_{1i}\xi_{2i}\frac{t}{2}$ for (warp fiber/resin layer)

  $t_i^2 = (1-\mu(1-V_f))\xi_{1i}(1-\xi_{2i})\frac{t}{2}$ for (weft fiber/resin layer)

Once the thicknesses of the resin layers and the uni-directional composite layers have been determined, the next step is to determine the equivalent material properties for them. The resin layer is a homogeneous layer and hence it's material properties are those for pure resin, which are known from experiment and are given in the table 5.2.

5.2.1 Stiffness Properties for the Uni-Directional Composite Layers

This section illustrates the calculation of the gross material properties for the uni-directional composite layer based on rule of mixture formula[6]. In the rule of mixtures approach, it is assumed that there is no interaction between the two phases. There are only two types of material response; parallel (in which applied strain is the same in both the phases) and series (in which the applied stress is the same in both the

phases). The models developed are rudimentary from this point. However, despite this shortcoming, in the case of longitudinal modulus, E_L, rule of mixtures gives very reasonable results.

Longitudinal modulus, E_L

In the case of unit displacement applied in the x direction, the ends of all the fibers are gripped tightly and move one unit. Similarly the ends of the matrix move with the ends of the fibers in the x direction. Thus if there is perfect bonding between the two, it is reasonable to assume that the strain field is uniform in the x direction:

$$\epsilon_x^c = \epsilon_x^f = \epsilon_x^m \tag{5.1}$$

where ϵ_x^i refers to the normal strain experienced by material i in the x direction, and subscript c, refers to the composite, f, to fiber , and m, to matrix.

Rule of mixtures assumes that there is no interaction between fiber and matrix. Combining this assumption with the homogeneity of the composite as a whole, it can be concluded that in the case of longitudinal loading, all of transverse stresses for fiber, matrix and composite are exactly zero. With all the assumptions the final equation for E_L can be written as,

$$E_L = V_f E_L^f + (1 - V_f) E^m \tag{5.2}$$

The longitudinal modulus obtained in this case is not the same as that in the case of iso-strain approach. If, however, $\nu_{TL}^f = \nu^m$, in which case there is no interaction between the phases, than the iso-strain approach and the rule of mixtures approach give identical results.

Transverse elastic modulus, E_T

In the rule of mixture approach the transverse elastic modulus prediction is built upon the assumption that each phase experiences the same stress level in the applied load direction, *i.e.* $\sigma_y^c = \sigma_y^f = \sigma_y^m$. By assuming no interaction between the fiber and

matrix, the total deformation in the system will be given by the volumetric average of the strain on the fiber and the strain on the matrix. If there are negligible stresses in the other directions (no effects of different Poisson's ratios or interaction of fiber and matrix), then the transverse modulus can be calculated as

$$E_T = \frac{E_T^f E^m}{V_f E^m + (1 - V_f) E_T^f} \tag{5.3}$$

Longitudinal Poisson's ratio, ν_{TL}

When there is no fiber-matrix interaction it can be stated that the total transverse contraction of the body is the sum of the contractions of the individual elements. This leads to the relationship

$$\nu_{TL} = \frac{\left[E_T^f(1 - V_f) + E^m V_f\right]\left[V_f \nu_{LT}^f + (1 - V_f)\nu^m\right]\left[V_f E_L^f + (1 - V_f)E^m\right]}{E^m E_T^f} \tag{5.4}$$

Transverse shear modulus, G_T

The rule of mixture approach to transverse shear modulus is to consider the stress field identical in both fiber and matrix in the plane perpendicular to the fibers, leading to the result that the transverse shear modulus can be expressed as:

$$G_T = \frac{G_T^f G^m}{V_f G^m + (1 - V_f) G_T^f} \tag{5.5}$$

Transverse Poisson's ratio, ν_{TT}

Transverse Poisson's ratio ν_{TT} can be extracted from the rule of mixtures approach using the conditions of transverse isotropy to define this value. Hence

$$\nu_{TT} = \frac{E + T}{2G_T} - 1 \tag{5.6}$$

With respect to the present computational work table 5.2 gives the elastic properties of the constituents such as fiber and resin. Using the above simple model the material

properties for a single layer woven fabric composite plate are calculated and shown in table 5.3.

5.2.2 Prediction of Strength Properties for the Uni-Directional Composite Layers

Inspite of developments of elastic and stress analyzes, there are few techniques for prediction of strength properties of composite materials. Dow and Rammath[7] developed a strength analysis model using finite element method. They assumed sequential failure of matrix and fiber. After the matrix had failed, the contribution of the matrix to the composite strength was reduced. In the strength analysis, stress redistribution due to cracks or yarn debondings need to be considered. Boundary conditions should take into account the assumed defects. Pollock[8] investigated the tensile strength of carbon/carbon composites. Based on the microscopic observation of damage, yarn and matrix were modeled by a curved beam with supporting springs after crack initiation. This model is limited to the specific crack condition and thus, not suitable for other failure modes.

Chamis[10] presented strength formulas based on micro-structural analysis for uni-directional composite materials, which is adopted in the present work, and can be written as follows.

Longitudinal Tension :

$$X_T = V_f S_{ft} \tag{5.7}$$

Longitudinal Compression

(a) Fiber Compression

$$X_C = V_f S_{fc} \tag{5.8}$$

(b) Delamination/Shear

$$X_C = 10S + 2.5S_{mt} \tag{5.9}$$

Transverse Tension

$$Y_T = \left[1 - (\sqrt{V_f} - V_f)(1 - E_m/E_f)\right] S_{mt} \tag{5.10}$$

Transverse Compression

$$Y_C = \left[1 - (\sqrt{V_f} - V_f)(1 - E_m/E_f)\right] S_{mc} \tag{5.11}$$

In-Plane Shear

$$S = \left[1 - (\sqrt{V_f} - V_f)(1 - G_m/G_f)\right] S_{ms} \tag{5.12}$$

Where X_t, X_C, Y_T, Y_C and S are the strength parameters of the composite material. S_{ft} and S_{fc} are the tensile and compressive strengths of the fiber. S_{mt}, S_{mc}andS_{ms} are tensile, compressive and shear strengths of the matrix material. E_f and G_f are the elastic moduli of the fiber material, E_m and G_m are the elastic moduli of the matrix material and V_f is the fiber content by volume of the composite material.

5.3 Stiffness Characterization of a Woven Fabric Ply

Until now, in the simplified model, the thicknesses and material properties of each resin layer and each uni-directional layers have been determined. From this, the stiffness properties of the woven ply can be determined using the first order shear deformation theory. Extension to a composite plate with more than one woven fabric plies is straight forward; same first order shear deformation theory can be used to determine the stiffness properties. The simplified model for a typical composite plate with five woven fabric composite layers is shown in figure 5.2. Even though the present step is not necessary for carrying out a progressive failure analysis, the procedure outlined here has been used in the subsequent sections for obtaining the material properties for a composite plate with five woven fabric plies. The predicted material properties are then compared against test results to validate the correctness of the simplified model.

5.4 Experimental Background for Woven Fabric Composite Plates

The experiments for the woven fabric composite plates had been conducted by Moy *et al.* (see reference[11]). The experimental procedure remains the same as that for uni-directional composite plates as described in section 4.7. Twenty five woven fabric composite plates were tested to failure to investigate the effects of material composition, method of manufacture and panel aspect ratio on strength and stiffness under transverse pressure loading. The woven fabric panels relevant to this research were plain woven with 0/90 degrees rovings. The weight density of the reinforcement was 800 g/mm^2, the matrix was isophthalic polyester, Scott Bader Crystic-489. The panels were made up of five woven fabric plies, each with equal amount of fibers in the warp and weft directions. The fiber weight fraction was 0.27. The mechanical properties of the constituent materials are as shown in table 5.2.

The three plates relevant to this research referred as plate D (size 600mm $\times$ 600), Plate E (size 1200mm $\times$ 600mm) and plate F (size 1800 mm $\times$ 600mm) had aspect ratios of 1.0, 1.50 and 2.0 respectively. All the plates had a thickness of 2.83mm. All plates were produced using a vacuum-assisted resin injection-moulding technique. Here the reinforcing fabrics were cut to size and placed in the flat mould. The mould was then vacuum-sealed with a flexible covering and catalysed resin was sucked into the mould using a vacuum pump. After the correct quantity had been injected the vacuum was maintained until the laminate had cured. The vacuum seal was then removed and the edges trimmed as necessary. Panels produced in this way are often called *scrimp* panels. Typical load-deflection curves are given in figure 5.3. Typical damage pattern of plate D from the photograph taken in the laboratory is shown in figure 5.4.

5.5 Extension of the Damage Model

In section 2, a woven fabric ply was simplified as a combination of resin layers and uni-directional composite layers. In section 3, the simplification procedure for a composite plate with woven fabric plies was discussed. With these simplifications, the progressive

failure methodology developed in the last chapter for uni-directional composite materials can be applied to a composite plate with woven fabric plies. Several aspects of a progressive failure analysis, such as material property degradation scheme, ABAQUS implementation and the equilibrium aspects have already been discussed in the last chapter in detail. Progressive failure analysis is based on the assumptions that (a) the damage is localized in nature and (b) the damaged material can be substituted with an equivalent material with degraded properties. Three forms of damage and their possible combinations are considered in this research. They are (i) matrix crack, (ii) fiber breakage and (iii) fiber matrix shear. Since the plates considered were very thin, of short-span to thickness ratio of as large as 200, delamination was unlikely to occur and hence was not considered. The properties of the damaged material are adjusted as the loading and progression of damage continues. Because of the large aspect ratio of the plates out-of -plane stresses are assumed to be in-significant and hence are neglected in the progressive failure analysis. The stress analysis is done using the general purpose finite element program ABAQUS[12]. A uniform mesh size of 20×20 (400 elements) was used. The progressive failure analysis methodology uses the C^0 four node shell element S4R of the ABAQUS element library based on first order shear deformation theory, due to its better performance in large deformation analysis. The element has six degrees of freedom(three displacement and three rotation components). The element has one in-plane integration point and three through-the-thickness integration points for each layer. In a numerically integrated finite element method, material properties are selected at Gauss integration points. Therefore in the present analysis at each Gauss point, damage or failure was determined by comparing the current stress state with a specified failure criterion. To simulate damage, material properties at each failed Gauss point were reduced to values representing the particular type of damage that had occurred as shown in table 5.1. In this table the FV(variables in ABAQUS) quantities specify whether failure has occurred or not. FV1 corresponds to matrix crack; FV1=1 indicates failure due to matrix crack and FV1=0 indicates no matrix crack at an integration point. Similarly FV2=1 represents failure due to fiber/matrix shear and FV3=1 indicates failure due to fiber breakage.

5.6 Numerical Results

5.6.1 Material Properties Results

Table 5.2 shows the mechanical properties for the fiber and resin which had been used as constituent materials for the woven fabric composite plates. The simplified model developed earlier in this chapter was used to calculate the material properties of the equivalent uni-directional composite plates. They are listed in table 5.3. To confirm the validity of the simplified model, the material properties are compared with test results. However, experimental material properties are available only for the entire woven fabric composite plate. Therefore the simplified model was then extended to calculate the material properties of the five layer woven fabric composite plate. This was performed using the finite element program ABAQUS. First order shear deformation theory was used for this purpose.

The results for the longitudinal Young's modulus E_L are listed in table 5.4. The table gives predictions for E_L at different orientations to the warp directions along with the test results for them. In addition, the present model is compared against those predicted by Feng[13]. In Feng's work, the uni-directional composite layer is first subjected to in-plane strain components individually. For each individual case the constitutive relationship is derived. These are then super-imposed to obtain the constitutive relationship for the general strain state of the composite material. The classical laminated plate theory is then used for obtaining the stiffness properties of a woven fabric ply. It can be seen that the present method gives more accurate results than those given in reference[13]. Comparison against other simplified models in literature has not been shown in this table since they appear in reference[13]. Also the main focus of this chapter is to carry out a progressive failure analysis for woven fabric composite plates, rather than material property predictions for them. The sole purpose of developing the simplified model was to extend the progressive failure model developed in the last chapter to woven fabric composite plates. Table 5.5 compares the predicted shear modulus and Poisson's ratios for the woven fabric composite plate with those obtained in reference[13]. For this case experimental results were not available.

The marginal improvement in property predictions as compared to Feng[13]'s results

can be attributed to the fact that in the later case classical lamination theory was used for predicting the plate properties in contrast to the first order shear deformation theory used in the present case. Also the expressions used for predicting the material properties for the equivalent uni-directional composite plates in reference[13] are more involved as compared to the rule of mixtures approach adopted in the present procedure. Presently, the implementation of the rule of mixtures approach can be found in many commercial finite element programs including ABAQUS.

5.6.2 Central Deflection Results

Figure 5.5 compares the central deflection results due to the progressive failure model, finite element method (with out any damage) with the experimental results. The progressive failure results give better predictions when compared to the finite element results. The error in the later case was more towards the upper end of the load-deflection curves. In the initial stage the load deflection curve (from experiment) was highly nonlinear. This justifies the assumption of geometric nonlinearity in the progressive failure model. The progressive failure results were always below those of the finite element model (no damage). This is because damage in the former case reduced the structural stiffness and therefore there was more deformation at the same load level.

5.6.3 Damage Patterns and Final Failure

Figures 5.6 to 5.14 show the damage pattern obtained using the progressive failure model for plate D at different loads. The resin cracking pattern was different to that obtained in the uni-directional case (plate A). The first ply failure was due to matrix cracking. It occurred at a load of 0.02 MPa. For this no experimental value is available. However, this value seems reasonable, when compared to the first ply failure load for plate A (table 4.3). At 0.05 MPa, about 5 percent of material points had failed by matrix cracking. Unlike the uni-directional case, all the layers of the woven fabric composite plate had damage in the form of matrix cracking. At this load the crack was already advancing towards the center in the last ply. When the load was increased further, cracks started advancing towards the center in all the plies (figure

5.7). At a load of 0.10 MPa cracks also appeared along the remote transverse directions (x=0,x=600). Failure due to fiber-matrix shear first appeared at a load of 0.14 MPa in the first ply. With further increase in pressure, it propagated to the second and fifth ply. Gradually it was advancing to the center, although the damaged region due to fiber-matrix shear was concentrated in the corner regions. This is in contrast to the uni-directional case, where the damaged region due to fiber matrix breakage ran parallel to the x axis. In each ply the damage was symmetric. At 0.30 MPa about 28 percent of the material points had failed by matrix cracking. Just before failure about 58 percent of the material points had failed by matrix cracking and about 4.7 percent material points had failed by fiber-matrix shear. The failure occurred at a load of 0.45 MPa. The test failure was 0.424 MPa. This is because of the simplification of the woven fabric composite plate as a stacking sequence of uni-directional composite plates. At this stage the fourth ply had substantial number of material points failed due to matrix cracking. Unlike the uni-directional case, there was no clear indication of the failure load for woven fabric composite plates. The damage pattern predicted in these figures correlate well with the experimental observations. For example, the deep black lines parallel to the x axis in the experimental damage pattern (figure 5.4) correspond to the resin crackings in figure 5.14. In this case, the ultimate failure was due to the effect of both the matrix cracking failure and fiber-matrix shearing failure, whereas the ultimate failure in the uni-directional case was due to fiber failure. This shows that the weave architecture does contribute to increasing resistance to fiber failure.

5.7 Conclusion

In this chapter a simple theoretical model is presented for prediction of elastic properties of woven fabric composite plates. The model can estimate the stiffness properties of the woven fabric composite plate from the knowledge of the material properties of the constituents. A progressive failure analysis has been carried out on the simplified model. Comparison with experimental data has shown to be satisfactory.

The response of a woven fabric composite material is dependent on the constituent material properties, and physical location and orientation of the fiber. Therefore the quantification of the geometrical structure of the reinforcement affects the distribution

of stresses in a woven fabric composite plate. In the present case, the total quantity of fiber in the plain weave composite layer is distributed in two uni-directional composite layers. This method has been seen to work well for this particular type of woven fabric composite material, where the curvature was too small. However in the event that the curvature increases, there will be the effect of stress concentrations, which have to be take into account while estimating the strength quantities of the woven fabric composite materials.

5.8 References

1. Blackketter, D.M., Walrath, D.E. and Hansen, A.C., Modeling Damage in a Plain Weave Fabric-Reinforced Composite Material, J. of Composite Technology and Research, Vol. 15, pp.136-142 (1993)

2. Whitcomb, J. and Srirengan, K., Effect of Various Approximations on Predicted Progressive Failure in Plain Weave Composites, Composite Structures, Vol. 34, pp. 13-20 (1996)

3. Naik, R.A, Failure Analysis of Woven and Braided Reinforced Composites, J. of Comp. Mat., Vol. 17, pp.2334-2336(1995)

4. Vandeurzen, P.H., Ivens, J. and Verpoest, I., An Analytical Model of the Failure Process in Woven Fabric Composites, 8th Europ. Conf. on Comp. Mat., ECCM-8,Naples, Vol. 4, pp. 627-634 (1998)

5. Guedes, J.M. and Kikuchi, N., Preprocessing and Postprocessing for Materials Based on The Homogenization Method with Adaptive Finite Element Methods, Comput. Meth. in Appl. Mech. and Engg., Vol. 83, pp. 143-198 (1990)

6. Bogdanovich, A.E. and Pastore, C.M., Mechanics of Textile and Laminated Composites, Chapman and Hall, London(1996).

7. Dow, N.F. and Rammath, V., Analysis of Woven Fabrics for Reinforced Composite Materials, NASA CR 178275 (1987).

Table 5.1: Material Property Degradation Scheme

Failure Mode	Material Properties				FV1	FV2	FV3
No Failure	E_x	E_y	ν_{xy}	G_{xy}	0	0	0
Matrix Failure	E_x	0	0	G_{xy}	1	0	0
Fiber/Matrix Shear Failure	E_x	E_y	0	0	0	1	0
Matrix Failure and Fiber/Matrix Shear Failure	E_x	0	0	0	1	1	0
Fiber Breakage	0	0	0	0	0	0	1
Matrix Failure and Fiber Breakage	0	0	0	0	1	0	1
Fiber/Matrix Shear Failure and Fiber Breakage	0	0	0	0	0	1	1
All Failure Modes	0	0	0	0	1	1	1

8. Pollock, P.B., Tensile failure in 2-D Carbon-Carbon Composites, Carbon, Vol. 28, pp. 717-732(1990).

9. Naik, R.A., Analysis of Woven and Braided Fabric Reinforced Composites, NASA CR-194930 (1994).

10. Chamis, C.C., Simplified Composite Micro-Mechanics Equations for Mechanical, Thermal and Moisture-Related Properties, Engineer's Guide to Composite Materials, American Society for Metals, Vol. 17, pp. 399-413

11. Moy, S.S.J., Shenoi, R.A. and Allen, H.G., Strength and Stiffness of Fiber Reinforced Plastic Plates, Proceedings of the Institution of Civil Engineers, Vol. 116, No. 2 1996, pp. 204-220

12. ABAQUS/Standard User's Manual, Version 5.6, Hibbit,Karlsson and Sorensen, Inc, 1996, RI, USA

13. Feng, Z.N., Thin FRP Composite Panels Under High Transverse Pressure, PhD Thesis, University of Southampton, 1998

Table 5.2: Mechanical Properties of E-glass(Yarn)/polyester(Resin)

	Yarn Properties	Resin Properties
Stiffness(MPa)	E_f=70000	E_m=3500
G_f=26923	G_m=1346	
Strength(MPa)	S_{ft}=2400	S_{mt}=65
Strength(MPa)	S_{fc}=2160	S_{mc}=130
		S_{ms}=65

Table 5.3: Stiffness and Strength Properties of Each Layer in the Equivalent Uni-Directional Composite Plate

Stiffness Properties	Strength Properties
E_x(MPa) = 39875	X_T(MPa)=1050
E_y(MPa) = 14181	X_C(MPa)=950
ν_{xy}= 0.3	Y_T(MPa)=55
G_{xy}(MPa) = 5127	Y_C=110
	S(MPa)=55

Table 5.4: Comparison of Longitudinal Young's Modulus E_L

Inclination to the warp direction (in degrees)	E (Present Model)	E (Feng[12])	E (Test)
0	27.17	27.2	27.1
22.5	20.1	19.8	19.2
45	15.77	15.6	15.6
67.5	20.6	19.8	20.7
90	27.17	27.2	27.0

Table 5.5: Comparison of Overall Shear Modulus and Poisson's Ratio

Inclination to the warp direction (in degrees)	G (Present Model)	G (Feng[12])	ν_{xy} (Present Model)	ν_{xy} (Feng[12])
0	5.02	5.1	0.156	0.157
22.5	7.0	7.1	0.156	0.157
45	11.7	11.8	0.156	0.157
67.5	7.0	7.1	0.156	0.157
90	5.23	5.10	0.156	0.157

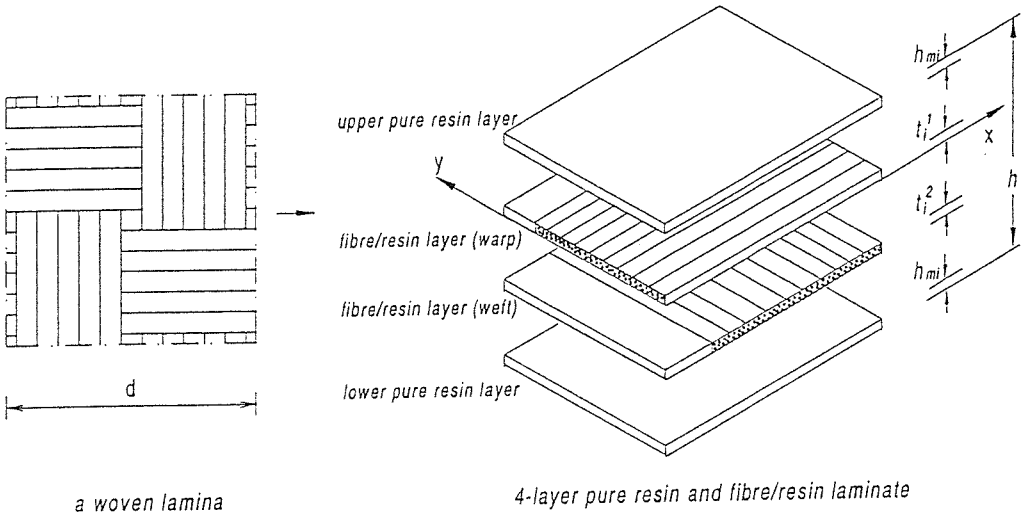

Figure 5.1: A Woven Lamina in the Simplified Model

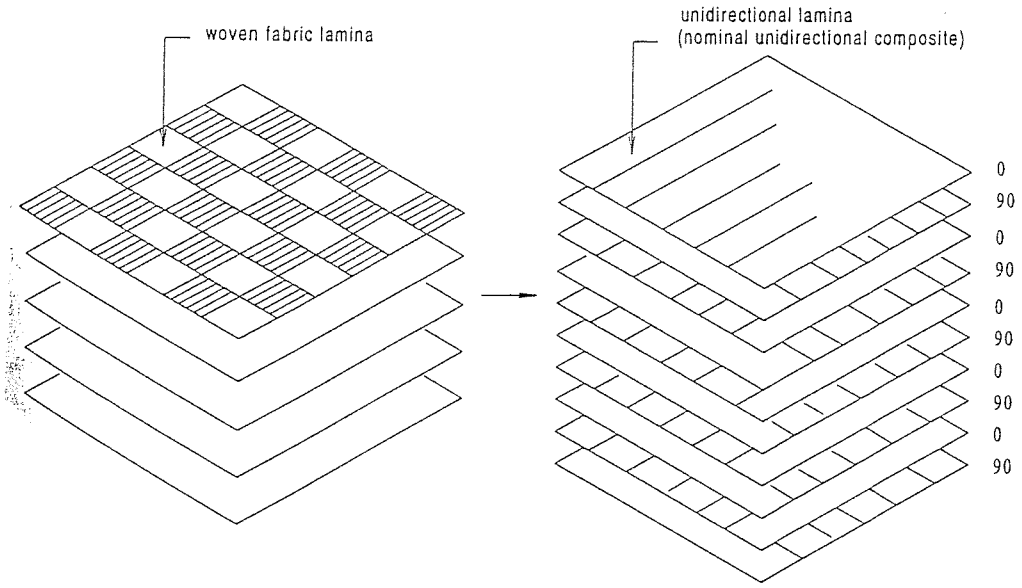

Figure 5.2: A Five-Layer Woven Fabric Composite Plate is Simplified as 10-Layer Cross-Ply Uni-Directional Composite Plate

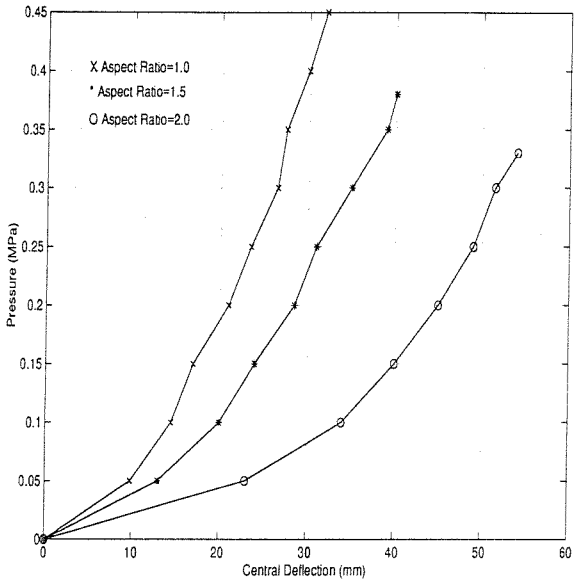

Figure 5.3: Load-Central Deflection Graphs : Test Results

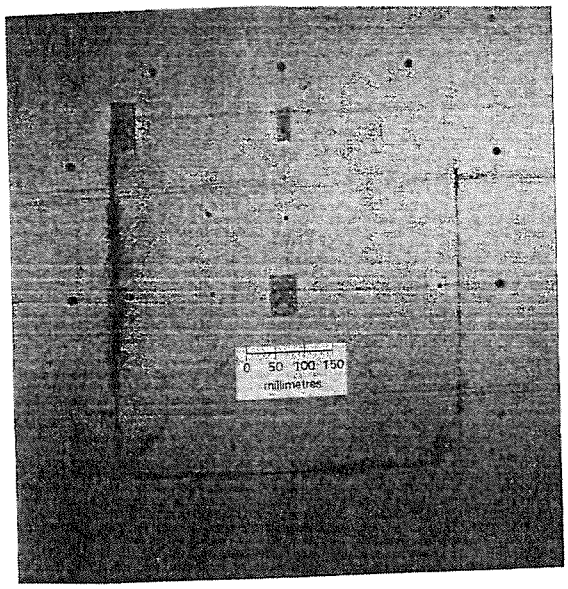

Figure 5.4: Detail of Failure Mechanism for Plate D (From Experiment)

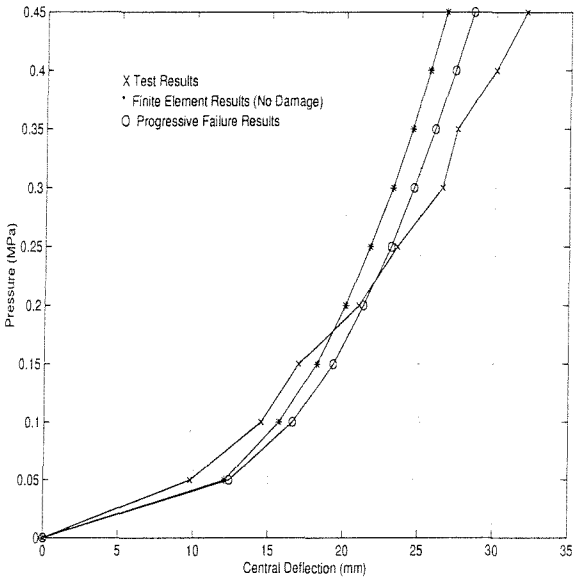

Figure 5.5: Central Deflection for Plate D

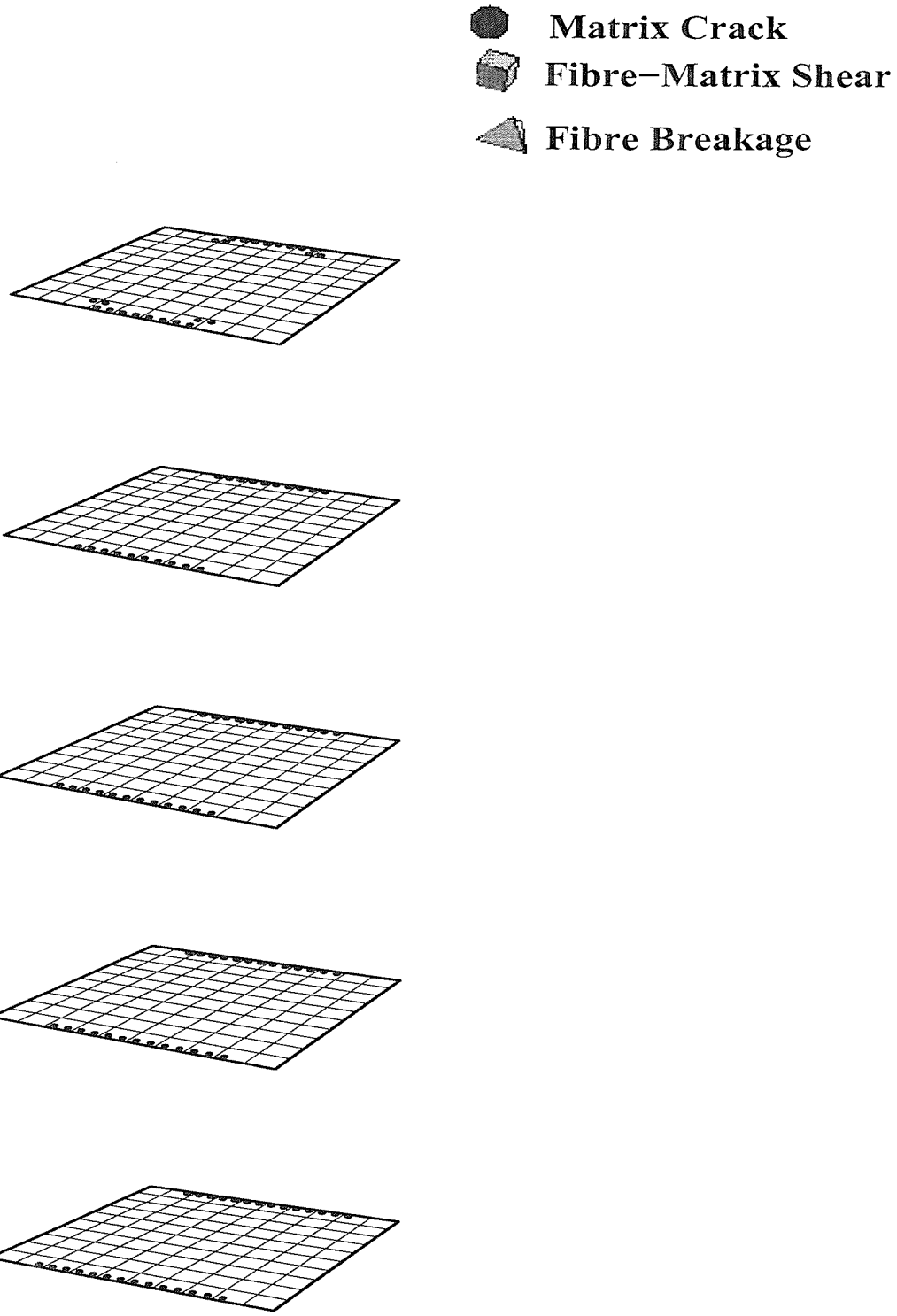

Figure 5.6: Damage Pattern for Plate D at 0.05 MPa

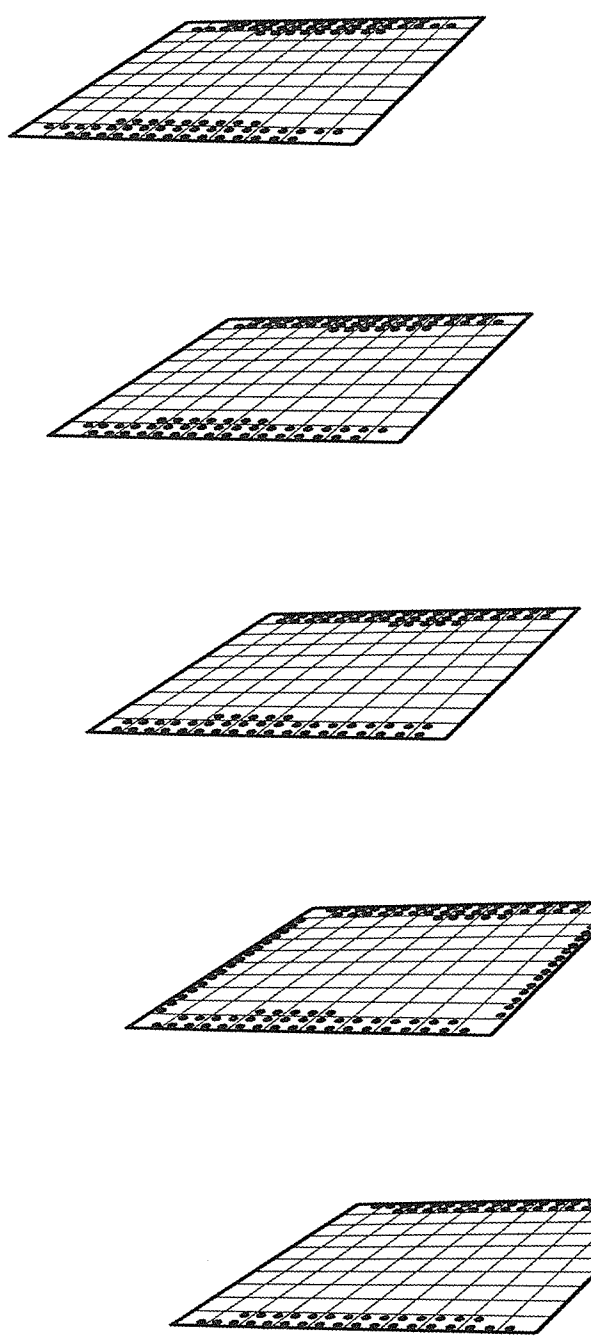

Figure 5.7: Damage Pattern for Plate D at 0.10 MPa

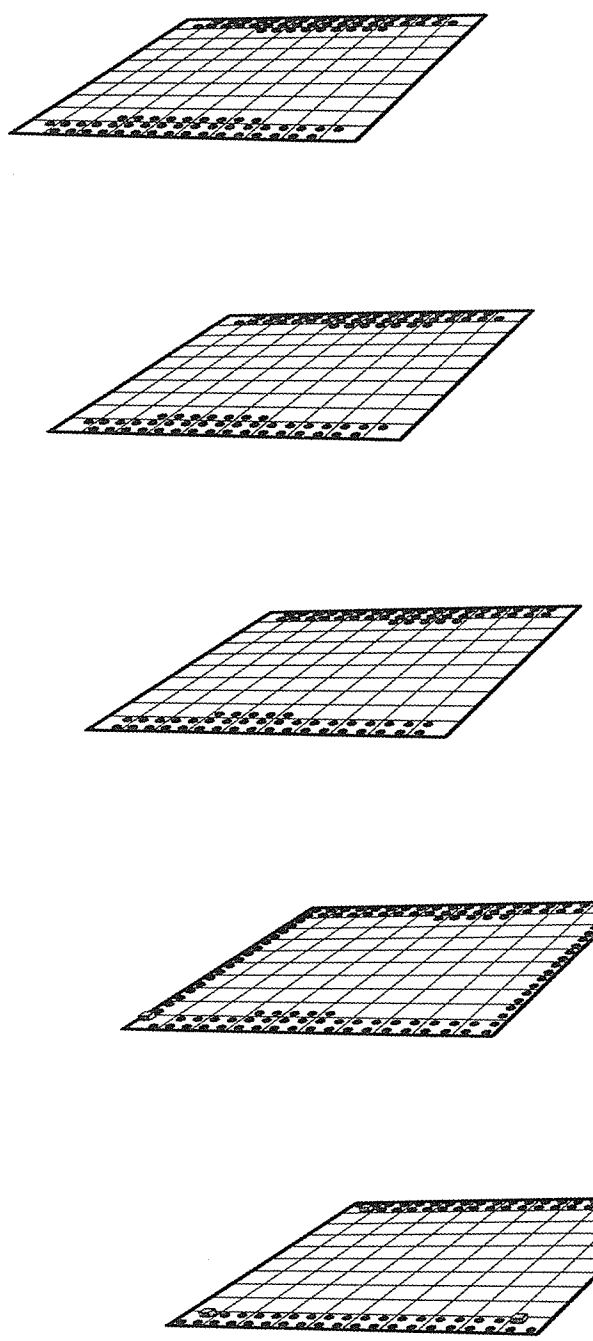

Figure 5.8: Damage Pattern for Plate D at 0.15 MPa

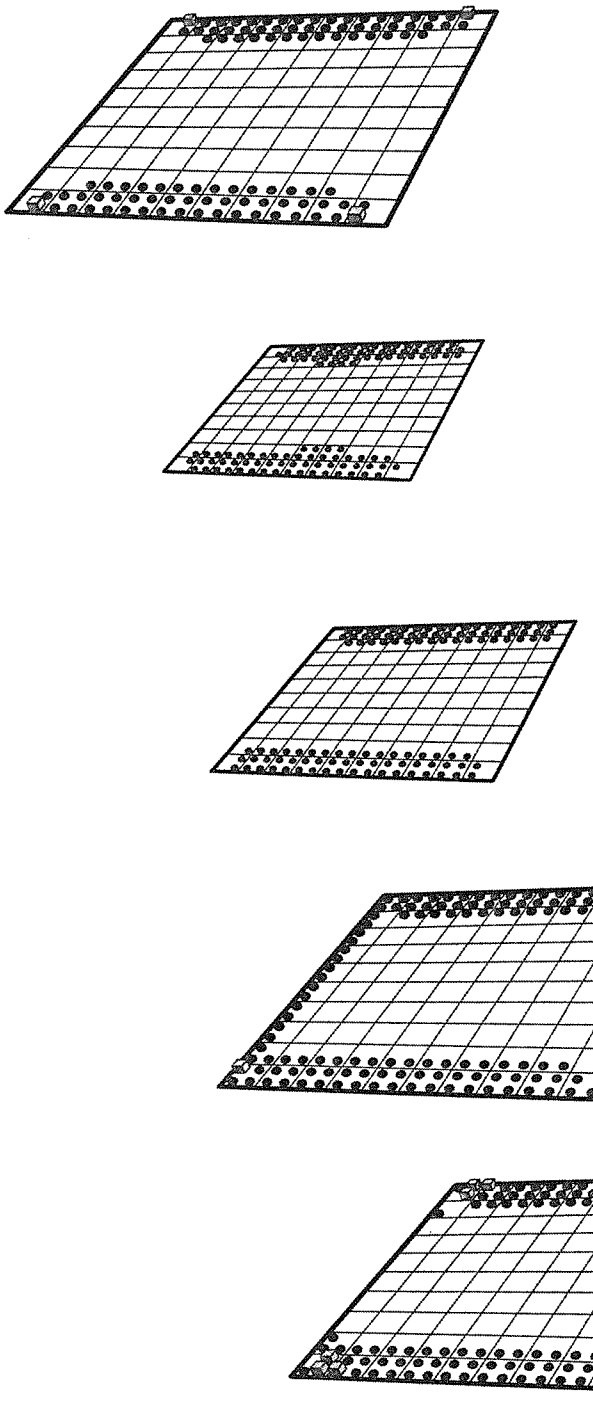

Figure 5.9: Damage Pattern for Plate D at 0.20 MPa

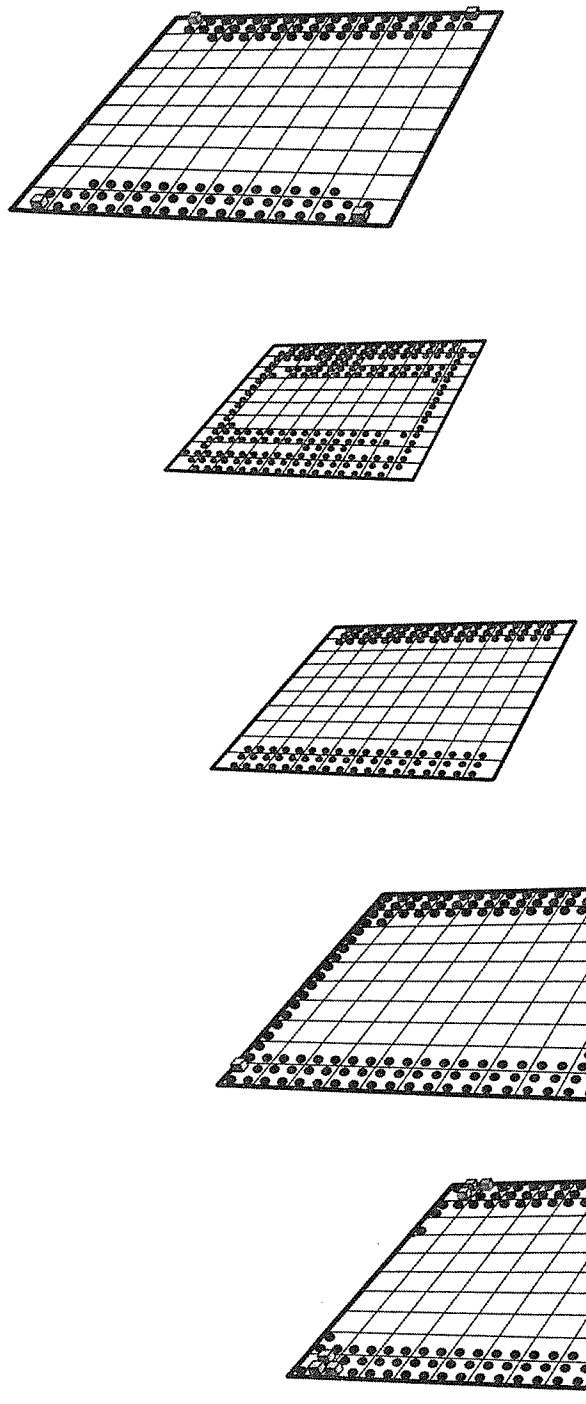

Figure 5.10: Damage Pattern for Plate D at 0.25 MPa

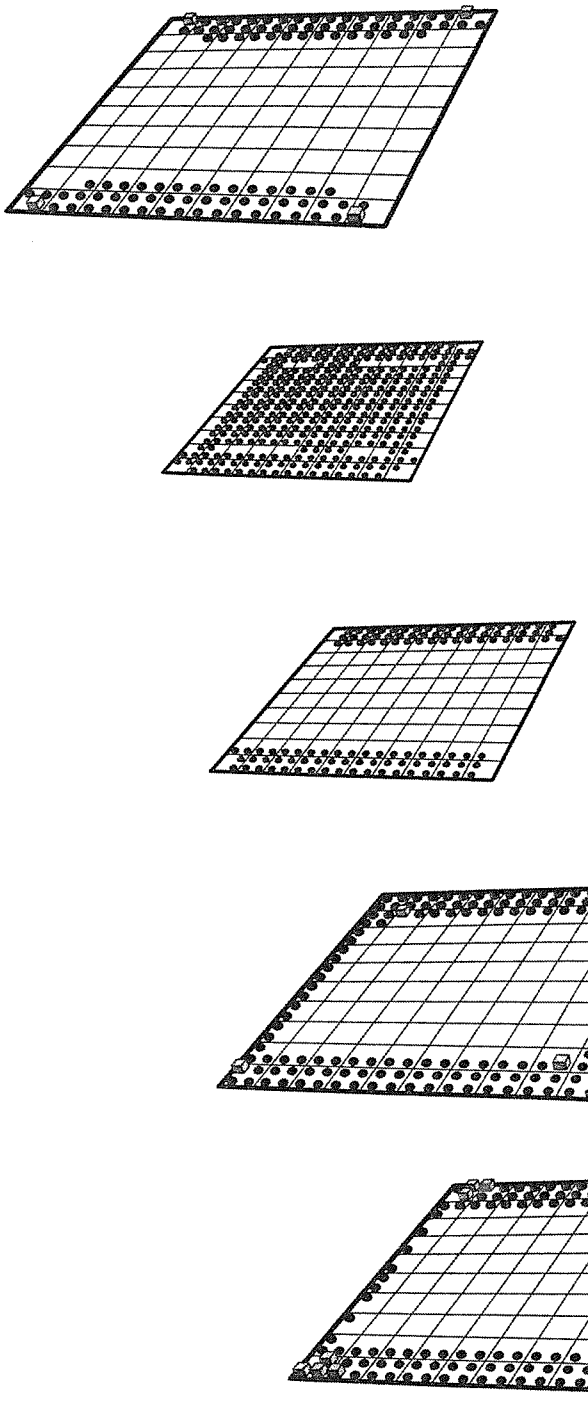

Figure 5.11: Damage Pattern for Plate D at 0.30 MPa

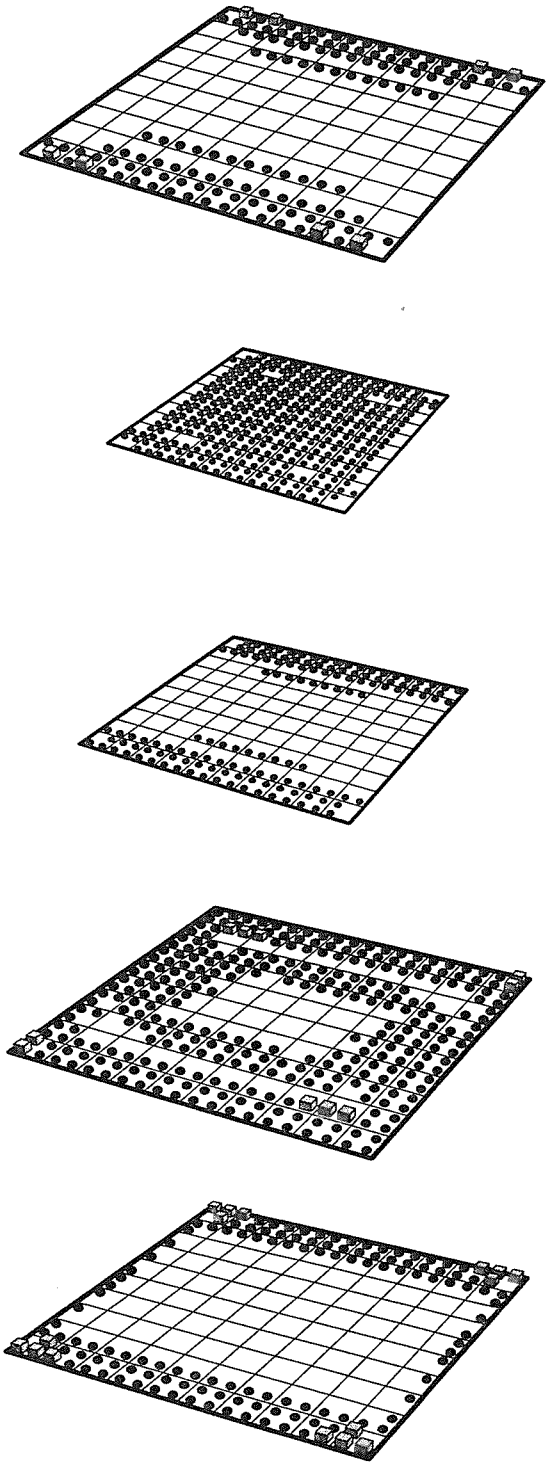

Figure 5.12: Damage Pattern for Plate D at 0.35 MPa

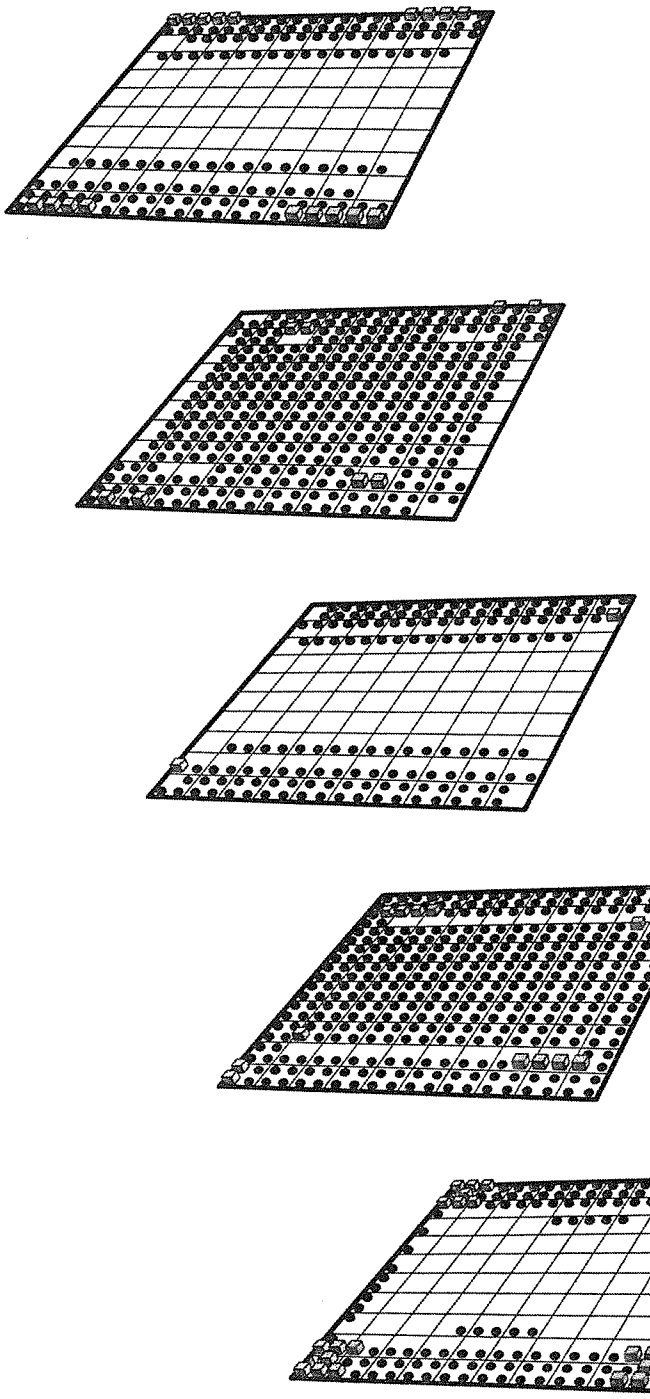

Figure 5.13: Damage Pattern for Plate D at 0.40 MPa

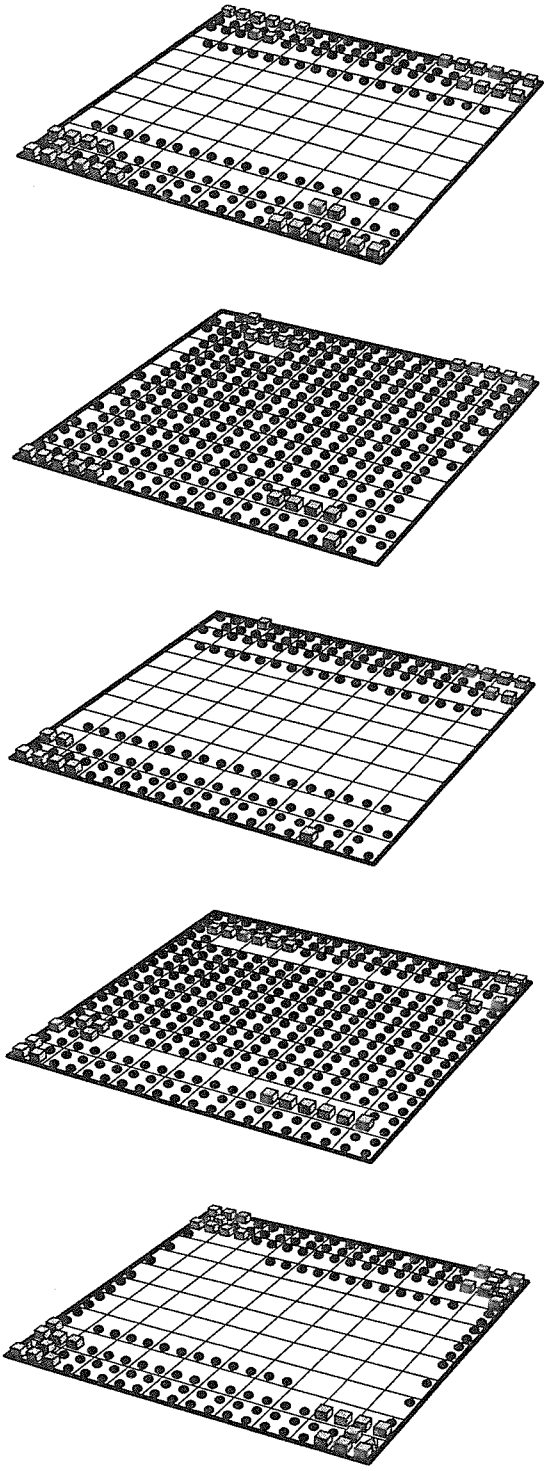

Figure 5.14: Damage Pattern for Plate D at 0.45 MPa (Just Before Failure)

Chapter 6

Stress Analysis of 2-D Orthotropic Structures Using the Boundary Element Method

6.1 Introduction

In the last two chapters the progressive failure methodology based on the finite element method was applied to uni-directional and woven fabric composite structures. The other available numerical method of stress analysis is the boundary element method. An important feature of the BIE method is that instead of attempting to find an approximate solution for the governing differential equation throughout the relevant solution domain, as in domain methods such as finite element or finite difference approaches, the equation is converted into an integral form, often involving only integrals over the boundary of the solution domain. Consequently, only the boundary has to be discretized in order to carry out the integrations. The dimensionality of the problem is thereby effectively reduced by one: a three dimensional volume problem becomes a two-dimensional surface one, while a two-dimensional plane problem involves only one-dimensional line integrations. Also, because the interior of a solution domain is not discretized, there is much less approximation involved in representing the solution variables.

In the analysis of complex problems created by the use of composite materials a de-

tailed and accurate calculation of stresses in the regions of rapid stress variation is often required for general design purposes. For these cases where the resolution of high stress gradients and complex geometries is required, the boundary element method is particularly well suited. The literature available on BIE implementation in isotropic elasticity is large[1,2,3]. However it is only comparatively recently that numerical implementations for anisotropic problems have been reported. Rizzo and Shippy[4] presented the first application of the BEM to plane anisotropic problems, while Vogel and Rizzo[5] presented an integral representation for three-dimensional problems. Deb and Banerjee[6] have applied the method of particular integrals to the case of two-dimensional anisotropic problems in the case of inertial and centrifugal loads where a closed form solution is available. Deb *et, al*[7] presented a BEM formulation for two and three-dimensional anisotropic thermo-elasticity using particular integrals. A more general formulation has been presented by Grundemann[8] based on Fourier series expansions.

In this chapter, stress analysis of 2-D orthotropic structures is carried out using the boundary element method. Computational accuracy of different element types, such as quadratic, linear and constant, are assessed. The deformation, and gradient quantities such as stresses and strains obtained, can be used in the stress-based or strain-based failure criteria for carrying out a failure assessment for them. An attempt is made to keep this chapter as self-contained as possible. The next section reviews the two distinct approaches for the integral equation formulation in orthotropic elasticity. Section 3 outlines the necessary fundamental solutions for carrying out a boundary element analysis. The numerical implementation aspects are discussed in section 4. The core of this chapter is section 5 , in which a novel method is developed for computation of singular integrals. Numerical examples are presented in section 6 and finally, concluding remarks are given in the last section.

6.2 Integral Equation Approaches for 2-D Orthotropic Plane Problems

Various approaches to the numerical implementation of BIE in anisotropic elasticity can be found in the literature. Broadly they can be grouped into two categories.

In the first, the isotropic fundamental solution (Kelvin's solution) is still used. This results in a volume integral term associated with the anisotropy of the material, which is numerically treated by discretizing the domain into internal cells[9]. In the second category, anisotropic fundamental solutions similar to Kelvin's solution for isotropic elasticity are used. These fundamental solutions can be based on functions of either the real variable or the complex variable.

Rizzo and Shippy[4] first used the two-dimensional anisotropic fundamental solution presented by Green[10] in a real variable direct boundary integral equation formulation. Constant elements were used in modeling the geometry and approximating the field variables such as displacements and tractions. Mahajerin and Sikarskie[11] used BIE based on real variables for calculating stress concentration factors in double lap joints for different hole sizes. Constant elements were used in the numerical implementation. Vable and Sikarskie[12] presented analytical expressions for integrals of Green's functions for BIE based on real variables. BIE based on the real variable approach was also used by Benjumea and Sikarskie[13]. Snyder and Cruse[14] were the first to use the complex variable anisotropic fundamental solution for determining stress intensity factors in linear elastic, finite anisotropic plates under conditions of plane stress or plane strain and containing a single traction free crack. This spurred further work based on the complex variable fundamental solutions. Tan *et, al*[15] used the BIE based on complex variable fundamental solutions for solving some inclusion problems. Tan and Gao[16] used the BIE method to solve stress concentration problems. Lee and Mal[17] presented a complex-variable approach, where the integral equations were discretized in the complex plane. Perez and Wrobel[9] developed an alternative integral-equation formulation for the numerical analysis of homogeneous anisotropic linear elastostatic problems. This led to a form of Somigliana's identity which included a domain term that accounts for anisotropy of the material.

6.3 The BIE Method For Plane Orthotropic Elasticity

The development of the boundary element method for orthotropic materials under plane stress follows the same steps as in isotropic elasticity[1,2,3]. It is based on unit load solutions in an infinite body known as the fundamental solutions. Use of these solutions with the Betti-Rayleigh reciprocal work theorem and carrying out the appropriate mathematical limiting operations will result in the BIE for the displacements at an interior point p due to tractions and displacements on the surface at a boundary point Q. In the absence of body forces it can be written as follows:

$$u_k(p) + \int_\Gamma T_{kl}(p,Q)u_k(Q)d\Gamma(Q) = \int_\Gamma U_{kl}(p,Q)t_k(Q)d\Gamma(Q) \tag{6.1}$$

where $u_k(p)$ are the displacements in the x_k directions at the interior point p, $u_k(Q)$ and $t_k(Q)$ are the displacements and tractions respectively at the boundary point Q, and the kernel functions U_{kl} and T_{kl} are unit load solutions in an infinite domain and are as given in the next two subsections. From the expressions for the fundamental solutions it can be inferred that the first integral in equation (6.1) has $\frac{1}{r}$ singularity and the second integral has $\log\frac{1}{r}$ singularity when p approaches the boundary of the domain.

6.3.1 The Real Variable Approach

For a homogeneous orthotropic body under plane stress, use of Hooke's law, the equations of equilibrium and the compatibility conditions result in the governing equation as,

$$S_{22}\frac{\partial^4\phi}{\partial x_1^4} + (2S_{12} + S_{66})\frac{\partial^4\phi}{\partial x_1^2\partial x_2^2} + S_{66}\frac{\partial^4\phi}{\partial x_2^4} = 0 \tag{6.2}$$

Where S_{mn} are the elastic compliances of the material. In terms of engineering constants, these compliances may be expressed as:

$$S_{11} = 1/E_1;\ \ S_{22} = 1/E_2$$

$$S_{66} = 1/G_{12}; \quad S_{12} = -\nu_{12}/E_1 \tag{6.3}$$

If equation 6.2 is re-written as:

$$\left(\frac{\partial^2}{\partial x_1^2} + \alpha_1 \frac{\partial^2}{\partial x_2^2}\right)\left(\frac{\partial^2}{\partial x_1^2} + \alpha_2 \frac{\partial^2}{\partial x_2^2}\right)\phi = 0 \tag{6.4}$$

then it can be shown that the α_i satisfy the following equations:

$$\alpha_1 + \alpha_2 = (2S_{12} + S_{66})/S_{22} \tag{6.5}$$

$$\alpha_1 \alpha_2 = S_{11}/S_{22} \tag{6.6}$$

Here the α_i are taken to be real and positive which is true for a large number of materials including those materials for which results are reported.

Thus, the solution of a two-dimensional problem reduces to finding a solution of equation (6.4) that satisfies the boundary conditions of the problem.

The stress function which satisfies equation (6.4) and corresponds to an isolated force at the origin in an infinite sheet can be found in (equation. 4.1 of) Green's work[10]. The displacement field corresponding to this stress function has been derived by Rizzo and Shippy[4] and is written as:

$$U_{kl} = K_a \begin{bmatrix} \alpha_1^{\frac{1}{2}} A_2^2 \log r_1 - \alpha_2^{\frac{1}{2}} A_1^2 \log r_2 & -A_1 A_2(\theta_1 - \theta_2) \\ -A_1 A_2(\theta_1 - \theta_2) & \alpha_1^{\frac{-1}{2}} A_1^2 \log r_1 - \alpha_2^{\frac{-1}{2}} A_2^2 \log r_2 \end{bmatrix} \tag{6.7}$$

Here $K_a = \frac{1}{\beta}$ and β is the magnitude of the force components, associated with the stress function, at the origin, acting in the positive x_i direction , as identified by Green[10], and is given by:

$$\beta = 2\pi(\alpha_1 - \alpha_2)S_{22} \tag{6.8}$$

Other constants are given by:

$$A_i = S_{12} - \alpha_i S_{22} \tag{6.9}$$

$$r_i^2 = x_1^2 + \alpha_i^{-1} x_2^2 \tag{6.10}$$

$$\theta_i = \arctan(x_2/\sqrt{\alpha_i} x_1) \tag{6.11}$$

Differentiation of the above displacement field with respect to x_1 and x_2 and substitution in Hooke's law results in the fundamental traction fields due to concentrated loads at the origin of the coordinate system. These can be written as follows:

$$T_{kl} = K_a \begin{bmatrix} x_k n_k \left(\frac{A_1}{\sqrt{\alpha_2} r_2^2} - \frac{A_2}{\sqrt{\alpha_1} r_1^2}\right) & \left(M_1 \frac{A_1}{r_1^2} - M_2 \frac{A_2}{r_2^2}\right) \\ \left(M_1 \frac{A_1}{\sqrt{\alpha_1} r_1^2} - M_2 \frac{A_2}{\sqrt{\alpha_2} r_2^2}\right) & x_k n_k \left(\frac{A_1}{\sqrt{\alpha_1} r_1^2} - \frac{A_2}{\sqrt{\alpha_2} r_2^2}\right) \end{bmatrix} \tag{6.12}$$

where

$$M_i = \sqrt{\alpha_i} x_1 n_2 - \frac{1}{\sqrt{\alpha_i}} x_2 n_1 \tag{6.13}$$

and n_i are the two components of the unit outward normal.

6.3.2 The Complex Variable Approach

This approach also originates from equation (6.2). By introducing operator $D_s, (s = 1, 2, 3, 4)$, as

$$D_s = \frac{\partial}{\partial x_2} - \mu \frac{\partial}{\partial x_1}$$

equation (6.2) becomes

$$D_1 D_2 D_3 D_4 (\phi) = 0 \tag{6.14}$$

and μ_s are the four roots of the characteristic equation

$$S_{11}\mu^4 - S_{16}\mu^3 + (2S_{12} + S_{66})\mu^2 - S_{26}\mu + S_{22} = 0 \tag{6.15}$$

Where $S_{16} = S_{26} = 0$ for an orthotropic material.

Lekhnitskii[31] has shown that the four roots of this equation are never real and are always distinct so long as the material is not isotropic. They may be denoted by

$$\mu_j = \alpha_j + i\beta_j$$

$$\overline{\mu}_j = \alpha_j - i\beta_j \qquad j = 1,2 \tag{6.16}$$

Where $i = \sqrt{(-1)}$ and $\beta_j > 0$ from thermodynamic considerations. Thus the characteristic directions may be denoted by

$$z_j = x_1 + \mu_j x_2 \qquad j = 1,2 \tag{6.17}$$

and their complex conjugates.

With this background and following the usual definitions of the fundamental solutions; point source solution in an infinite sheet, the explicit expressions for the displacement and traction kernel functions can be derived. These expressions have been derived in reference[14]. They are given below.

$$U_{kl} = 2Re[p_{l1}a_{k1}Log(z_1) + p_{l2}a_{k2}Log(z_2) \qquad k,l = 1,2 \tag{6.18}$$

$$T_{k1} = 2n_1 Re[\mu_1^2 a_{k1}/z_1 + \mu_2^2 a_{k2}/z_2] - 2n_2 Re[\mu_1 a_{k1}/z_1 + \mu_2 a_{k2}/z_2] \tag{6.19}$$

$$T_{k2} = 2n_1 Re[\mu_1 a_{k1}/z_1 + \mu_2 a_{k2}/z_2] - 2n_2 Re[a_{k1}/z_1 + a_{k2}/z_2] \qquad k = 1,2 \tag{6.20}$$

Where the first subscript refers to the direction of the displacement of the boundary point Q caused by a unit load at the interior load point p in the direction given by the the second subscript.

6.4 Numerical Implementation

To solve the BIE, equation (6.1) numerically, the boundary of the solution domain may be divided into a series of line elements, each with three nodes. The boundary geometry, displacements and tractions over each of these elements may be assumed to vary, as in the present work, in a quadratic manner. Substitution of these isoparametric representations into equation (6.1) will result in a set of linear algebraic equations for the unknown displacements and tractions at the nodes on the boundary of the solution domain. These linear algebraic equations may then be solved by standard matrix solution techniques.

6.5 Numerical Integration

The accuracy of the boundary element method for elastostatics problems is critically dependent upon the proper evaluation of the boundary integrals. These integrals, which involve the fundamental solution and element shape functions, present, in two-dimensional elasticity, a singular behavior of the order $\log \frac{1}{r}$ and $\frac{1}{r}$ for the displacements and tractions fundamental solutions respectively, where r is the distance from a source point to the element under evaluation.

The use of the Gaussian quadrature integration rule has been shown to give satisfactory results when the source point is far from the field element over which the integration is being carried out. For the case when the source point and the field point are coincident (singular integrals) or they are at a short distance in comparison with the size of the element (nearly singular integrals) various numerical integration schemes have been used over the years in order to limit the error of the numerical integration required. It was found that accuracy can be maintained with some degree of computational efficiency by methods that test the relative proximity of source points and boundary elements being integrated, and strategically assign the number and location of integration points to be employed in the integrations. Generally, algorithms that exploit this concept have relied on either an element subdivision such as the works of Lachat and Watson[18] and Jun *et al*[19] or a co-ordinate transformation technique as presented by Telles[20].

The use of Taylor series expansion proposed originally for singular integrals by Aliabadi *et al.*[21] have been receiving a great deal of attention lately with the works of Guiggiani and Gigante[22] and Guiggiani *et al.*[23] on a general formulation for singular and hyper-singular integrals and Cruse[24] for near singular integrals.

The earliest approach for calculating the strongly singular integrals has been the use of the rigid body motion technique[25] that indirectly gives the sum of these integrals and the free term coefficients. Another approach has been to regularize the singular integral equations in which the strength of the highest singularity is reduced by order one. The literature available on regularization techniques is too extensive to discuss here. For weakly singular integrals, numerical techniques, including special weighted quadratures and mapping methods have been reported in the literature. Tanaka *et al*[26]

have summarized the regularization procedures for both singular and hyper-singular integral equations that have appeared in the literature and therefore no attempt is made here to discuss these techniques. It is evident that mathematical similarity often exists in these techniques. In a series of papers Guiggiani *et al*[23,27,28,22] have tried to evaluate the strongly singular and hyper-singular integrals directly. In these papers the original boundary is recast with an exclusion zone e_ϵ and a spherical boundary bump S_ϵ (figure 6.1). Integration over S_ϵ is performed analytically, independent of discretization. For calculating the limit of the integral over $\Gamma - e_\epsilon$, the exclusion zone is mapped on to the intrinsic coordinate space and the singular integrands are expanded into Laurent series about the singular point. The singular integrals in the series expansion are evaluated analytically with canceling of the divergent terms, the limit is taken.

The rest of this section briefly describes the computational methodology adopted for computing the singular integrals in 2-D BEM. For more details, reference can be made to Padhi *et al.*[29].

Because of the singular nature of the fundamental solutions, equation (6.1) has to be set up in a limiting form to obtain the boundary integral equation suitable for numerical implementation. Assuming the body can be represented as shown in figure 6.1 with the point P (which is really a boundary point) as an internal point surrounded by part of a spherical surface S_ϵ of radius ϵ, equation (6.1) can be written as

$$u_k(P) + \int_{\Gamma - e_\epsilon + S_\epsilon} T_{kl}(P,Q) u_k(Q) d\Gamma(Q) = \int_{\Gamma - e_\epsilon + S_\epsilon} U_{kl}(P,Q) t_k(Q) d\Gamma(Q) \qquad (6.21)$$

As discussed in references[23,27] , the surrounding zone S_ϵ need not be a spherical surface. To arrive at the boundary integral equation, the limit of equation (6.21) has to be found as $\epsilon \to 0$. If the integrals in equation (6.21) are broken into summation of integrals over the regions $\Gamma - e_\epsilon$ and S_ϵ and their limits as $\lim_{\epsilon \to 0}$ are studied, it can be shown that the limit quantity which often needs special treatment is

$$I = \lim_{\epsilon \to 0} \int_{\Gamma - e_\epsilon} T_{kl}(P,Q) u_k(Q) d\Gamma(Q) \qquad (6.22)$$

6.5.1 Direct Numerical Evaluation of the Limit

The limiting integral is evaluated using Euler's transformation technique as follows. Even though the individual integrands in the right hand side of equation (6.21) are not defined at $\epsilon = 0$, the integral quantity I exists and can be evaluated without evaluating the integrands at the singular point.

A sequence of values of ϵ decreasing in magnitude and approaching but not equal to zero are chosen. These values can be represented as $\epsilon_0, \epsilon_1, \epsilon_2 ... \epsilon_n$ and the corresponding finite integral values can be represented as $I_0, I_1, I_2 ... I_n$. The limit of this sequence, $\lim_{n\to\infty} I_n$, is the desired quantity, and is calculated as follows. If a new sequence is formed as

$$I_1 - I_0, I_2 - I_1, \cdots I_n - I_{n-1} \tag{6.23}$$

then

$$\lim_{n->\infty} I_n = I_0 + \lim_{n->\infty} (I_1 - I_0 + I_2 - I_1 + \cdots I_n - I_{n-1}) \tag{6.24}$$

The second part of the right hand side can be approximated from n difference quantities using Euler's transformation technique (see appendix) which gives an infinite sum through finite sampling as

$$\lim_{n\to\infty} (I_1 - I_0 + I_2 - I_1 + \cdots I_n - I_{n-1}) = EulerSum\,(I_1 - I_0 + I_2 - I_1 + \cdot sI_n - I_{n-1}) \tag{6.25}$$

Once the approximated infinite sum is calculated, it is back substituted in equation (6.24) and the limiting value of the integral is found.

6.5.2 Computer Implementation

The above algorithm for obtaining the limit of a function has been implemented in the symbolic computer program *Mathematica 3.0* [30] as a standard AddOn Package. The corresponding function is NLimit. All the limit integrals are evaluated directly using the Euler's transformation technique. No unbounded terms arise when the singular point p is taken to the boundary, since the unbounded divergent terms cancel each other

out. The implementation of Euler's transformation technique for finding an infinite sum makes no assumptions regarding the strength of singularity or dimensionality of the problem. Therefore it can be extended to more complicated 3-D and hyper-singular formulations. The number of finite terms to choose in the Euler's transformation technique depends on rate of convergence of the function for which the limit is to be evaluated. In the present analysis, five terms were satisfactory.

The computing work was done on a Silicon Graphics Work Station running under Irix 6.0 operating system with an 195 MHZ IP28 Iris processor with 128 Mbytes of main memory.

6.6 Numerical Examples

Four examples are considered for illustration purposes. In all cases three different element types; constant, linear and quadratic are studied for comparison purposes. Furthermore, in each problem, the number of nodes is kept constant for all the three element types, so as to attain a realistic comparison of numerical efficiencies. No units have been chosen so that any compatible set of units, whether SI or Imperial, can be used provided they are consistent. Also in the examples whenever boundary stresses are determined, the stresses along the tangential direction to the boundary are determined from differentiation of the shape functions and use of the constitutive equations.

Example 1: This deals with an infinite plate with a circular hole, at the boundary of which uniform hydrostatic pressure is applied. The material properties are

$$E_x = 1.2; \qquad E_y = 0.6$$

$$G_{xy} = 0.7; \qquad \nu_{xy} = 0.071$$

This problem is solved using 12 quadratic boundary elements along the hole boundary. Following usual boundary element discretization, since the domain is infinite, the node numbering is done in reverse (clockwise) direction. To compare the numerical efficiency of the present approach with the results obtained in literature, the same problem is solved with 24 linear elements and 24 constant elements, so that the number of nodes remains same.

Figure 6.2 shows the numerical results for hoop stress ($\sigma_{\theta\theta}$) obtained using the present approach along with the analytical results due to Lekhntiskii[31]. The error is found to be less than 0.5 % when quadratic elements are used, whereas it is about 3% with linear elements and more than 10% with constant elements. It may be noted that although accurate results were obtained by Rizzo and Shippy[4], considerably more nodes were used (24 nodes for one quarter of the hole), which will increase both the computational time and the computer storage space significantly.

Figure 6.3 compares the deformed shape of one quarter of the hole boundary of unit radius with the exact one, which is an ellipse[31]. A' and B' represent the deformed positions of the corresponding points A and B on the hole boundary. The deformed shape obtained using quadratic, linear and constant elements are shown in the same figure, with the average error being 0.5%, 3% and 10% respectively.

Example 2: This deals with an infinite orthotropic plate containing a circular hole at the surface of which tangential stress is applied(figure 6.4). The boundary element mesh and the material properties remain the same as in example 1. Figure 6.4 shows the hoop stress distribution along the boundary of the hole. Results are given for one quarter of the hole, at 7.5^o intervals proceeding counterclockwise around the edge of the hole starting at the x-axis. As can be seen, the present approach gives an error less than about 0.5%.

Example 3: Here the infinite plate, with a circular hole at the center is subjected to remote tension in the x-direction. Again the boundary element discretization remains the same as in example 1. Two cases are considered. First the grains(fibers) are oriented in the x-direction($E_x > E_y$). Figure 6.5 shows the numerical results for the hoop stress $\sigma_{\theta\theta}$ for this case. In the second case the grains(fibers) are oriented in the y-direction($E_x < E_y$) and the corresponding numerical results for hoop stress $\sigma_{\theta\theta}$ at the hole boundary are shown in figure 6.6. In both cases exact solutions are taken from Lekhntiskii[31]. For both cases the error when using quadratic elements was less than 1%, while it was about 3% and 10% respectively when linear and constant elements were used.

Example 4: This considers an infinitely long(in z direction) orthotropic plate simply supported along the long edges(x=0, x=L) and subjected to sinusoidally dis-

tributed load at the top surface of the form $q(x) = q_0 \sin(\pi x/L)$. It is assumed to be under plane strain condition.

The material parameters for this problem are as follows:

$$E_x = 25 \times 10^6 \quad E_y = E_z = 10^6$$

$$G_{xy} = G_{xz} = 0.5 \times 10^6 \quad G_{yz} = 10^6$$

$$\nu_{xy} = \nu_{xz} = \nu_{yz} = 0.25$$

To compare the present results with Pagano's 3-D elasticity solution[32] the stresses and displacements are normalized in the form of Pagano and are written as:

$$\overline{w} = \frac{100 E_y h^3 w(L/2, 0)}{q_0 L^4}; \qquad \overline{y} = \frac{y}{h} \qquad \text{and} \qquad \overline{\tau}_{xy} = \frac{\tau_{xy}(0, y)}{q_0} \tag{6.26}$$

where w is the maximum central deflection, h is plate thickness and q_0 is the maximum amplitude of the sinusoidally distributed load at the top surface. This problem is solved using 8 quadratic elements(for aspect ratio L/h=4), although more elements were added for higher aspect ratios. Since the problem is one of plane strain modified compliances were used.

Figure 6.7 compares the normalized maximum deflection obtained by the present approach using quadratic, linear and constant elements with the results given by the 3-D elasticity solution[32] for different L/h ratios. As can be seen present BEM results with quadratic elements closely follow the elasticity solution with less than 0.5% error, while the errors using linear and constant elements are 3% and 10% respectively.

Figure 6.8 compares the normalized shear stress across the depth of the plate obtained by the present approach with that given by the 3-D elasticity solution[32]. Again present numerical solution shows an error of less than 0.5% when quadratic elements are used. However in this case constant elements gave more accurate results(error 10%) than the linear ones(error 25%)

6.7 Conclusion

In this chapter Euler's transformation technique has been successfully used for stress analysis of 2-D orthotropic structures using the boundary element method. A comparative study has been made of the BIE procedure using constant, linear and quadratic elements in the discretization. For problems involving bending, in which a rapidly varying traction field is prescribed as the boundary condition, it was found that both constant and linear elements gave highly in-accurate results, while the error with quadratic elements was less than 1%.

In general, the use of the Euler' transformation technique requires the choice of a number of terms to use in the limit evaluation process. Despite having been developed for two-dimensional anisotropic elasticity, this technique is completely general and can, therefore, be applied to a wide range of problems from potential theory to elasticity. To the author's knowledge there is no other scheme with similar approach available in the BEM literature, making this technique a completely original approach to tackle the problem of computation of singular integrals in boundary element method.

The stress measures obtained from the present boundary element procedure, can be post-processed for various purposes. For example, composite failure criteria can be applied to these quantities and a failure assessment for 2-D orthotropic structures can be made. However, presently no results are presented in this regard, since the aim of this chapter was to develop a computational methodology for computation of singular integrals.

6.8 References

1. Brebbia, C.A., Telles J.C.F. and Wrobel, L.C., *Boundary Element Techniques*, Springer-Verlag, Berlin 1984.

2. Becker A.A., *The Boundary Element Method in Engineering*, McGrawhill, London 1992.

3. Rizzo, F.J., An Integral Equation Approach to Boundary Value Problems of Classical Elastostatics, *Quarterly J. of Appl. Math.* 25, 83-95(1967).

4. Rizzo, F.J. and Shippy, D.J., A method for stress Determination in Plane Anisotropic Body, *J. of Comp. Mat.* 4, 36-61(1970).

5. Vogel, S.M. and Rizzo, F.J., An Integral Equation Formulation of Three-Dimensional Anisotropic Elastosttaic Boundary Value Problems, *Journal of Elasticity*, Vol. 3, pp. 203-216(1973).

6. Deb, A. and Banerjee, P.K., BEM for General Anisotropic 2D Elasticity Using Particular Integrals, *Communications in Applied Numerical Methods*, Vol. 6, pp. 111-119(1990).

7. Deb, A., Henry, D.P. and Wilson, R.B., Alternative BEM Formulation for 2- and 3-D Anisotropic Thermo-elasticity, *International Journal of Solids and Structures*, Vol. 27, pp. 1721-1738(1991).

8. Grundemann, H., A General Procedure Transferring Domain Integrals Onto Boundary Integrals in BEM, *Engineering Analysis With Boundary Elements*, Vol. 6, pp. 214-222(1989).

9. Perez M.M. and Wrobel L.C., An Integral Equation Formulation for Anisotropic Elastostatics, *ASME J. of Appl. Mech.* 63, 891-902(1996).

10. Green A.E., A Note on Stress Systems in Aelotropic Materials, *Philos. Mag.* 34, 416-418(1943).

11. Mahajerin, E. and Sikarskie, D.L., Boundary Element Study of a Loaded Hole in an Orthotropic Plate, *J. of Comp. Mat.* 20, 375-389(1986).

12. Vable, M. and Sikarskie, D.L., Stress Analysis in Plane Orthotropic Material by the Boundary Element Method, *Int. J. of Solids and Structures* 24, 1-11(1988).

13. Benjumea, R. and Sikarskie, D.L., On the Solution of Plane Orthotropic Elasticity Problems by an Integral Method, *ASME J. of Appl. Mech.*, 39, 801-808(1972)

14. Snyder, M.D. and Cruse, T.A., Boundary Integral Equation Analysis of Cracked Anisotropic Plates, *Int. J. of Fracture* 11, 315-328(1975).

15. Tan, C.L., Gao, Y.L. and Afagh, F.F., Anisotropic Stress Analysis of Inclusion Problems Using the Boundary Integral Equation, *J. of Strain Anal.* 27, 67-76(1992).

16. Tan, C.L. and Gao, Y.L., Boundary Element Analysis of Plane anisotropic Bodies with Stress Concentration and Cracks, *J. of Composite Structures*, Vol. 20, pp. 17-28(1992).

17. Lee, K.J. and Mal A.K., A Boundary Element Method for Plane Anisotropic Elastic Media, *ASME J. of Appl. Mech.* 57, 600-606(1990).

18. Lachat, J.C. and Watson, J.O., Effective Numerical Treatment of Boundary Integral Equations: A Formulation for Three-Dimensional Elastostatics, Int. J. for Num. Meth. in Engg., Vol. 10,pp. 991-1005 (1976)

19. Jun, L., Beer G. and Meek, J.L., Efficient Evaluation of Integrals of Order $1/r, 1/r^2, 1/r^3$ using Gauss Quadrature, Engg. Anal., Vol. 2, pp. 118-123, (1985).

20. Telles, J.C.F., A Self-Adaptive Co-ordinate Transformation for Efficient Numerical Evaluation of General Boundary Element Integrals, Int. J. for Num. Meth. in Engg., Vol.24, pp. 959-973 (1987).

21. Aliabadi, M.H. and Hall. W.S., Taylor Expansions for Singular Kernels in the Boundary Element Method, Int. J. for Num. Meth. in Engg., Vol. 21, pp. 2221-2236(1985).

22. Guiggiani, M., Gigante, A., A General Algorithm for Multi-Dimensional Cauchy Principal Value Integrals in the Boundary Element Method, ASME J. of Applied Mech., Vol. 57, pp.906-915(1990)

23. Guiggiani, M., Krishnasamy, G., Rudolphi, T.J. and Rizzo, F.J., A General Algorithm for the Numerical Solution of Hyper-singular Boundary Integral Equations, ASME J. of Appl. Mech., Vol. 59, 604-614 (1992)

24. Cruse, T.A., A New Integration Algorithm for Nearly Singular BIE Kernels, Boundary Integral Methods, Theory and Applications, Morino, L. and Piva, R. (Eds.), Springer-Verlag, pp. 162-171(1990).

25. Rizzo, F.J. and Shippy, D.J., An Advanced Boundary Integral Method for Three Dimensional Elasticity, Int. J. for Num. Meth. in Engg., Vol. 1, pp. 1753-1768 (1977)

26. Tanaka, M., Sladek, V. and Sladek, J., Regularization Techniques Applied to Boundary Element Methods, ASME Appl. Mech. Rev., Vol. 47, no. 10, 457-489 (1994)

27. Guiggiani, M., Hyper-singular Formulation for Boundary Stress Evaluation, Engg. Anal. with Bound. Elem., Vol. 13, pp. 169-179 (1994)

28. Guiggiani, M. and Casalini, P., Direct Computation of Cauchy Principal Value Integrals in Advanced Boundaru Elements, Int. J. for Num. Meth. in Engg., Vol 24, pp. 1711-1720 (1987)

29. G S Padhi, R A Shenoi, S S J Moy and G L Hawkins, A Quadratic Boundary Element Implementation in Orthotropic Elasticity Using the Real Variable Approach, *Communications in Numerical Methods in Engineering*, Vol. 16(2000).

30. Wolfram, S., *Mathematica, A system for Doing Mathematics by Computer*, Addison-Wesley, RedWood City, CA(1991).

31. Lekhntiskii, S.G., *Theory of Elasticity of an Anisotropic Elastic Body*, Holden-Day, San Francisco(1963).

32. Pagano, N.J., Exact Solutions for Composite Laminates in Cylindrical Bending, *J. of Comp. Mat.* 3, 398-411(1969).

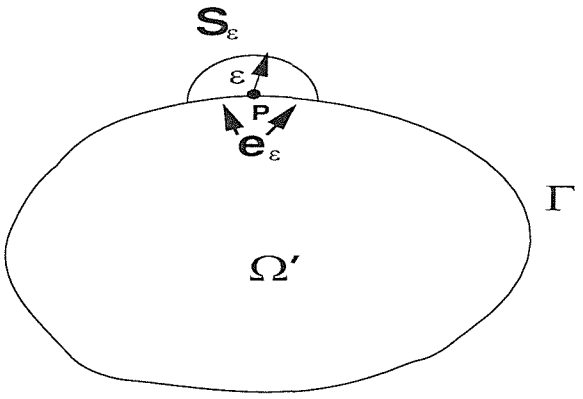

Figure 6.1: Exclusion of the singular point P by a vanishing neighbourhood S_ϵ

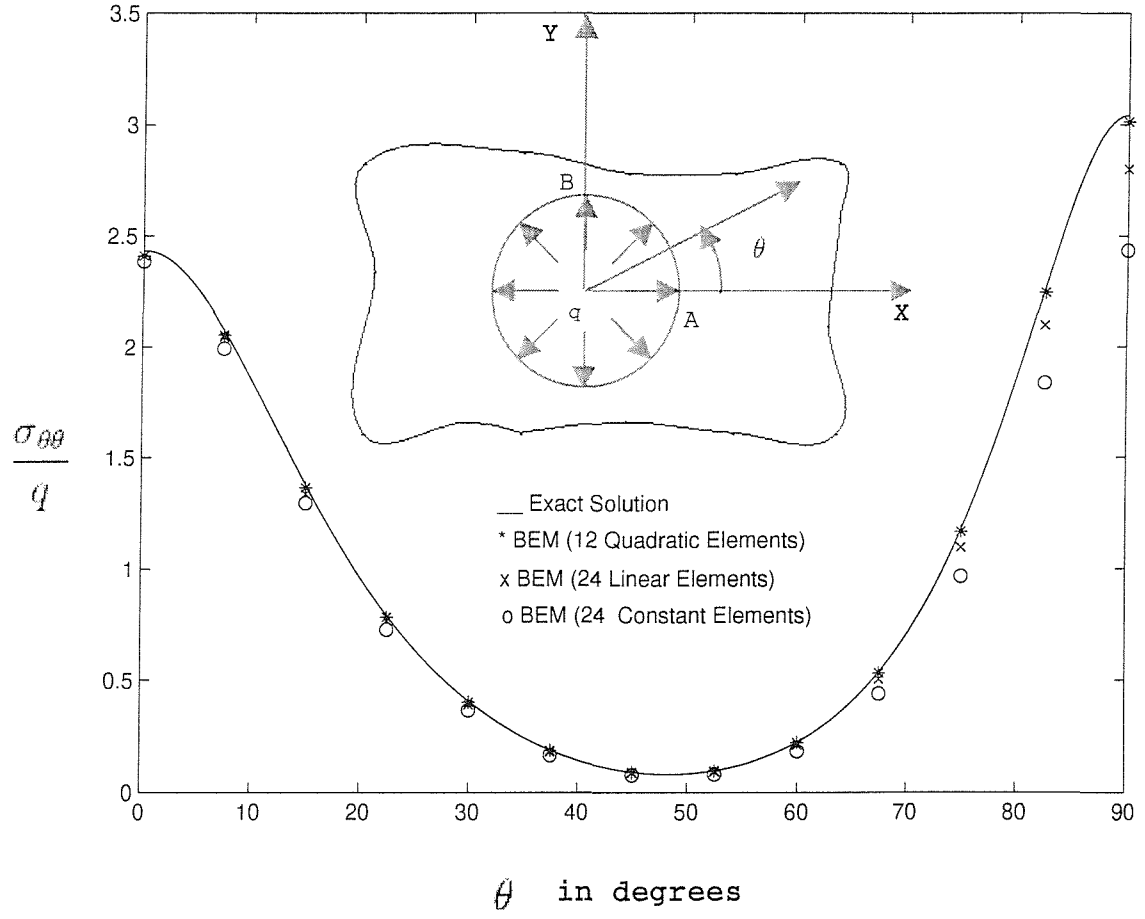

Figure 6.2: Normalized Tangential Stress at the Hole Boundary-(Infinite Plate With a Circular Hole)-Subjected to Hydrostatic Stress

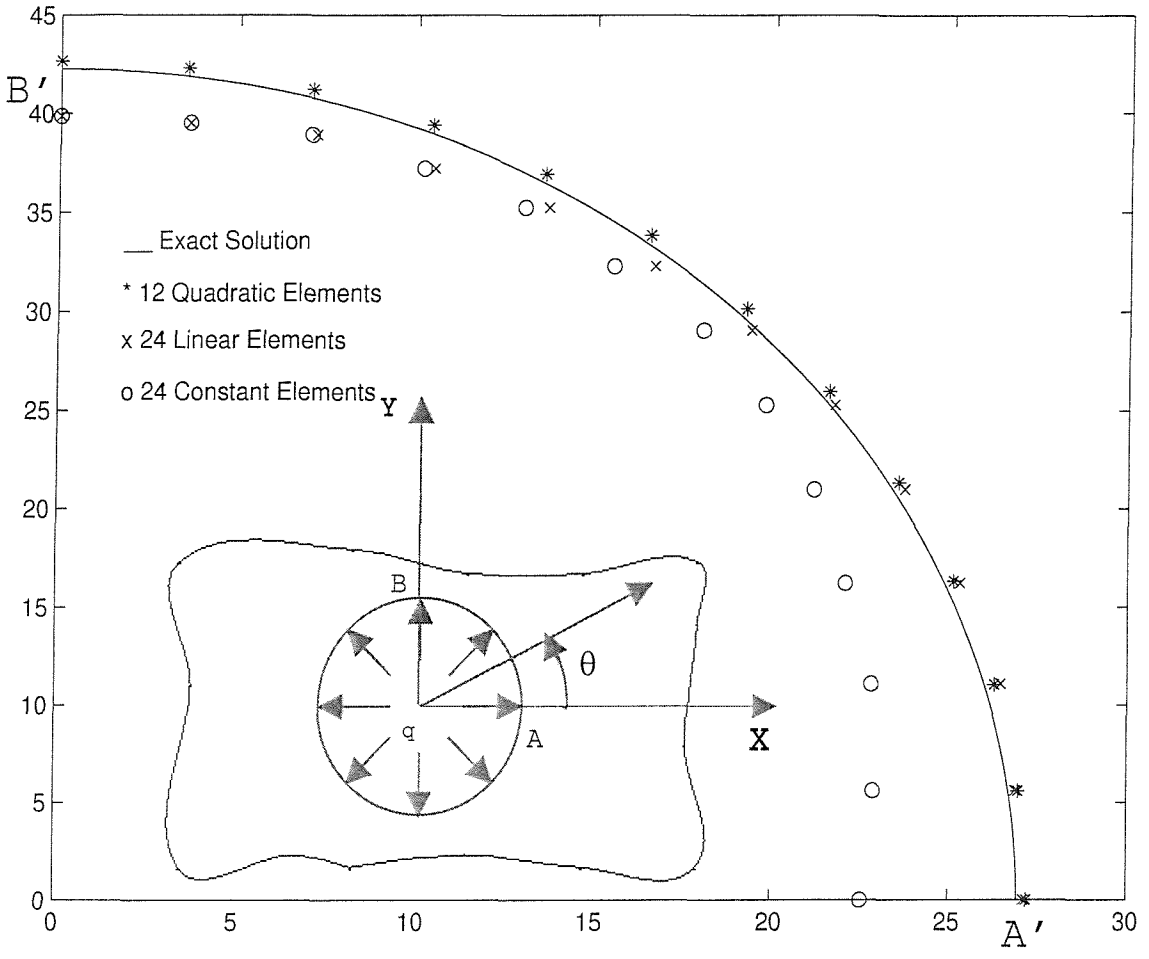

Figure 6.3: Deformed Shape of One Quarter of the Inner Boundary with Unit Radius (Infinite Plate With a Circular Hole)-Subjected to Hydrostatic Stress

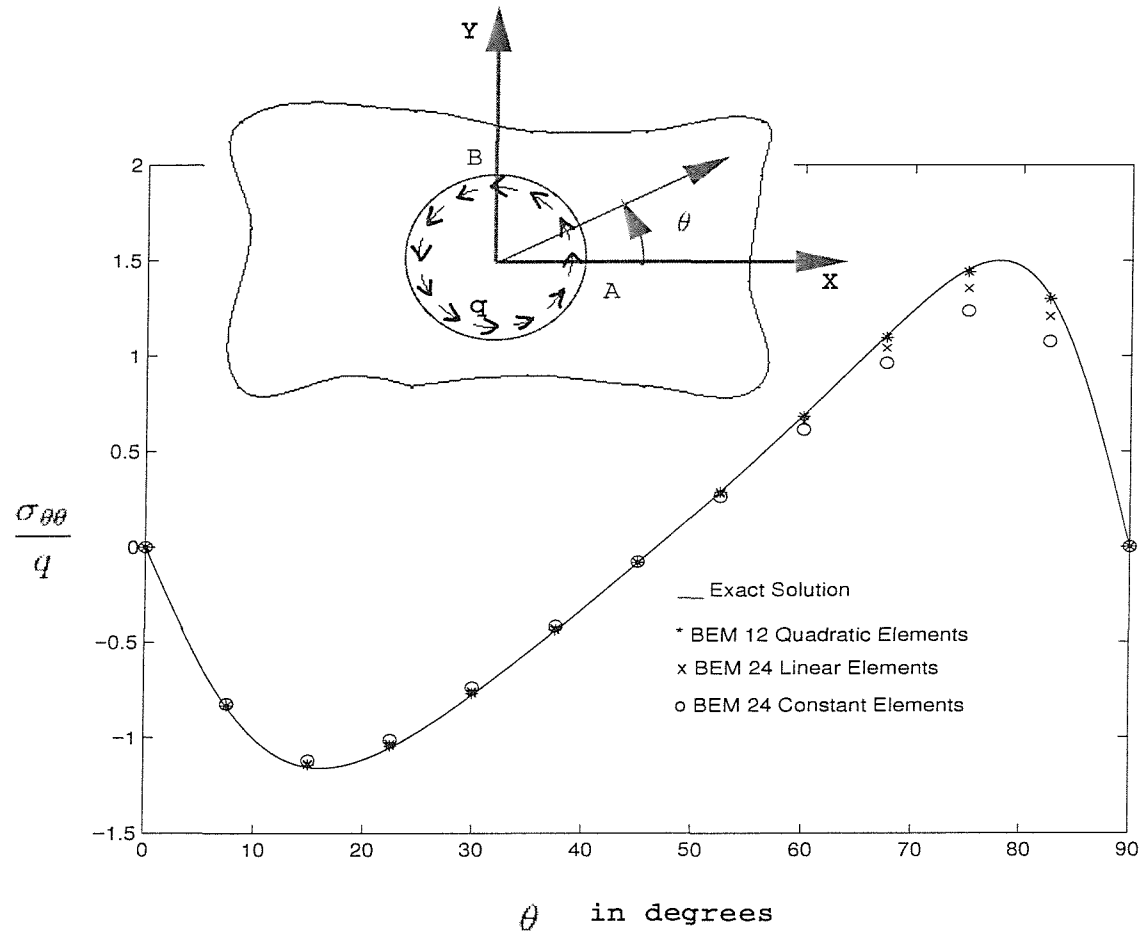

Figure 6.4: Normalized Tangential Stress at the Hole Boundary (Infinite Plate With a Circular Hole)-Subjected to Tangential Stresses

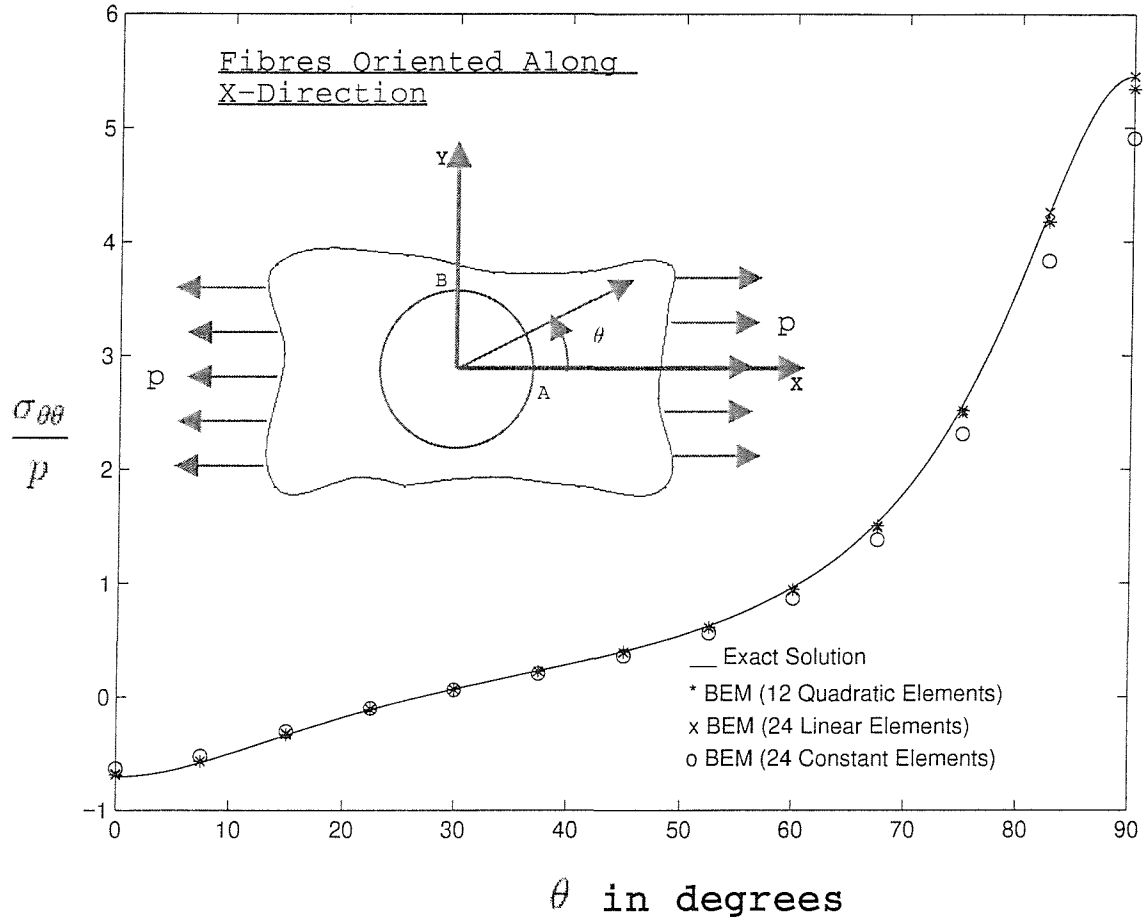

Figure 6.5: Normalized Tangential Stress at the Hole Boundary-(Infinite Plate With a Circular Hole)-Fibers Oriented Along the X-Direction-Subjected to Remote Tension in X-Direction

x

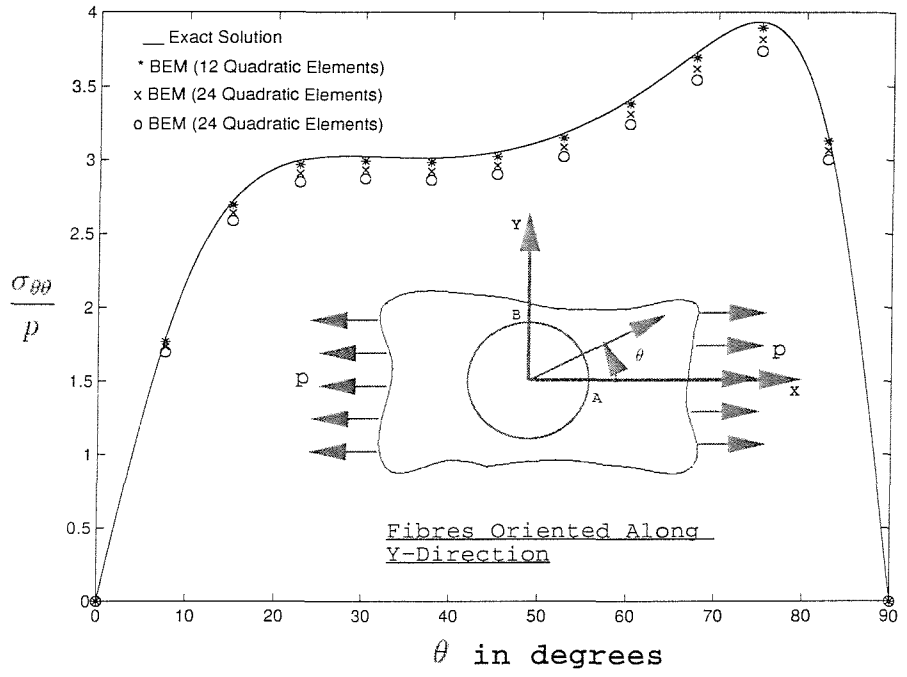

Figure 6.6: Normalized Tangential Stress at the Hole Boundary-(Infinite Plate With a Circular Hole)-Fibers Oriented Along the Y-Direction-Subjected to Remote Tension in X-Direction

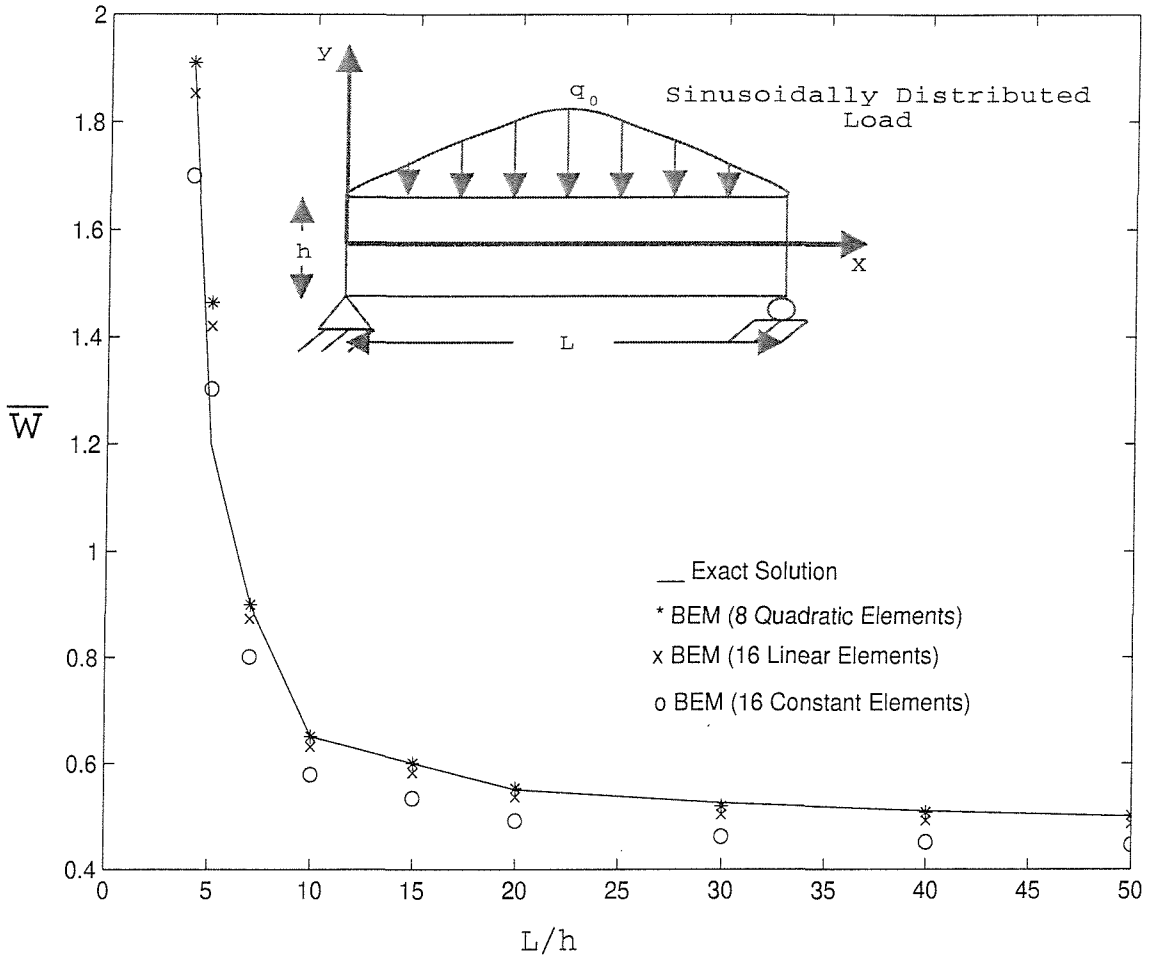

Figure 6.7: Normalized Maximum Deflection Vs. Length/Span Ratio, Infinitely Long Plate Under Sinusoidally Distributed Load

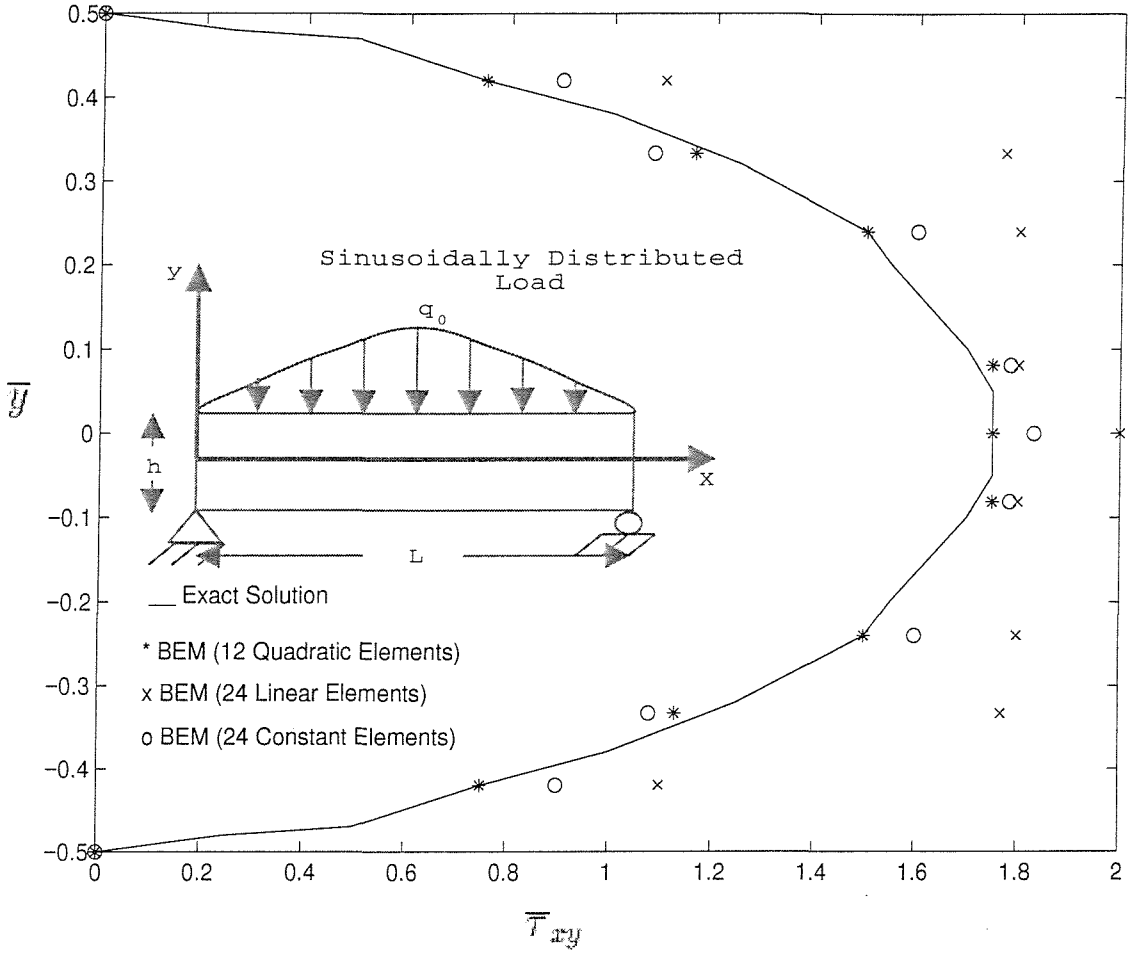

Figure 6.8: Normalized Transverse Shear Stress Distribution Across the Depth, at L/h=4, Infinitely Long Plate Under Sinusoidally Distributed Load

Chapter 7

Discussions and Future Projections

7.1 Discussions

A finite element based progressive failure methodology has been developed for predicting the nonlinear response, first ply failure and ultimate collapse strength of composite plates when loaded in bending. This progressive failure methodology is based on large deformation theory and contains most of the well established composite failure criteria. The progressive failure analysis uses C^0 shell elements based on first order shear deformation theory to calculate the in-plane stresses. The finite element program ABAQUS is used for this purpose. The different failure criteria are compared and assessed by performing analyzes on uni-directional and woven fabric composite structures. The model gives the exact location of occurance of the first ply failure. It can provide the information about the extent of damage and residual strength at any stage of loading.

The first class of laminated composite structures to be analyzed was uni-directional composite structures. Studies were performed to examine the effect of aspect ratios, load increment size and choice of failure criterion on the first ply failure load, nonlinear response and the ultimate collapse strength of these composite structures. The deformation results and the damage patterns obtained in the numerical model were compared against experimental results. Large number of load steps is taken to predict the first ply failure load correctly. Based on the numerical studies, most suitable failure criteria for predicting the first ply failure load and the ultimate collapse loads are suggested.

The next class of composite structures analyzed was woven fabric composite plates. A simplified model was developed for analyzing this class of structures. The correctness of the simplified model was first demonstrated by comparing the material properties predicted by this model with those predicted by other models and with experimental results. The rule of mixtures approach and the first order shear deformation theory have been used while developing the simplified model. The model can provide the elastic material properties for a laminated composite plates with any number of woven fabric plies. The material properties results in this case closely followed the experimental values for longitudinal Young's modulus, shear modulus and the Poisson's ratio. The progressive failure methodology developed for uni-directional composite plates was then extended to the woven fabric composite plates. The propagation of damage for a square woven fabric composite plate was studied. This was compared against the experimental observations and contrasted against the damage patterns of the uni-directional ones. The simplified model is very simple to code in contrast to the finite-element-based micro mechanics approach which is computationally too expensive.

Lastly stress analysis of 2-D orthotropic structures was carried out using the boundary element method. A novel technique was developed for computation of the singular integrals in the BEM. The primary advantages of this technique are that the singular integrals are computed directly and numerically, without any analytical computations, and that corners and edges present no difficulties. These three features should make this approach attractive for most applications. The limit to the boundary provided a mathematically sound and physically sensible definition of the singular integrals, and leads to a direct, and completely general, evaluation algorithm. In the authors opinion, this is much simpler, conceptually and computationally, than 'regularizing' a non-existent integral (e.g., an 'exclusion zone' analysis). The task of carrying out the limiting process, admittedly onerous by hand, is conveniently automated with symbolic computation. The development of this method was motivated by the application of the boundary element method for complex laminated composite structures. Although this application involved the computation of singular integrals in two-dimensional elestostatics, there is no difficulty in extending this work to three dimensions. Once the procedures have been worked out for one application, it is relatively easy to modify the *Mathematica* scripts to generate the needed formulas for another application. This is

due to the fact that the nature of the corresponding kernel singularity, can be found, identical in other engineering applications. Thus, in creating a 3-D code, the existence of the 2-D script could be exploited to considerably shorten the development time.

The stress measures, obtained from using the boundary element method, can be postprocessed for carrying out a failure analysis for 2-D orthotropic structures. However, in this research, this was not investigated since the focus of the research related to the BEM was on the computational aspects rather than failure studies. The aim was to develop computational methodologies for efficient computation of singular integrals. Failure analysis for these 2-D orthotropic structures could be carried out very efficiently using the finite element method. However, again no attempt was made for failure analysis in this case, since more complex structures have already been analyzed in chapters 3 and 4.

The novelty aspects of this research are as follows.

- A computational damage model was developed for progressive failure analysis of laminated composite structures in *bending* with (1) geometric non-linearity, (2) large strains and large rotations, (3) material non-linearity because of local damage, (4) presence of bi-axial stresses. The numerical results are validated against test values. To the author's knowledge, there had been no similar work in the past literatures.

- The damage model was extended to laminated composite plates with plain woven fabric plies. A simplified model was developed in which a woven ply could be represented as a combination of pure resin layers and uni-directional composite layers. Even though this kind approach for woven fabric structures is not new, according to the author's view, the present simplified model is the simplest to code.

- A novel technique was developed for the computation of singular integrals in the two-dimensional boundary element method (BEM). In the author's opinion, this was the first attempt for directly and numerically computing the singular integrals in the boundary element method.

7.2 Future Research

7.2.1 A Novel Finite Element for Progressive Damage Analysis of Laminated Composite Structures

In an experiment the damage development is an evolution process. In the present numerical model (chapter 4) this was approximated with a set of discrete damage quantities. The present computational damage model was developed using the finite element program ABAQUS. The damage parameters were computed as a function of stress measures. The stress measures, however, are calculated from the other independent quantities (degrees of freedom) such as displacements and rotations. However, truly speaking damage development in a continuum is more of an independent process. Therefore just like displacements and rotations, it needs a unique presence of it's own in a finite element analysis. In other words, a true damage analysis can be performed if damage can be interpreted as a new degree of freedom, which the traditional finite elements do not have. The usual element development processes and the relevant numerical tests (patch tests) can be performed. The quantification of this degree of freedom will depend upon the appropriate damage quantities obtained from standard experiments.

7.2.2 Micro-Mechanics Based Progressive Failure Analysis of Woven Fabric Composite Structures

In chapter 5, a simplified model was developed for the analysis of woven fabric composite plates. However the model cannot carry out a detailed stress analysis at the micro level. For this a finite element based micro-mechanic model of woven fabric composite plates can be developed. The solid modelling program PATRAN can be used for this purpose. In this case the model involved will be three dimensional in nature. Once the finite element model is generated, the damage model developed in chapter 4 can be applied to the finite element model for studying the damage propagation and failure analysis of woven composites. However, in this case the damage model also has to be three-dimensional in nature and there has to be separate damage models for the

fiber and resin. The computational cost in this case is expected to be much higher. However, with the availability of the parallel computers, this task seems to be within the reach of research engineers.

7.2.3 Experimental Characterizations of Laminated Composite Structures

From chapter 5, section 5.6.1, it was clear that there were insufficient experimental data on material properties for comparison purposes. Test results are important for validation purposes, especially for composite materials, for which, on specific cases, analytic results are not available. This is true for composite materials with complex reinforcements, such as woven fabric composites. Model tests, such as uniaxial tension tests, pure shear tests and biaxial tension tests have been standardized and are common for composite materials. Certain test procedures such as the acoustic emision energy methods are used for detecting damage in a composite material. However, these are not enough. More experiments, especially for woven fabric composite materials are necessary for an efficient validation of computational models.

7.2.4 Improved Stress Computation of Composite Structures Using the Advanced Implementation of the Boundary Element Method

In chapter 6, a novel technique of computing the singular integrals in 2-D BEM was presented. Using this technique, primary quantities such as displacements for 2-D orthotropic structures were determined. The gradient quantities such as strains and stresses were determined with differentiation of the shape functions and use of the Hooke's laws. This process introduces extra errors associated with the shape functions in the discretization procedure. In the hyper-singular formulations of the boundary element method, stresses are computed more accurately. However, traditionally, just like singular integrals, computation of hyper-singular integrals involve somekind of analytic procedures. According to the author's opinion, the method developed in chapter 6, can be extended to hyper-singular integrals for a direct numerical computation of the

integral quantities. It is expected that in this case, the direct numerical computation procedure will provide more meaningful interpretation of the hyper-singular integrals.

7.2.5 Integration of the Finite Element Method and the Boundary Element Method for Efficient Numerical Characterization of Composite Materials

In the present research, the finite element method was applied for failure prediction of laminated and woven fabric composite plates. The boundary element method was used for computation of deformations and stresses in 2-D orthotropic structures. The logical extension to this research is to integrate FEM and BEM for computationally efficient damage model development for laminated composite structures. The main advantage offered by the FEM is it's ability to solve complex three dimensional problems more efficiently in the nonlinear deformation range. The main advantage offered by the BEM is it's superior numerical computational capability for simple domains and for the linear material behavior. The integration of the two methods will exploit the advantages offered by both the techniques. Since most practical problems have complex geometries and boundary conditions, the finite element method can be used for arriving at a global response. The structure can be divided into certain subdomians. The locations of these sub-domains can be strategically chosen. From the global finite element solution, the nodal force and displacement vectors can be transformed to the boundary of the sub-domains. The sub-domain is now ready with all the informations necessary to carry out a boundary element analysis. In this way the state of stresses and the subsequent damage parameters in the sub-domain can be computed more accurately using the BEM. Even though sub-domain techniques are not knew as such, the application of the BEM at the sub-domain level can be a novel approach. In the event of a damage analysis with geometric nonlinearity, the load history can be split into several sub-steps. The linearized sub-step can be analyzed as described above.

Chapter 8

Conclusion

This research was concerned with the numerical computation aspects of deformations, stresses, failure loads and damage patterns for laminated and two dimensional composite structures including plain woven fabric composite plates. In each case, numerical results were compared with experimental values or analytical solutions.

From the research carried out the following conclusions seem justified.

- Numerical failure modeling of composite structures could give much more information on the stress, damage and failure patterns of composite structures. No other existing techniques including the experimental methods would have been able to carry out such a rigorous study.
- For laminated composite structures in bending, in general, the ultimate failure load was found to be much higher than the first ply failure load. There was a pronounced effect of geometric nonlinearity, especially in the initial stage of loading.
- The curvature of the weave pattern in the woven fabric composite plates considered in this research was not significant. Therefore it is difficult to make conclusive comments on the effect of weave on the stiffness and strength for them. However, from the present research, it seems that there is an improvement in resistance to fiber failure for woven fabric composite plates.
- The method developed in chapter 6, for computation of singular integrals, was

novel, conceptually simple and easy to implement in a computer. It gave an added contribution towards the physical interpretation of the singular integrals.

Appendix A

Introduction to ABAQUS/Standard

A.0.6 Overview

ABAQUS/Standard is a general-purpose finite element program designed specifically for advanced structural analysis applications. A wide variety of problems can be addressed with the available modeling tools. ABAQUS/Standard is designed to run effectively on computers ranging from desktop systems running Windows NT or UNIX to departmental servers and supercomputers. Structures and continua can be modeled. One, tow and three-dimensional continuum elements are provided, as well as beams, membranes and shells. ABAQUS/Standard is a modular code: any combination of elements, each with any appropriate material model, can be used in the same analysis.

A.0.7 Features

ABAQUS/Standard uses a high-performance, sparse, multi-front equation solver to solve both symmetric and unsymmetric systems of equations and automatically uses the unsymmetric solution scheme when the physics of a problem demands it.

A.0.8 Nonlinear Analyses

In nonlinear problems the challenge is to provide a convergent solution at minimum cost. This challenge is addressed by automatic control of the time incrementation, which is provided for all relevant analysis procedures. The user defines a "step" (a

portion of the analysis history). ABAQUS/Standard then automatically selects the convergence tolerances and the increments required for the step. This approach is highly effective for nonlinear problems because the model's response may change drastically during an analysis step. Automatic control allows nonlinear problems to be run with confidence without extensive experience with the problem.

The user divides the loading histories into steps solely on the basis of convenience. For a purely linear analysis each step is essentially a load case. In a nonlinear analysis each step is typically one stage in the overall loading history. A Single analysis type is specified within each step.

In a nonlinear analysis the initial condition for each step is the state of the model at the end of the previous step. This dependency provides a convenient method for following complex loading histories. Each step is subdivided into increments ; in each increment ABAQUS/Standard iterates for equilibrium, using the full Newton method in most cases. The convergence criteria are determined automatically by ABAQUS/Standard, although the user can override these tolerances.

A.0.9 Static Analysis

Two approaches for static analysis are available. One is for cases in which a prescribed loading history must be followed. With this approach there is an option for ABAQUS to control localized unstable behavior automatically. The alternative is an arc-length (modified Riks) method, which is provided for globally unstable static problems such as post-collapse or post-buckling cases.

A.0.10 ABAQUS Elements

For three-dimensional applications 3- and 6-node triangular and 4-, 8-, and 9-node quadrilateral shells are available. All shell elements can model layered composites. The reference surface of the element, defined by the position of the nodes, can be placed at any location through the thickness of the shell.

A.0.11 Numerical Integration

Full-integration triangular shells and full- or reduced- integration quadrilateral shells are available. The shell section stiffness can be recalculated throughout an analysis to capture nonlinear material behavior, or it can be integrated once for economic solutions involving material response. In either case nonlinear geometric effects can be included. The shell elements in ABAQUS are true doubly curved shells. Both shear flexible("thick") and "thin" shell elements are provided. The initial thickness can be provided on an element or nodal basis, and the final thickness distribution can be recovered.

A.0.12 Solution Techniques

By default, ABAQUS/Standard uses a multi-frontal, block elimination technique, available only for both symmetric and unsymmetric matrices. This solver is highly optimized to minimize the CPU time and disk space required for sparse problems. It takes full advantage of parallel capabilities on high performance computers.

The user can also access a frontal solver that includes an automatic, internal, wavefront minimization algorithm. The user can choose any node and element and node numbering without invoking a solution time penalty.

A.0.13 Geometric Nonlinearity

ABAQUS/Standard uses complete, consistent kinematics for finite-strain calculations. Lagrangian and updated Lagrangian formulations are used for finite-strain elastic and elastic-plastic problems, respectively. ABAQUS/Standard generally uses the full Newton method for the solution of nonlinear equations. This approach is especially effective for the highly nonlinear cases that are commonly modeled with the program. Modified Newton methods are also available.

A.0.14 Problem Size and Performance

ABAQUS/Standard has no built-in limits on problem size. Smaller problems run entirely in main memory. Buffering to secondary storage occurs automatically as the problem size increases. ABAQUS/Standard performs efficiently on a wide range of computers and is particularly effective for large problems running on advanced computer architectures.

Appendix B

Summation of an Infinite Series via Finite Sampling Using Euler's Transformation Technique

Given any series

$$S = a_0 + a_1 + a_2 + a_3 + \cdots a_{n-1} + a_n + \cdots \tag{B.1}$$

define $x = \frac{a_n}{a_{n-1}}$, so that the series can be re-written as

$$S = a_0 + x\frac{a_1}{x} + x^2\frac{a_2}{x^2} + x^3\frac{a_3}{x^3} + \cdots x^{n-1}\frac{a_{n-1}}{x^{n-1}} + x^n\frac{a_n}{x^n} + \cdots \tag{B.2}$$

where n is the number of finite terms used to give an approximation to the infinite sum. The series can be re-written as

$$S = u_0 + u_1 x + u_2 x^2 + \cdots, \tag{B.3}$$

where $u_0 = a_0, u_1 = \frac{a_1}{x}, u_2 = \frac{a_2}{x^2}$ and so on. Using the relationships $Eu_0 = u_1, E^2u_0 = u_2, E^3u_0 = u_3$.....; then symbolically

$$S = \left(1 + Ex + E^2x^2 + \cdots\right) u_0 = \frac{1}{1 - Ex} u_0 \tag{B.4}$$

where E is a shift operator such that $Ef(x) = f(x+h)$ and h is the interval length. Using $E = \Delta + 1$, equation (A.4) can be re-written as

$$S = \frac{u_0}{1 - x - x\Delta} = \frac{1}{1-x}\left(\frac{u_0}{\left(1 - \left(\frac{x}{1-x}\right)\Delta\right)}\right) \tag{B.5}$$

where Δ is the difference operator such that $\Delta f(x) = f(x+h) - f(x)$, or $\Delta u_0 = u_1 - u_0$, $\Delta^2 u_0 = u_2 - 2u_1 + u_0$ etc.

The summation formula in equation (A.5) can now be re-written as

$$S = \frac{1}{1-x} \times \sum_{s=0}^{\infty} \left(\frac{x}{1-x}\right)^s \Delta^s u_0 \tag{A.6}$$

Using the difference quantities in the terms of the original sequence, equation (A.6) can be re-written as

$$S = \frac{1}{1-x} \times \sum_{s=0}^{\infty} \left(\frac{1}{1-x}\right)^s \Delta^s a_0 \tag{B.6}$$

This is Euler's transformation of the original series which is found to converge faster than the original series. It is not necessary to sum to infinity in equation (A.6); it will be sufficiently accurate to use a finite number of terms, (say, p), thus requiring the first p differences obtained from the terms starting at u_0.